

A Universal Load Balancing Principle and Its Application to Large Language Model Serving

Zixi Chen³, Tianci Bu^{2†}, Chendong Song^{1†}, Xin Lu^{2*},
Yinyu Ye^{1,4*}, Zijie Zhou^{1*}

¹*Department of Industrial Engineering and Decision Analytics, HKUST,
Clear Water Bay, Hongkong, China.

²Department of System Engineering, National University of Defense
Technology, 109 Deya Road, Changsha, 410073, Hunan, China.

³School of Mathematical Sciences, Peking University, Yiheyuan Road,
100871, Beijing, China.

⁴Department of Management Science and Engineering, Stanford
University, 450 Jane Stanford Way, Stanford, 94305, California, United
States.

*Corresponding author(s). E-mail(s): xin.lu.lab@outlook.com;
yyye@ust.hk; jerryzhou@ust.hk;

Contributing authors: chenzixi22@stu.pku.edu.cn; btc010001@gmail.com;
songcd@ust.hk;

†These authors contributed equally to this work.

Abstract

Load balancing—the allocation of work across parallel resources to reduce delay, energy and cost—is a pervasive challenge in science and engineering, from large-scale simulation and data processing to cloud and manufacturing operations. Motivated by the emerging bottleneck in large language model (LLM) serving, we study a particularly stringent regime of load balancing that arises in barrier-synchronized, stateful systems: work cannot be freely migrated and progress is gated by the slowest participant at each step, so heterogeneity and temporal drift in workloads create persistent stragglers and substantial idle time. LLM serving under data-parallel decoding provides a prominent modern instance: in production traces, barrier-induced idle can exceed 40% of compute time per decode step. Here we develop a universal load-balancing principle, which admits a step-wise finite-horizon integer-optimization formulation and yields worst-case guarantees: across LLM decode models and a broader class of non-decreasing workload drift

processes, it reduces long-run imbalance by a factor that grows with batch size and system scale. Extensive experiments corroborate the theory, showing substantial improvements in throughput and latency together with reductions in energy consumption. These results provide a general, theoretically grounded framework for load balancing, with immediate implications for sustainable LLM serving and broad relevance to other synchronization-gated resource-allocation problems.

1 Introduction

Load balancing—the problem of distributing work across parallel resources to minimize latency, energy, or cost—is a central challenge across the natural and engineering sciences and in large-scale service systems. In large-scale molecular dynamics and biomolecular simulations, dynamic load-balancing schemes are essential to maintain scalability as particles move and local density fluctuates [1, 2]. In climate and weather models, specialized load-balancing strategies are required to handle localized, high-intensity physics kernels and heterogeneous meshes, improving time-to-solution for global simulations and regional storm-surge predictions [3, 4]. Similar issues arise in cloud computing platforms [5, 6], manufacturing systems [7, 8], and emergency medical management [9, 10], where workloads and resource availability fluctuate over time. In this work, we study a new instance of this broad class: load balancing in large-scale LLM (Large Language Model) serving. This setting adds stringent constraints—jobs whose processing times are unknown and evolve as computation proceeds, per-request state that cannot be migrated between workers without prohibitive cost, and step-wise synchronization barriers across workers—that make it substantially more challenging than many classical load-balancing problems. Our goal is to develop a **universal and scientifically sound** load balancing principle that not only resolves this emerging bottleneck in LLM serving, but also applies, in appropriately simplified form, to more traditional load-balancing tasks.

Modern generative LLMs [11–15] have transformed artificial intelligence by achieving unprecedented performance in natural-language generation, reasoning, and task generalization across diverse domains. LLM serving refers to the process of hosting these models in production environments to process user prompts and generate responses in real time. Meeting this demand requires vast networks of AI datacenters that deliver timely and reliable inference at massive scale [16, 17]. Even considering OpenAI alone, its LLM serving services handle at least 2.5 billion user prompts per day [18], corresponding to roughly on the order of gigawatt-hour of electricity consumption daily [19]. As LLM usage continues to accelerate, the energy and cooling resources required for such inference are approaching practical and environmental limits—often referred to as the emerging energy wall [20]. Despite remarkable advances in model architecture and hardware acceleration, the overall efficiency and energy use of LLM serving remains constrained by how computational workloads are balanced across parallel workers.

In LLM serving, inference unfolds in two stages: a *prefill* stage that encodes the input prompt and initializes internal state, followed by a *decode* stage that generates the response one token at a time. In modern deployments, decoding is executed in parallel across many computational workers, and each token step typically includes a coordinated stage across workers (e.g., collective communication in model-parallel execution), which induces barrier synchronization: the step completes when the slowest worker finishes. As active requests evolve and complete at different times, per-worker workloads drift, creating persistent stragglers and forcing faster workers to idle. Figure 1 quantifies the resulting inefficiency in a real industrial trace: both the mean and median barrier-induced idle time exceed **40%** per decode step, wasting more than two-fifths of aggregate compute on average. This inefficiency scales directly into energy cost at fleet scale. Because GPUs draw substantial power even while waiting at synchronization barriers—idle time consumes energy [21] without producing useful computation—the 40% barrier-induced idle in Figure 1 represents not merely wasted time but wasted watts. Figure 2 demonstrates this concretely: reducing decode-stage imbalance via the approach introduced in this paper yields a **3.4%** reduction in total energy consumption relative to the default serving policy. At the scale of modern LLM deployments—where inference alone can consume gigawatt-hours of electricity daily—even single-digit percentage improvements translate to megawatt-hour savings with proportionate reductions in cooling load and carbon footprint. Moreover, as we establish theoretically, the improvement factor grows with system scale, implying that larger production deployments stand to benefit even more substantially. We next unpack the decode-side mechanics that create this imbalance and clarify why routing decisions are both critical and difficult.

To make the bottleneck precise, we outline the decode-side mechanics relevant to load balance. *Prefill–decode (PD) disaggregation* is the most common structure in LLM serving, where prompt encoding (prefill) and token-by-token generation (decode) run on distinct workers. When a request finishes prefill, the router assigns it to a decode worker; from that handoff onward the request remains on that decode worker. During decoding, each newly generated token appends one unit of key–value (KV) vectors to the per-request KV cache, so the cache grows linearly with response length. In practice, the decode stage is organized via *data parallelism (DP)*: each worker maintains a batch of active requests and their KV caches; migrating a request would require transferring its entire cache and is therefore impractical—assignments are effectively **sticky**, making the assignment decision crucial. At each decode step t , worker g performs the local attention compute for its request batch; the runtime $T_{\text{local}}^{(g)}(t)$ is approximately linear with the aggregate resident KV it must read and carry over. Once the local computation finishes, the system executes a *model-parallel* stage—such as expert parallelism (EP) or tensor parallelism (TP)—in which the forward pass is split across workers because the model (or its expert set) is partitioned across devices. This stage requires collective communication and is therefore *synchronous* across workers, taking time $T_{\text{sync}}(t)$. The per-step wall-clock time is thus

$$T_{\text{step}}(t) = \max_g T_{\text{local}}^{(g)}(t) + T_{\text{sync}}(t).$$

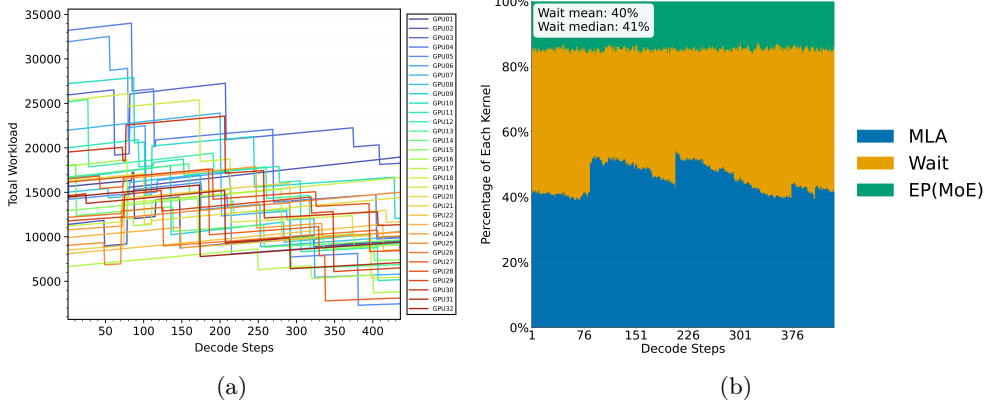


Fig. 1: Workload imbalance and idle time in 436 decoding steps over 3 minutes from a real industrial trace. **(a):** Dynamic total workload across 32 GPUs. At each step, the completion time for all GPUs is dictated by the heaviest workload unit, demonstrating significant and persistent workload imbalance. **(b):** Per-step idle time resulting from this imbalance. The yellow bars represent the average percentage of time that GPUs spend waiting during each decode step. With a mean (and median) idle time of 40% (and 41%), more than two-fifths of the aggregate computational resources are wasted on average per step.

As response lengths diverge across requests, these local times diverge, so the maximization term governs progress and induces persistent idle time for lightly loaded workers. Figure 3 illustrates the LLM serving system architecture and the load balancing barrier.

Balancing decode-time work is intrinsically difficult for three coupled reasons. **(i) Unknown and evolving workloads.** The response length of a request is unknown at assignment. Although several studies predict decode length from prefill features [22–26], the inherent randomness of generation and the limited information in these features result in low prediction accuracy. **(ii) Online, non-stationary arrivals.** Requests finish prefill and arrive to the router sequentially, so decisions must be made without knowledge of the future mix of lengths. Moreover, the frequency of arrival varies over time and is hard to model, so even an arrival distribution for decode is unavailable. **(iii) Sticky assignments with drifting load.** Once placed, a request cannot be migrated without moving its entire KV cache. Each request’s decode is processed on a single decode worker for its entire lifetime. Meanwhile, per-worker load changes at every step (Figure 3): continuing requests add one token’s workload, completed requests remove their entire workload, and newly admitted requests add their KV cache from the prefill step. Early placement errors therefore persist and compound.

Together, these constraints define an online routing problem with unknown, time-varying job sizes under hard synchronization barriers, in which classical policies such as round-robin or join-shortest-queue can be systematically misaligned with

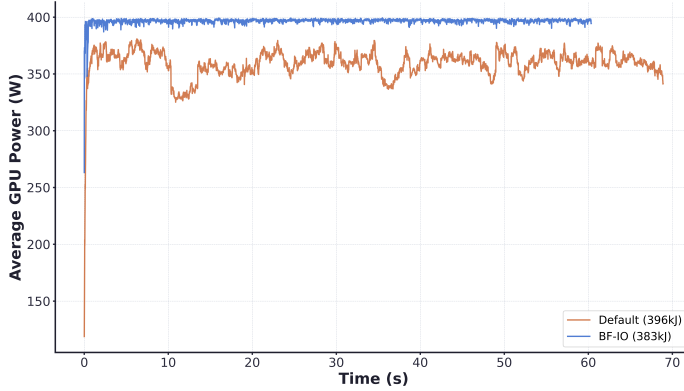


Fig. 2: Instantaneous GPU power consumption over time under the default policy and the approach introduced in this paper (BF-IO). Total energy, computed as the time integral of instantaneous power, is 396 kJ for the default and 383 kJ for BF-IO—a 3.4% reduction. BF-IO draws slightly higher instantaneous power (reflecting improved GPU utilization from reduced barrier idling), but completes the same workload in less time; the resulting shorter integration window yields lower total energy consumption.

the true objective and perform poorly. Because the barrier-induced bottleneck is architectural and the workload mix is inherently non-stationary, improvements that depend on a particular trace or dataset are insufficient; what is needed is a *universal* load-balancing principle that is robust across deployments and adversarial arrival patterns. Appendix A.1 reviews related work, including the limitations of classical load-balancing policies in this setting.

2 Results

We summarize the main findings of this work in two parts. First, we introduce a *universal* load-balancing principle for sticky assignment systems with barrier synchronization and show that it admits a clean optimization formulation and rigorous worst-case guarantees. Second, we instantiate the principle in the decode-stage DP bottleneck of LLM serving, design a sustainable routing policy, and demonstrate substantial improvements on both public and proprietary workloads.

2.1 A universal load-balancing principle: Balance a Short Future

Scientific structure: a step-wise integer-optimization formulation.

At each assignment step, the Balance Future with Integer Optimization principle (BF-IO) chooses assignments that minimize a short-horizon prediction of future imbalance (Section 4). We write this decision as a finite-horizon *integer optimization* over binary assignment variables, subject to per-worker capacity constraints and full utilization of available slots, in the spirit of classical linear- [27, 28] and integer-optimization [29]

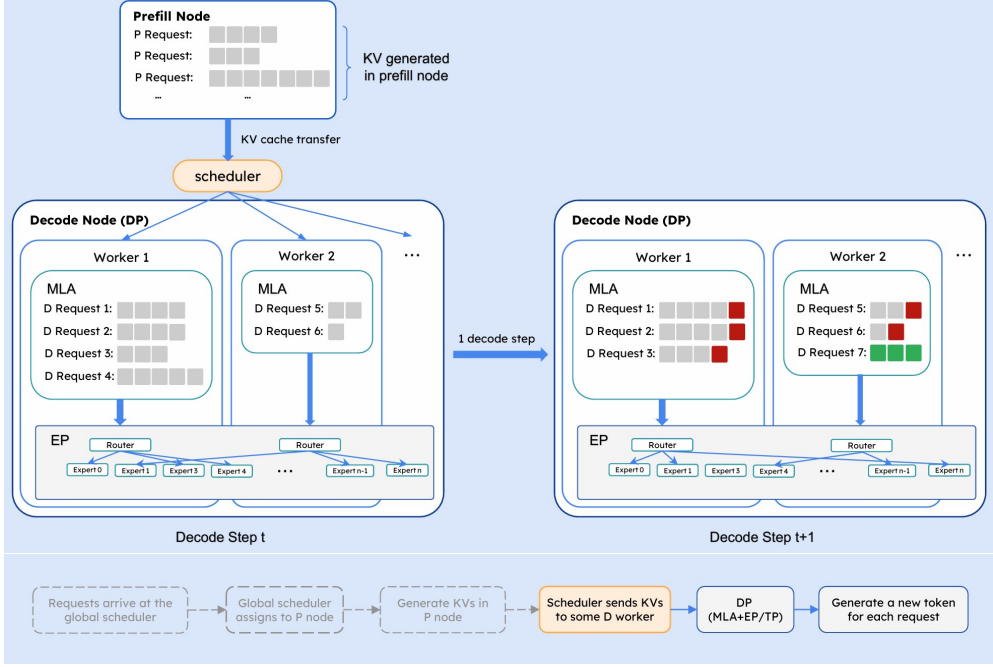


Fig. 3: Prefill-decode serving and the decode-stage load-balancing barrier. **Left (Decode Step t):** Prefill workers build each request’s KV cache and hand the request to the scheduler, which assigns it to a decode worker; the assignment is sticky because migrating the KV cache is impractical. Each decode worker processes a batch of requests during the local compute stage (Multi-head Latent Attention). Gray squares indicate the resident KV cache per request. After local compute, all workers must begin the EP stage synchronously. The step time is therefore governed by the slowest local stage: here, Worker 2 must wait for Worker 1, exposing the load-balancing bottleneck. **Right (Decode Step t+1):** Every active request produces one token, appending to its KV cache (red square). Completed requests leave the batch (e.g., Request 4), and newly prefetched requests may be admitted by the scheduler to a worker (e.g., Request 7 with green square). Because request lengths differ and assignments are sticky, per-worker loads drift from step to step, creating persistent imbalance that limits throughput and energy efficiency. **Legend:** gray = existing KV cache; red = KV added by the current step; green = newly admitted request after prefill.

formulations used in scientific and engineering applications. Concretely, the step- k decision is characterized by the integer program (IO), whose objective is the accumulated predicted imbalance over a short window and whose feasible set encodes the sticky assignment rule and slot constraints. This formulation makes explicit that decode-time load balancing is not merely a heuristic dispatch problem: it is an online sequence of structured combinatorial optimization problems with a barrier-driven objective.

A counterintuitive information suggested: short lookahead, not full-job prediction.

A central insight is that effective load balancing in barrier-synchronized systems does *not* require accurate prediction of the *total* remaining workload of newly arriving jobs—a task that is notoriously unreliable in LLM inference and many other domains. Instead, our BF-IO principle relies on a weaker and more robust signal: a short lookahead description of the *near-future evolution* of the *currently active* jobs, not the newly arriving jobs. Intuitively, the barrier cost at time k is dominated by which workers are likely to become stragglers in the *next* few steps; decisions can be revisited at subsequent steps as new arrivals are observed, so errors about the distant future can be corrected by future routing choices. This is precisely the regime where short-horizon prediction is feasible: while forecasting the full completion time of a long job may be difficult, predicting whether an ongoing job will finish within a small window is often considerably easier (and can be performed using lightweight signals, or even manual rules in some settings).

2.2 Provable theoretical guarantees under worst-case settings

Guaranteed improvement in the LLM serving model.

We build a mathematical model in Section 3 for the LLM DP decode load imbalance problem, where each active request contributes an increasing KV workload until termination. Then, we provide worst-case theoretical guarantees, where arrivals may be chosen adversarially in Section 5. We rigorously prove that even under this worst-case arrival model, BF-IO provably reduces long-run imbalance relative to the real baseline algorithm by a factor $\Omega(\sqrt{B \log G})$ that grows with system scale (Theorem 1, Theorem 2), where B is the per-worker batch size and G is the number of workers. This scaling is significant: it shows that the benefit of principled balancing *increases* with cluster size and batching, precisely the regime in which industrial huge serving systems operate.

Universality beyond LLMs: a broad class of drifting workloads.

The LLM analysis exploits the fact that per-request workload drifts by one unit during processing, but the same phenomenon occurs far more broadly. We therefore extend the theory to a general non-decreasing drift model in which all active jobs share a bounded, time-varying workload increment sequence $(\delta_k)_{k \geq 1}$, encompassing the classical constant-workload case ($\delta_k \equiv 0$), standard LLM decoding with unit-step KV growth ($\delta_k \equiv 1$), speculative decoding where multiple tokens may be accepted per step ($\delta_k \geq 1$) and and memory-efficient architectures employing cache compression or sparse attention (Section 5.1). Theorem 3 shows that the same scale-sensitive improvement persists in this general setting: BF-IO achieves a worst-case imbalance-reduction factor of order $\Omega(\sqrt{B \log G})$ relative to the baseline under the worst-case arrival sequences.

Beyond its immediate implication for system design, the mathematical proof introduces a technically involved analytical route for studying online load balancing under

stickiness and barrier coupling; we view this as a novel and reusable perspective for future theoretical work on load balancing in modern, stateful parallel systems.

2.3 Resolving a decode-stage load balancing bottleneck in LLM serving

Decode-stage load imbalance as a dominant efficiency bottleneck

We establish that decode-stage load imbalance constitutes a dominant efficiency bottleneck in production-scale LLM serving with large-scale EP/TP synchronization. In such deployments, each token step is barrier-gated by the slowest data-parallel worker; heterogeneity in resident KV footprints therefore translates directly into idle time on faster workers while they await synchronization. Our analysis of real industrial traces quantifies this inefficiency: Figure 1b shows that the average fraction of compute time lost per decode step exceeds **40%**, representing more than two-fifths of aggregate GPU resources wasted at barriers, which results in a **3.4%** energy waste. Crucially, the magnitude of this waste varies sharply with arrival patterns and request characteristics, indicating that improvements tied to any single trace or dataset are insufficient—a finding that motivates our focus on a universal principle with worst-case guarantees.

Empirical results on open and proprietary workloads.

We evaluate BF-IO through extensive numerical simulations to assess whether the theoretical improvements translate into practical efficiency gains. We evaluate BF-IO on (i) public datasets and (ii) proprietary industrial workloads under matched serving configurations (Section 6). Across these settings, BF-IO consistently reduces imbalance and improves system efficiency relative to the default baselines used in real industries. Concretely, on the public workload, BF-IO improves throughput by **14%**, reduces latency by **13%**, and reduces energy consumption by **3.4%**.

3 Model and Baseline Policy

We consider a general online assignment problem with G computational workers. Each worker $g \in [G]$ has a maximum concurrency of $B \in \mathbb{N}$, meaning that at most B requests can be processed simultaneously on g . The discrete time horizon is indexed by $k \in \{0, 1, \dots, K\}$, where K can be taken large (and later set to infinity in asymptotic analyses).

Arrival instance and workload profiles.

Let \mathcal{I} denote the set of all requests in a given arrival instance. Each request $i \in \mathcal{I}$ arrives at some step $k_i \in \{0, \dots, K\}$ and may be assigned to a worker at any step $x_i \geq k_i$. Once assigned, the request is processed on a *single* worker until completion; we do not allow migration between workers (assignments are *sticky*) and we do not preempt processing.

The processing requirement of request i is represented by a *workload profile*

$$W_i = (w_i^{(1)}, w_i^{(2)}, \dots, w_i^{(o_i)}),$$

where $o_i \in \mathbb{N}$ is the total number of processing steps for request i , and $w_i^{(j)} \geq 0$ denotes the workload contributed by i in its j -th processing step. Thus, once i starts processing at time x_i , it occupies exactly o_i consecutive steps $x_i, x_i + 1, \dots, x_i + o_i - 1$, and its workload at time k (while active) is $w_i^{(k-x_i+1)}$.

Two simple examples illustrate this notation. If a request i has constant workload 5 in each of 3 steps, then $W_i = (5, 5, 5)$. In LLM inference, if a request i has a KV-cache load that grows linearly with the number of generated tokens and starts with prefill size 3, then a run of 4 decoding steps corresponds to $W_i = (3, 4, 5, 6)$. In general, the full profile W_i is *unknown* to the scheduler at arrival time; it is treated as fixed but unobserved.

Policies and per-step workloads.

A non-anticipative policy π specifies, for each request i and each step $k \geq k_i$, whether to assign i at time k , and if so to which worker $g \in [G]$, subject to the capacity constraint that at most B requests are actively processed on each worker at every step. Let $g(i)$ denote the worker to which request i is assigned under policy π , and x_i its assignment time.

For each worker g and step k , define the active set

$$\mathcal{A}_g(k) = \{i \in \mathcal{I} : g(i) = g, x_i \leq k < x_i + o_i\},$$

i.e., the set of requests that are currently being processed on worker g at time k . The instantaneous workload of worker g at time k is then

$$L_g(k) = \sum_{i \in \mathcal{A}_g(k)} w_i^{(k-x_i+1)}. \quad (1)$$

We denote by

$$L_{g^*}(k) = \max_{g \in [G]} L_g(k)$$

the maximum workload across all workers at time k .

Imbalance and objective.

In many parallel systems, including data-parallel LLM decoding, the processing time of a step on a worker is linear in its workload, and all workers must wait for the slowest worker at each step (a barrier). Thus, the *idle* work at step k —the total amount of work that other workers could have done if they were as heavily loaded as the busiest worker—is proportional to

$$\text{Imbalance}(k; \pi) = \sum_{g=1}^G (L_{g^*}(k) - L_g(k)) = G \cdot L_{g^*}(k) - \sum_{g=1}^G L_g(k), \quad (2)$$

where we make the dependence on the policy π explicit. Over a finite horizon $\{1, \dots, K\}$, we define the *average imbalance* of a policy π as

$$\text{AvgImbalance}(\pi) = \frac{1}{K} \sum_{k=1}^K \text{Imbalance}(k; \pi).$$

Our goal is to design an assignment policy π that makes $\text{AvgImbalance}(\pi)$ as small as possible. Intuitively, this corresponds to maximizing the amount of “useful” work performed each step and minimizing the total idle time induced by waiting for the slowest worker at the barrier.

4 Method: A Universal Load Balance Principle

In the fully agnostic model of Section 3, where the scheduler has no information about W_i beyond arrivals and completions, no policy can differentiate between two requests with the same arrival time if their future workloads are indistinguishable. In practice, however, many systems expose *partial* information about the near future. Our goal in this section is to formalize a minimal and broadly feasible form of such information, and then to develop a load-balancing principle that uses it in a disciplined way.

Short lookahead workload information.

We introduce a short lookahead window of length $H \in \mathbb{N}$ and assume that, at each step k , the scheduler may observe for every active request i an estimate of its contributions to future workloads over the next H steps *after* the current one. Formally, let

$$\widehat{W}_i^H(k) = (\widehat{w}_i^{(1)}(k), \widehat{w}_i^{(2)}(k), \dots, \widehat{w}_i^{(H)}(k))$$

denote any prediction of the workloads that request i will contribute in its next H processing steps, i.e., at times $k+1, \dots, k+H$, conditional on the information available at time k . When i finishes before H further steps, we interpret the remaining entries as zeros. The special case $H = 0$ corresponds to having *no* lookahead beyond the current step: the scheduler only knows the current workloads $\{L_g(k)\}$ and has no predictive signal about $k+1, k+2, \dots$

This interface captures situations where the total workload of a job is hard to predict at arrival, but its *short-term* behavior is easier to infer once the job has progressed. In LLM serving, for example, the total number of decode steps for a request is difficult to predict accurately from the prompt alone, yet once a response is near completion (e.g., exhibits “in conclusion”, closing punctuation, or termination tokens), it becomes much easier to estimate whether the request will complete within the next H steps. In the LLM serving setting, the per-step workload is driven by the KV cache, which grows by one token per decode step until termination, so $\widehat{W}_i^H(k)$ effectively reduces to a prediction of *whether* and *when* a request will finish within the lookahead window. As another example, consider a multi-stage document-processing pipeline where early stages have highly variable runtimes, but once a document reaches the final stage, sensors or partial results reveal that only a short, nearly deterministic

tail of work remains; here, $\widehat{W}_i^H(k)$ summarizes this remaining tail, even if the total processing time from arrival was unpredictable.

The universal Balance Future with Integer Optimization principle (BF-IO).

Given access to short lookahead workload information, we now state our universal load-balancing principle. At a high level, the scheduler should choose assignments that make the *future* workloads across workers as balanced as possible, rather than greedily equalizing only the current step. To make this precise, fix a window length $H \geq 0$ and consider step k . Let $R_{\text{wait}}(k)$ be the set of waiting requests, and let $\text{cap}[g](k)$ be the number of free slots on worker g at that time. An *allocation* at step k consists of disjoint subsets $\{S_g(k)\}_{g \in [G]}$ of $R_{\text{wait}}(k)$, with

$$S_g(k) \subseteq R_{\text{wait}}(k), \quad S_g(k) \cap S_{g'}(k) = \emptyset \text{ for } g \neq g', \quad |S_g(k)| \leq \text{cap}[g](k) \text{ for all } g.$$

We write

$$S(k) = \bigcup_{g \in [G]} S_g(k)$$

for the set of all requests admitted at step k . For any such allocation $S(k)$, the induced per-worker sets $\{S_g(k)\}$ determine an updated active set $\{\mathcal{A}_g(k)\}$ and hence a predicted load trajectory over the next H steps, using the profile estimates $\{\widehat{W}_i^H(k)\}$ for all active and newly admitted jobs.

Let $L_g(k)$ denote the current workload on worker g at time k and $L_g(k+h)$ the *predicted* workload at time $k+h$ under allocation $S(k)$ for $h \geq 1$, and let $\text{Imbalance}(k+h)$ be the corresponding imbalance as in Equation (2). The Balance–Future principle is then to choose, at each step k , an allocation $S(k)$ that minimizes the *accumulated predicted imbalance* over the window:

$$J(S(k)) = \sum_{h=0}^H \text{Imbalance}(k+h),$$

where $h=0$ uses the current workloads and $h \geq 1$ uses the predicted workloads based on $\{\widehat{W}_i^H(k)\}$.

This minimization can be achieved via an integer optimization. Introduce binary decision variables $x_{ig} \in \{0, 1\}$ indicating whether request $i \in R_{\text{wait}}(k)$ is assigned to worker g at step k , and define

$$S_g(k; x) := \{i \in R_{\text{wait}}(k) : x_{ig} = 1\}, \quad S(k; x) := \bigcup_{g \in [G]} S_g(k; x),$$

so that $S(k; x)$ is the admitted set induced by the assignment matrix $x = \{x_{ig}\}$. We write $J_k(x) := J(S(k; x))$ for the accumulated predicted imbalance cost at step k . Let

$$U(k) := \min \left\{ |R_{\text{wait}}(k)|, \sum_{g=1}^G \text{cap}[g](k) \right\}$$

denote the number of slots that can be filled at step k (either all waiting requests, or all free capacity, whichever is smaller). Then the optimal minimization choice at step k is the solution of the following integer optimization:

$$\begin{aligned}
\min_{\{x_{ig}\}} \quad & J_k(x) = J(S(k; x)) \\
\text{s.t.} \quad & \sum_{g=1}^G x_{ig} \leq 1, \quad \forall i \in R_{\text{wait}}(k) \quad (\text{each request assigned to at most one worker}), \\
& \sum_{i \in R_{\text{wait}}(k)} x_{ig} \leq \text{cap}[g](k), \quad \forall g \in [G] \quad (\text{per-worker capacity constraints}), \\
& \sum_{g=1}^G \sum_{i \in R_{\text{wait}}(k)} x_{ig} = U(k), \quad (\text{full utilization of available slots or waiting requests}), \\
& x_{ig} \in \{0, 1\}, \quad \forall i \in R_{\text{wait}}(k), \forall g \in [G].
\end{aligned} \tag{IO}$$

An optimal solution x^* to (IO) yields the selected allocation $\{S_g^*(k)\}_{g \in [G]}$ with

$$S_g^*(k) := S_g(k; x^*) = \{i \in R_{\text{wait}}(k) : x_{ig}^* = 1\}.$$

In words, at each step BF-IO solves an integer optimization that simultaneously assigns requests to workers and minimizes a finite-horizon prediction of future imbalance.

We capture this procedure in the following step-wise pseudocode. Conceptually, the “inner loop” that enumerates feasible allocations and chooses the one minimizing J corresponds exactly to solving the integer optimization (IO).

Although BF-IO (Algorithm 1) is not globally optimal over the entire time horizon $\{0, \dots, K\}$, it explicitly balances across the *near future* rather than acting myopically. When $H = 0$, the window collapses to the current step and $J(S(k))$ reduces to $\text{Imbalance}(k)$; the algorithm selects the assignment that best equalizes the *next* workloads $\{L_g(k)\}$, using no lookahead beyond the current step. Larger H allows the scheduler to anticipate near-term completions and avoid assignments that look good now but create pronounced imbalance a few steps later.

Intuition and choice of window length H .

The Balance–Future principle can be understood as a compromise between two extremes. When H is very small (e.g., $H = 0$), the scheduler only equalizes the current-step workloads; this is cheap and prediction-free but can be short-sighted, because it ignores imminent completions that would quickly relieve heavy workers or jobs that are about to enter the system. At the other extreme, taking H very large is also undesirable: the algorithm optimizes the effect of current assignments over a long window *without* knowing future arrivals or the future assignment decisions that will be made within that window, so its predictions become increasingly speculative and dominated by unmodeled randomness. In practice, a moderate window H —large enough to see a few steps of meaningful tail behavior, but small enough that predictions remain informative and computational costs stay low—strikes the right balance (See Figure 4).

Algorithm 1: Balance–Future Algorithm (BF-IO)

Input: Waiting set $R_{\text{wait}}(k)$, active sets $\{\mathcal{A}_g(k)\}$, free slots $\{\text{cap}[g](k)\}$, lookahead window length H

Output: Assignments $\{S_g(k)\}_{g \in [G]}$ at step k

Compute the number of admissible assignments:

$$U(k) \leftarrow \min \left\{ |R_{\text{wait}}(k)|, \sum_g \text{cap}[g](k) \right\};$$

Enumerate all feasible allocations $\{S_g(k)\}$ with $S_g(k) \subseteq R_{\text{wait}}(k)$, $|S_g(k)| \leq \text{cap}[g](k)$ for all g , $S_g(k) \cap S_{g'}(k) = \emptyset$ for $g \neq g'$, and $|\bigcup_g S_g(k)| = U(k)$;

for each feasible allocation $\{S_g(k)\}$ **do**

Form $S(k) \leftarrow \bigcup_{g \in [G]} S_g(k)$;

Simulate the predicted load trajectory $\{L_g(k+h)\}_{h=0}^H$ for this allocation using $\{\widehat{W}_i^H(k)\}$;

Compute the imbalance cost

$$J(S(k)) = \sum_{h=0}^H \text{Imbalance}(k+h);$$

Select an allocation $\{S_g^*(k)\}$ that minimizes $J(S(k))$ (equivalently, solves the integer optimization (IO));

Assign requests according to $\{S_g^*(k)\}$;

Our theory in Section 5 shows that even the purely myopic case $H = 0$ already yields strong worst-case gains over FCFS-type policies, and our experiments in Section 6 confirm that modest $H > 0$ can further improve performance when realistic predictive signals are available.

5 Theoretical Guarantee of the Load Balance Principle in LLM Inference

In Section 4, we introduced the Balance–Future (BF-IO) as a universal principle for load balancing under sticky assignments and barrier synchronization. In this section, we provide theoretical guarantee for its effectiveness by analyzing its performance in the LLM decode serving setting and then discussing extensions to more general workload patterns. Our primary focus is the data-parallel (DP) decoding bottleneck in LLM serving: we show that, under a realistic overloaded regime and for any adversarial arrival instance, BF-IO achieves significantly smaller imbalance than the baseline First-Come-First-Serve (FCFS) policy used in many real systems. A detailed description of the baseline FCFS policy can be found in Appendix B. We then outline how the

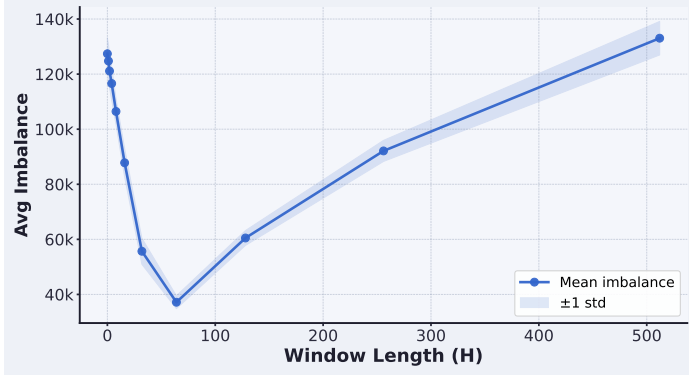


Fig. 4: Intuition for selecting the window length H , evaluated across values from 0 to 500. This analysis uses an implementation of the Algorithm BF-IO in the LLM serving context. Further implementation and experimental details are provided in Sections 6.

analysis framework extends beyond LLM serving to a broader family of load balancing problems.

LLM serving-specific workload model.

We specialize the general model of Section 3 to the DP decode stage of LLM serving. Recall that G denotes the number of computational workers (e.g., GPUs) and B the maximum batch size (number of requests that can be processed simultaneously on a single worker). We assume that $\sqrt{G} = \tilde{o}(B)$, which is an extremely mild assumption in practice: typical batch sizes are $B \in [64, 128]$, whereas the number of workers G is at most in the hundreds in real deployments.

As in Section 3, each request i is represented by a *workload profile*

$$W_i = (w_i^{(1)}, w_i^{(2)}, \dots, w_i^{(o_i)}),$$

where $o_i \in \mathbb{N}$ is the total number of processing steps for request i , and $w_i^{(j)} \geq 0$ denotes the workload contributed by i in its j -th processing step. In the LLM setting, the initial workload $w_i^{(1)}$ corresponds to the prefill size, which we denote by s_i . We assume that the prefill lengths $\{s_i\}$ are i.i.d. draws from an unknown bounded distribution $\mathcal{D}_{\text{prefill}}$ supported on $\{1, \dots, s_{\max}\}$, and let σ_s be the standard deviation of $\mathcal{D}_{\text{prefill}}$. We impose a non-degeneracy condition: there exists $\kappa_0 \in (0, \frac{1}{2}]$ such that

$$\kappa_0 \leq \frac{\sigma_s}{s_{\max}} \leq \frac{1}{2}.$$

The upper bound follows from Popoviciu's inequality, which implies $\sigma_s/s_{\max} \leq 1/2$ for any distribution supported on an interval of length s_{\max} . The lower bound $\kappa_0 > 0$ simply rules out pathological cases where almost all prompts have essentially identical prefill length.

After prefill, LLM decoding proceeds token by token. Once request i starts decoding, it occupies exactly $o_i - 1$ consecutive decode steps and its k -th decode step ($k \in [o_i - 1]$) requires workload $s_i + k$, reflecting the growth of its KV cache. We assume that the decode lengths $\{o_i\}$ are i.i.d. draws from an unknown distribution $\mathcal{D}_{\text{decode}}$ on $\{1, 2, \dots\}$. Thus the full workload profile of request i takes the form

$$W_i = (s_i, s_i + 1, \dots, s_i + o_i - 1).$$

Overloaded arrival instances.

We now formalize the overloaded regime, which is the relevant regime for LLM serving: if the system were lightly loaded, all requests could be processed immediately without sophisticated scheduling. Intuitively, an arrival instance is overloaded if, at every step, there are “many more” pending requests than free slots. Moreover, we assume that no single prefill-length class dominates the pool. The latter condition reflects the empirical fact that real workloads contain a variety of prompt lengths rather than being concentrated on a single fixed prefill size.

Formally, at each step k , let \mathcal{I}_k denote the set of requests that are pending in the waiting pool, and let

$$\mathcal{R}_k = \{(s_i, o_i) : i \in \mathcal{I}_k\}$$

denote the multiset of their prefill and decode lengths. For $\ell \in \{1, \dots, s_{\max}\}$, define the length class

$$\mathcal{R}_k(\ell) := \{i \in \mathcal{I}_k : s_i = \ell\}.$$

Let $C_k = \sum_{g=1}^G c_g(k)$ denote the total number of free slots at step k , where $c_g(k)$ is the number of available batch slots on worker g .

Definition 1 (Overloaded arrival instance family \mathcal{I}) An arrival instance I is called *overloaded* if, for every step k ,

$$\min_{\ell \in \{1, \dots, s_{\max}\}} (|\mathcal{R}_k \setminus \mathcal{R}_k(\ell)|) \geq C_k.$$

Let \mathcal{I} denote the family of all overloaded arrival instances.

In words, even after removing all requests belonging to whichever single prefill-length class is most numerous at step k , the remaining pool still contains at least C_k requests and can therefore fill all free slots freed in step k . This condition is typically satisfied in heavily loaded real systems: prompt lengths exhibit substantial diversity, and the number of pending requests is far larger than the instantaneous capacity.

Specialization of BF-IO to $H = 0$.

As discussed in Section 4, BF-IO can, in principle, use a short lookahead window of length $H \geq 0$. From an analytical perspective, however, rigorous control of the dynamics for $H \geq 1$ is extremely involved, because current assignments interact with future arrivals and future decisions within the window. In this section we therefore focus on the case $H = 0$, where BF-IO reduces to selecting, at each step, the assignment that minimizes the *current-step* imbalance. As we will show, even this purely myopic

variant achieves substantial improvement over FCFS in the LLM decode model. This is fantastic since we demonstrate that modest $H > 0$ yields further gains when realistic predictive signals are available in Section 4.

Imbalance improvement ratio (IIR).

We compare BF-IO and FCFS via an *imbalance improvement ratio*, which measures, in the worst arrival instance, the long-run factor by which BF-IO reduces average imbalance relative to FCFS. For a given arrival instance $I \in \mathcal{I}$ and policy $\pi \in \{\text{BF-IO}, \text{FCFS}\}$, let $\text{AvgImbalance}(\pi; I)$ denote the time-average imbalance defined in Section 3. We define

$$\mathbf{IIR} = \inf_{I \in \mathcal{I}} \left(\lim_{K \rightarrow \infty} \frac{\mathbb{E}[\text{AvgImbalance}(\text{FCFS}; I)]}{\mathbb{E}[\text{AvgImbalance}(\text{BF-IO}; I)]} \right),$$

where the expectation is taken over the randomness in the prefill and decode lengths (s_i, o_i) drawn from $\mathcal{D}_{\text{prefill}}$ and $\mathcal{D}_{\text{decode}}$. The arrival sequence I itself is chosen adversarially from \mathcal{I} ; in particular, the adversary can choose any number of arrivals at each step, subject only to the overloaded condition. Larger values of **IIR** correspond to larger worst-case improvements of BF-IO over FCFS.

Directly lower bounding **IIR** in full generality is challenging. To build intuition, we first study a warm-up setting in which all decode lengths are homogeneous: $o_i = o$ for every request i . In this case, the dynamics simplify substantially: once GB jobs are admitted, they run in perfect lockstep for o decode steps and then all complete simultaneously. Under the overloaded condition (so that every worker runs at full batch capacity), the per-step imbalance within a round of o steps is constant; optimizing long-run average imbalance reduces to optimizing the imbalance right after each batch admission.

Theorem 1 (Warm-up: Homogeneous decode lengths) *Consider the homogeneous-decode model $o_i = o$ for all requests i . There exists a universal constant $c > 0$ such that*

$$\mathbf{IIR} \geq c \kappa_0 \sqrt{B \log G} \cdot \frac{G}{G-1} = \Omega(\sqrt{B \log G}). \quad (3)$$

Proof intuition: In the homogeneous-output setting, each admission round is structurally simple: once GB jobs are admitted, they run in perfect lockstep for o token steps and then all finish simultaneously. As a result, all steps in the round share the same inter-device imbalance, and minimizing the long-run time-average imbalance is equivalent to minimizing the imbalance *immediately after admission* in each round.

On the BF-IO side, this reduction means that BF-IO is effectively solving a static bin-packing problem in every round: partition the GB prompt lengths into G groups of size B to minimize the maximum per-device load. A simple exchange argument shows that any such optimal assignment must be s_{\max} -balanced: the difference between the heaviest and lightest devices can never exceed s_{\max} . This immediately implies that the expected BF-IO imbalance per round is at most $(G-1)s_{\max}$, independent of the detailed shape of the prefill-length distribution.

On the FCFS side, the story is almost the opposite. Under size-agnostic FCFS admission and an overloaded pool, each device simply sees B i.i.d. prompt lengths.

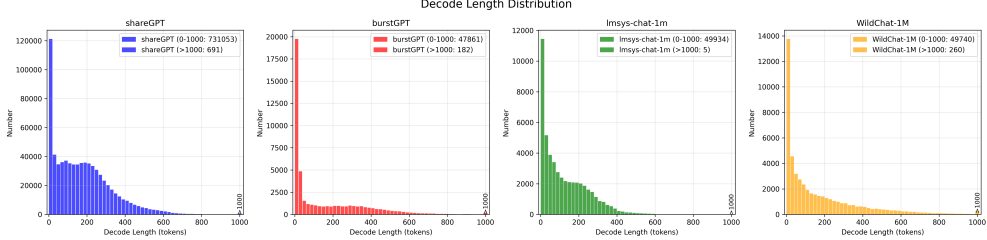


Fig. 5: Empirical distributions of decode lengths from production LLM traces [30–33]. Decode lengths exhibit the geometric (discrete-exponential) pattern.

The per-device loads $S_g = \sum_{j=1}^B s_{g,j}$ are thus i.i.d. with variance $\sigma_s^2 B$. For large B , the central limit theorem (and a Berry–Esseen bound) shows that S_g behaves approximately Gaussian. Taking the maximum over G such devices amplifies these fluctuations: with constant probability, at least one device deviates above the mean by order $\sigma_s \sqrt{B \log G}$. This produces an expected FCFS imbalance of order $G \sigma_s \sqrt{B \log G}$, while BF-IO keeps the imbalance of order $(G - 1)s_{\max}$. The non-degeneracy condition $\sigma_s/s_{\max} \geq \kappa_0 > 0$ then yields an imbalance-reduction factor of order $\sqrt{B \log G}$, uniformly over all overloaded arrival instances. The complete proof is deferred to Appendix C.1. \square

Inhomogeneous setting.

The homogeneous-decode assumption $o_i = o$ in Theorem 1 serves as a warm-up: it is analytically convenient but clearly unrealistic for LLM inference, whose responses exhibit substantial variability in length. Empirical studies in Fig 5 on both open-source ([30–33]) and production traces show that decode lengths typically follow a heavy right-skewed pattern well approximated by a geometric (or discrete exponential) distribution: most responses terminate quickly, while a non-negligible tail runs for many tokens. Motivated by this evidence, we now consider an inhomogeneous setting in which decode lengths are random and independent across requests. Specifically, we assume

$$o_i \sim \mathcal{D}_{\text{decode}} = \text{Geo}(p) \quad \text{i.i.d. for each request } i,$$

for some $p \in (0, 1)$, so that the mean and variance of o_i are $1/p$ and $(1 - p)/p^2$, respectively. Under this more realistic decode model, the next theorem shows that BF-IO still achieves a worst-case imbalance improvement factor of order $\Omega(\sqrt{B \log G})$, with an explicit dependence on both the prefill and decode variability.

Theorem 2 (Inhomogeneous decode lengths) *Consider the inhomogeneous-decode model in which $o_i \sim \text{Geo}(p)$ i.i.d. for each request i with some $p \in (0, 1)$. Then, there exists a universal constant $c > 0$ such that*

$$\mathbf{IIR} \geq c \frac{p}{s_{\max}} \sqrt{\sigma_s^2 + \frac{1-p}{p^2}} \frac{G}{G-1} \sqrt{B \log G} = \Omega(\sqrt{B \log G}). \quad (4)$$

Proof intuition

Under geometric output lengths with unit per-step growth, the stochastic dynamics of loads under FCFS and BF-IO differ sharply. On the FCFS side, each slot behaves as a simple renewal process: its size increases deterministically by one each step until a geometric completion occurs, at which point it resets to a fresh prompt length S . In stationarity, a snapshot of a slot therefore looks like

$$(\text{prompt}) \ S + (\text{age}) \ A,$$

where S has variance σ_s^2 and A is geometric with mean $(1-p)/p$ and variance $(1-p)/p^2$, independent of S . This yields a per-slot “snapshot” variance

$$\sigma_{\text{snap}}^2 = \sigma_s^2 + \frac{1-p}{p^2}.$$

Aggregating B i.i.d. slots on each device gives per-device loads with variance $\sigma_{\text{snap}}^2 B$, and comparing G such independent devices, standard Gaussian extreme-value theory shows that *at least one* device sits of order $\sigma_{\text{snap}} \sqrt{B \log G}$ above the mean with constant probability. This creates a typical FCFS imbalance of order $G \sigma_{\text{snap}} \sqrt{B \log G}$.

On the BF-IO side, the analysis from Part 1 shows that, despite the asynchronous completions, the myopic balancing rule enforces a contraction of the inter-device gap: in each step, pre-admission loads shrink by a factor roughly $(1-p)$, and the subsequent assignment step of BF-IO prevents the gap from growing by more than s_{\max} , up to small error events. Over time, this yields a steady-state average gap of order s_{\max}/p , independent of (B, G) up to lower-order terms. Since instantaneous imbalance is at most $(G-1)$ times the gap, the long-run average imbalance under BF-IO is at most $(G-1)s_{\max}/p$, while FCFS incurs imbalance of order $G\sigma_{\text{snap}} \sqrt{B \log G}$. The resulting imbalance-reduction ratio is therefore of order

$$\frac{G \sigma_{\text{snap}} \sqrt{B \log G}}{(G-1) s_{\max}/p} \asymp \frac{p \sigma_{\text{snap}}}{s_{\max}} \sqrt{B \log G},$$

matching the homogeneous-output case in $\sqrt{B \log G}$ scaling, but with the snapshot variance σ_{snap}^2 capturing the additional variability introduced by geometric completion times. The complete proof can be found in Appendix C.2.

5.1 Theoretical Guarantee of BF-IO in General Cases

The LLM-specific analysis above exploits a particular structure of the workload profiles,

$$W_i = (s_i, s_i + 1, \dots, s_i + o_i - 1),$$

where each alive request gains one unit of KV load per decode step. This captures current DP decoding architectures, but many other load-balancing problems do *not* obey this linear drift. A classical example is the constant-workload setting, where each

job has a fixed processing requirement per step and

$$W_i = (s_i, s_i, \dots, s_i) \quad (o_i \text{ copies of } s_i),$$

which arises naturally in traditional CPU or manufacturing workloads. Even within LLM serving, future systems may reduce or compress KV usage dynamically so that per-step cost does not grow exactly by $+1$; instead, every alive request may experience a common but time-varying increment that reflects changes in the underlying architecture or memory-management policy.

To encompass these scenarios, we consider a more general class of *non-decreasing workload drift* models. We retain the prefill and decode assumptions from the inhomogeneous LLM model—namely, s_i drawn from a bounded prefill distribution with variance σ_s^2 and decode lengths $o_i \sim \text{Geo}(p)$ i.i.d. for some $p \in (0, 1)$ —but relax the per-step growth pattern as follows.

Definition 2 (Non-decreasing Workload Drift) There exists a deterministic sequence $(\delta_k)_{k \geq 1}$ with

$$0 \leq \delta_k \leq \delta_{\max} \quad \text{for all } k \geq 1,$$

where δ_{\max} is a non-negative constant independent of (B, G) , such that for every request i ,

$$w_i^{(1)} = s_i, \quad w_i^{(j)} = s_i + \sum_{t=1}^{j-1} \delta_t, \quad j = 2, \dots, o_i.$$

In words, all alive requests share the same nonnegative increment δ_k at global step k ; workloads are non-decreasing over time and their per-step growth is uniformly bounded. The LLM decode model with linear KV growth corresponds to the special case $\delta_k \equiv 1$ for all k , while the constant-workload model corresponds to $\delta_k \equiv 0$. More sophisticated architectures, in which per-step KV work is throttled or sparsified over time, are captured by intermediate patterns with $0 < \delta_k < 1$ or time-varying δ_k . The following theorem shows that BF-IO continues to enjoy a *worst-case* imbalance improvement factor of order $\sqrt{B \log G}$ relative to FCFS in this more general setting.

Theorem 3 (General non-decreasing workload drift) *Consider the inhomogeneous-decode model in which $o_i \sim \text{Geo}(p)$ i.i.d. for each request i with some $p \in (0, 1)$, and assume the non-decreasing drift structure in Definition 2. Then there exists a universal constant $c > 0$, depending only on $(\sigma_s^2, p, \delta_{\max}, s_{\max})$, such that*

$$\mathbf{IIR} = \inf_{\mathcal{I}} \frac{\text{AvgImbalance}(\text{FCFS}; \mathcal{I})}{\text{AvgImbalance}(\text{BF-IO}; \mathcal{I})} \geq c \frac{p \sigma_s}{s_{\max}} \frac{G}{G-1} \sqrt{B \log G} = \Omega(\sqrt{B \log G}). \quad (5)$$

Proof intuition: Compared with the “ $+1$ per step” case, the core structure of the BF-IO analysis remains unchanged: the gap contraction still comes entirely from completions, not from the deterministic per-step growth. When every survivor gains a common increment δ_k at step k , each device’s load is shifted by exactly $B\delta_k$, so the inter-device gap $D(k-1)$ is unaffected by this drift; only the random removals from

completions change the spread. As a result, the separation lemma (which enforces $D(k) \lesssim A^{\text{Pre}}(k) - Bp$ on good completion-count events) still holds since it depends only on prompt sizes and binomial completions, not on the specific value of δ_k . The main technical adjustments are (i) in the concentration lemma, where the per-slot summands are now bounded by $\Lambda(k) + \delta_{\max}$ instead of $\Lambda(k)$, so the Bernstein bound is applied with a slightly larger envelope, and (ii) in the envelope/age accounting, where we use that an alive job of age r has size at most $s_{\max} + \delta_{\max}r$, so the excess $\Lambda(k) - s_{\max}$ is controlled by δ_{\max} times the maximum age. The geometric tail of the output length then yields the same exponential decay in age (up to constants depending on δ_{\max}), and hence the same $O(s_{\max}/p)$ bound on the long-run average gap as in the +1 case. In other words, as long as the per-step increments are common across jobs and uniformly bounded, the contraction mechanism and the averaging argument that underpin the BF-IO upper bound survive unchanged; only the constants in the concentration and tail estimates are rescaled by δ_{\max} .

In the constant +1 model, the slot-level process under FCFS is a homogeneous Markov chain that admits a clean stationary representation: at any snapshot, each slot contains “prompt + geometric age”, and the age has variance $(1-p)/p^2$. With a time-varying drift sequence (δ_k) , the chain for $Y_{g,b}(k)$ becomes non-homogeneous, but the key stochastic structure survives: completions still occur as i.i.d. $\text{Bernoulli}(p)$ trials, independent of job sizes and of the drift. This means that at any step k , the prompt length of the current job in a slot is still an independent copy of S , and the number of drift steps it has accumulated—its age—still has geometric tails with parameter p , regardless of the past. The per-slot snapshot can therefore be written as

$$(\text{prompt}) + (\text{sum of the last } A_k \text{ drifts}),$$

where A_k has uniformly bounded moments and δ_k is uniformly bounded. This immediately implies that the per-slot variance is uniformly bounded below by σ_s^2 (from the prompt) and the third moment is uniformly bounded above, independent of time. Summing B such independent snapshots on each device yields loads with variance of order B , and a Berry–Esseen bound (in its non-identical version) shows that each device’s load fluctuates on the \sqrt{B} scale and is close to Gaussian. Taking the maximum over G devices then produces an excess of order $\sqrt{B \log G}$ above the average device load, with constant probability, exactly as in the homogeneous case. Thus, even though the per-slot chain is no longer time-homogeneous and lacks a simple stationary law, the bounded and common per-step drift leaves the *order* of the FCFS imbalance unchanged: its expected size remains $\Theta(G\sqrt{B \log G})$. This concludes that the imbalance-reduction factor is at least on the order of $\sqrt{B \log G}$. The complete proof can be found in Appendix C.3. \square

6 Experiments

We implement a numerical simulation framework to evaluate different scheduling strategies for GPU-based request processing. This section describes the experimental setup, evaluation metrics and numerical result of different routing strategies.

6.1 Request Generation

To simulate realistic LLM inference workloads, we use request traces from the BurstGPT dataset [34]. Each request is characterized by a triplet (s_i, o_i) , where s_i denotes the prompt (input) length, o_i the actual output length.

Dataset.

The BurstGPT dataset captures production-level LLM serving patterns, including the heavy-tailed distribution of output lengths commonly observed in real deployments. We extract the `input_tokens` and `output_tokens` fields from the dataset to construct our simulation workload. This approach ensures that our experiments reflect realistic request characteristics, such as the variability and correlation structure present in actual user queries.

6.2 Simulation Environment

The router simulator models an online setting with G GPU workers, each supporting up to B concurrent requests (batch size). Key components include:

- **Undiscovered queue:** Requests not yet revealed to the router.
- **Wait queue:** Candidate requests available for routing decisions.
- **Active sets \mathcal{A}_g :** Requests currently executing on GPU g .
- **Load tracking L_g :** Total token load on GPU g , defined in Equation (1).

Time Progression Model.

Each simulation step advances time by:

$$\Delta t = C + t_\ell \cdot \max_{g \in [G]} L_g \quad (6)$$

where C is a fixed overhead constant and t_ℓ is the per-token generation latency. During each step, all active requests generate one token. A request i completes when $\tau_i \geq o_i$.

Online Revelation.

The simulator maintains a revelation target R ; whenever $|\text{wait_q}| < R$, additional requests are revealed from the undiscovered queue. This models realistic online arrival patterns. The default configuration of our experiment is $G = 32$ GPUs, $B = 72$ batch size, $R = 128$ revelation target.

Routing Strategies.

We evaluate four scheduling policies: (i) FCFS, (ii) Join-Shortest-Queue (JSQ), (iii) BF-IO ($H = 0$), (iv) BF-IO ($H = 20$)

6.3 Evaluation Metrics

We evaluate routing performance using four metrics. Let G denote the number of GPUs, $\mathcal{A}_g^{(k)}$ the active requests on GPU g at step k , and $L_g(k) = \sum_{i \in \mathcal{A}_g^{(k)}} w_i^{(k-x_i+1)}$

the instantaneous workload on worker g , where $w_i^{(j)}$ is the workload contributed by request i in its j -th processing step.

Average Imbalance.

Following the theoretical framework, we adopt the average imbalance as the primary metric. At each step k , the instantaneous imbalance is defined as:

$$\text{AvgImbalance} = \frac{1}{K} \sum_{k=1}^K \text{Imbalance}(k) \quad (7)$$

In addition to the theoretically motivated imbalance metric, we evaluate two metrics that directly reflect real-world LLM inference efficiency:

Throughput.

Throughput measures the token processing rate (tokens/second):

$$\text{Throughput} = \frac{\sum_{k=1}^K |\mathcal{A}^{(k)}|}{\sum_{k=1}^K \Delta t^{(k)}} \quad (8)$$

where $\mathcal{A}^{(k)} = \bigcup_g \mathcal{A}_g^{(k)}$ denotes all active requests at step k , and $\Delta t^{(k)} = C + t_\ell \cdot \max_g L_g(k)$ is the wall-clock duration of step k . Since step duration is governed by the maximum load across workers, reducing imbalance directly increases throughput.

Time Per Output Token (TPOT).

TPOT captures per-request latency as perceived by users:

$$\text{TPOT} = \frac{1}{N} \sum_{i=1}^N \frac{t_i^{\text{finish}} - t_i^{\text{start}}}{o_i} \quad (9)$$

where t_i^{start} and t_i^{finish} are the start and completion times of request i , and o_i is its output length. Requests assigned to heavily loaded GPUs experience longer per-step durations due to the barrier synchronization, resulting in higher TPOT. This metric is widely used in production LLM serving systems to measure user-facing latency.

Energy Consumption.

We measure total energy consumption (in Joules) as the time integral of instantaneous GPU power:

$$E = \int_0^T P(\text{mfu}(t)) dt \quad (10)$$

where $\text{mfu}(t)$ denotes the Model FLOPs Utilization (mfu) at time t —the ratio of observed computational throughput to the GPU’s theoretical peak FLOPs capacity.

Therefore, the instant mfu at time t is positively related to the instant throughput at t . [21] validates instantaneous power is a sublinear function of utilization:

$$P(\text{mfu}) = P_{\text{idle}} + (P_{\text{max}} - P_{\text{idle}}) \cdot \left(\frac{\text{mfu}}{\text{mfu}_{\text{sat}}} \right)^{\gamma} \quad (11)$$

with idle power $P_{\text{idle}} = 100\text{W}$, peak power $P_{\text{max}} = 400\text{W}$, saturation threshold $\text{mfu}_{\text{sat}} = 0.45$, and scaling exponent $\gamma = 0.7$. The sublinear exponent $\gamma < 1$ captures a critical inefficiency: GPUs draw substantial power even at low utilization. Under barrier synchronization, workers waiting at the barrier operate near P_{idle} while contributing zero throughput; reducing imbalance converts this idle power draw into useful token generation, directly improving energy efficiency. Details of MFU computation and parameter calibration are provided in Appendix D.

6.4 Results

Load Trajectory Analysis.

Figure 6 visualizes the per-worker token load trajectories over approximately 4000 decode steps for four scheduling strategies on a 16-GPU configuration. Each colored line represents the total token load $L_g(k)$ on a single worker across time.

The results reveal stark differences in load balancing effectiveness:

- FCFS maintains a persistent load gap of approximately 40k–50k tokens between the heaviest and lightest workers. This spread translates directly into barrier-induced idle time, as lightly loaded workers must wait for the straggler at each decode step.
- JSQ, despite being workload-aware, exhibits even worse imbalance than FCFS. This counterintuitive result aligns with the theoretical analysis: JSQ uses queue length (number of requests) as a proxy for workload, which poorly approximates actual token load when request sizes vary significantly. Heavy requests accumulate on certain workers, creating persistent stragglers.
- BF-IO ($H = 0$) dramatically reduces the load spread to approximately 5k–10k tokens. Even without lookahead information, myopically minimizing instantaneous imbalance at each assignment step yields substantial improvements over size-agnostic policies.
- BF-IO ($H = 20$) achieves the tightest load balance, with worker loads nearly indistinguishable throughout execution. The 80-step lookahead enables the scheduler to anticipate near-term completions and avoid assignments that would create transient imbalance.

Quantitative Metrics Comparison.

Table 1 summarizes the performance metrics across all evaluated strategies. We report average imbalance, throughput, and TPOT, each averaged over multiple simulation runs with different random seeds.

Table 1 summarizes the performance metrics across all evaluated strategies. We report average imbalance, throughput, TPOT, and energy consumption, each averaged over multiple simulation runs with different random seeds.

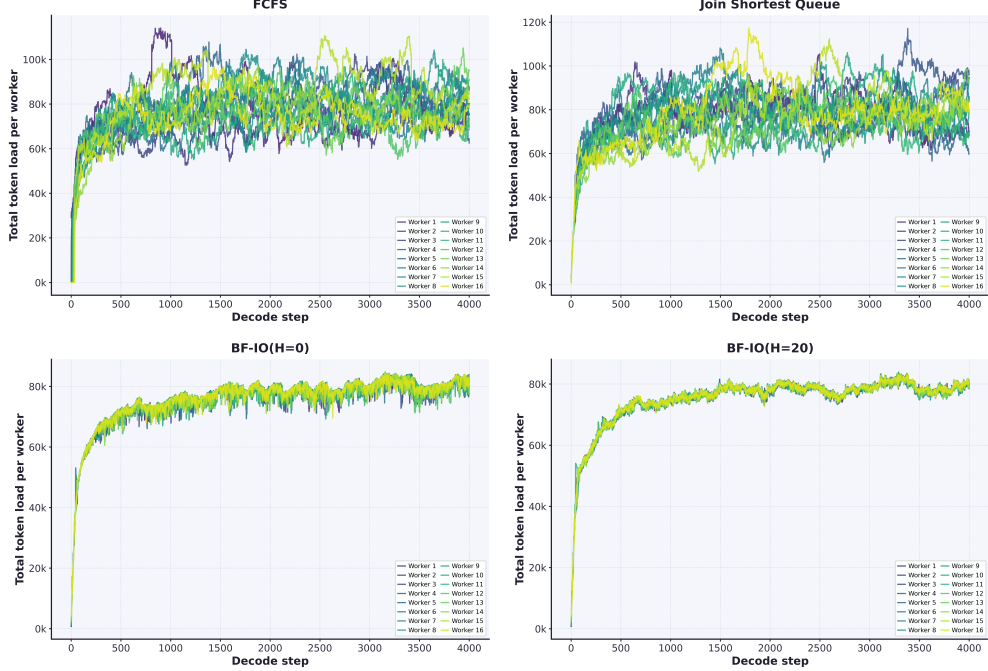


Fig. 6: Per-worker token load trajectories under four scheduling strategies. **Top-left:** FCFS exhibits persistent load spread between 60k–110k tokens, with substantial inter-worker variance throughout execution. **Top-right:** JSQ shows even greater imbalance, with peak loads exceeding 120k while other workers remain around 80k. **Bottom-left:** BF-IO ($H = 0$) achieves significantly tighter load clustering around 80k tokens. **Bottom-right:** BF-IO ($H = 20$) produces the most balanced distribution, with all workers maintaining nearly identical loads throughout the simulation.

The results in Table 1 demonstrate that BF-IO significantly outperforms baseline policies across all metrics. Compared to FCFS, BF-IO ($H = 20$) reduces average imbalance by $17\times$ (from 27.9 to 1.65), while improving throughput by 14% (from 8.00 to 9.13×10^4 tok/s) and reducing TPOT by 13% (from 1.42 to 1.25×10^{-2} s/tok). Additionally, BF-IO ($H = 20$) achieves a 3.3% reduction in energy consumption (from

Table 1: Performance comparison of scheduling strategies.

Strategy	Avg Imbalance \downarrow	Throughput \uparrow (10^4 tok/s)	TPOT \downarrow (10^{-2} s/tok) \downarrow	Energy \downarrow (kJ)
FCFS	27.9	8.00	1.42	396
JSQ	28.2	7.99	1.42	396
BF-IO ($H = 0$)	2.92	9.03	1.26	386
BF-IO ($H = 20$)	1.65	9.13	1.25	383

396 kJ to 383 kJ). FCFS and JSQ exhibit nearly identical performance across all metrics, confirming that both strategies are effectively size-agnostic and fail to exploit workload heterogeneity. The comparison between BF-IO ($H = 0$) and BF-IO ($H = 20$) shows that even without lookahead, workload-aware assignment achieves substantial gains; incorporating short-horizon prediction further reduces imbalance by 44% (from 2.92 to 1.65) and provides incremental improvements in throughput, latency, and energy efficiency.

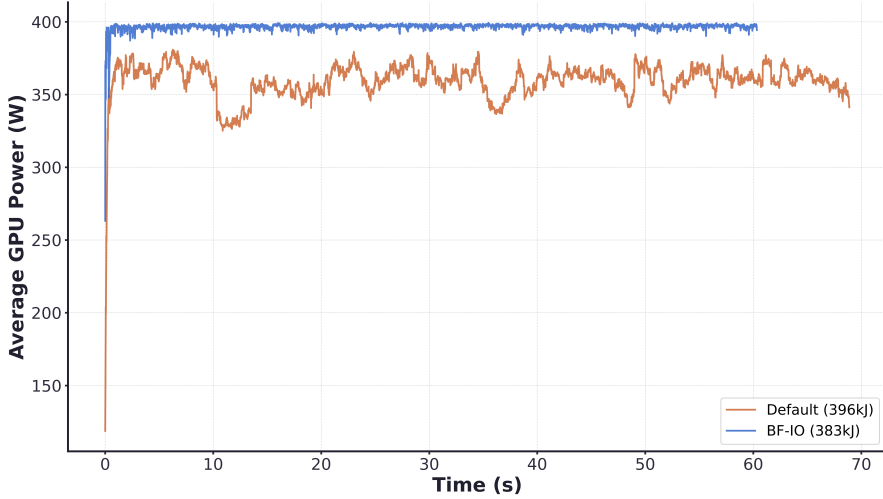


Fig. 7: Average GPU power consumption over time for FCFS and BF-IO ($H = 20$).

Figure 7 illustrates the average GPU power consumption over time for the FCFS and BF-IO ($H = 20$) scheduling strategies. The BF-IO strategy maintains a consistently high power draw around 395–400W throughout the experiment, whereas the Default strategy exhibits significant fluctuations between 330W and 380W.

Although BF-IO operates at higher instantaneous power levels, it achieves lower total energy consumption (383 kJ vs. 396 kJ). This counterintuitive result can be attributed to improved load balancing: BF-IO keeps all GPUs uniformly utilized, avoiding idle periods and reducing the overall execution time. In contrast, the power dips observed in the Default strategy indicate periods of underutilization caused by load imbalance across GPUs. These results demonstrate that better workload distribution not only improves throughput and latency but also leads to improved energy efficiency.

7 Discussion and Conclusion

7.1 Summary of contributions

This work develops a universal load-balancing principle for barrier-synchronized systems with sticky assignment decisions. We formalize the principle as BF-IO, which selects assignments by minimizing a short-horizon prediction of the imbalance metric

induced by the slowest worker via an integer optimization. We establish worst-case, scale-sensitive guarantees for BF-IO under adversarial arrivals in the LLM decode model and extend the analysis to a broader class of non-decreasing workload drift processes. On the empirical side, extensive numerical experiments on both public benchmarks and proprietary industrial traces demonstrate that BF-IO substantially reduces imbalance, improves throughput, and lowers energy consumption relative to widely deployed baselines.

7.2 Broader relevance beyond LLM serving

Although the LLM serving bottleneck motivates our study, the abstraction captured by BF-IO is broader: many scientific and engineering workloads evolve in discrete steps, include at least one synchronization point (explicitly or implicitly), and bind work to a device or process for efficiency reasons (data locality, memory residency, or stateful execution). Two representative examples illustrate how the short-lookahead philosophy transfers.

Large-scale linear algebra and matrix computation.

Many high-performance linear algebra kernels (e.g., blocked matrix factorizations, tiled matrix multiplication, and iterative solvers) execute as task graphs over sub-matrices/tiles. Even when per-kernel costs are relatively stable, effective completion times of “jobs” (usually several hours) are hard to predict far in advance due to cache effects, contention, and dependence constraints. Nevertheless, short lookahead information is often readily available from the runtime: tile-based systems maintain progress counters and DAG readiness queues, and a node can infer whether it will finish a set of outstanding tile tasks within the next few scheduling quanta by tracking (i) the number of remaining tiles on the critical path, (ii) the fraction of tiles already completed in the current panel/update phase, and (iii) convergence indicators for iterative methods (e.g., residual norms approaching tolerance). In such settings, BF-IO can be applied by treating each core/GPU as a worker, using short-horizon completion signals for currently running tasks, and routing or admitting new tasks to reduce load imbalance.

Adaptive multi-physics simulations with mesh refinement.

A second example arises in physics and geoscience simulations that use adaptive mesh refinement (AMR) or adaptive particle resolution [35, 36]. Here the per-step workload on each rank/accelerator can drift as refinement/coarsening changes the number of cells/particles and as localized physics kernels activate (e.g., shocks, phase boundaries, or localized forcing). Long-run workload is difficult to forecast because refinement decisions depend on evolving solution features, but near-term evolution is often predictable: refinement criteria are computed at regular intervals from local error indicators, gradients, or thresholded physical diagnostics, so it is feasible to estimate whether a region will remain refined (or be coarsened) over the next few time steps. Because time stepping typically includes synchronization (global reductions, halo exchanges, or coordinated stage boundaries), the slowest rank gates progress.

Under these conditions, a short-lookahead policy like BF-IO is natural: it uses near-term refinement/coarsening signals of *ongoing* regions to guide assignment of newly generated work units (e.g., blocks, patches, or particle batches) so as to reduce barrier-induced idle time.

These examples share the key property exploited by BF-IO: while predicting the *total* remaining runtime of a newly arriving unit of work is unreliable, predicting whether *ongoing* work will finish within a short window is often feasible from progress signals, diagnostics, or domain structure. This makes short lookahead a practical and portable information interface across scientific workloads.

7.3 Limitations and future directions

Several limitations suggest clear directions for future work.

System interfaces and buffering.

Our strongest theoretical guarantees are developed under a centralized waiting-pool abstraction. Some serving engines bind requests immediately to per-worker queues, which reduces the scheduler’s ability to reshape batches at slot-release times and can weaken future-aware balancing when queueing delays exceed the lookahead window. A promising direction is to develop a full theory for the “instant-dispatch” interface (routing to per-worker FIFO queues) and to quantify how short-horizon signals degrade as activation delays grow.

Model scope.

Our general theory covers a broad class of non-decreasing workload drift processes, motivated by stateful execution where work grows with accumulated state. Some systems exhibit decreasing or highly non-monotone per-step workloads (e.g., aggressive pruning, adaptive compression, or multi-phase jobs with alternating heavy/light stages). Extending worst-case theory to such regimes, and characterizing when monotonicity is essential, remains open.

Multi-objective serving.

Real deployments often optimize multiple objectives simultaneously (tail latency, fairness across tenants, service-level objective compliance, and energy caps). Although the BF-IO objective aligns well with barrier-induced idle reduction, integrating fairness and service-level objective constraints into the short-horizon optimization—while preserving millisecond decision budgets—deserves dedicated study.

Appendix A Supplementary Materials for Section 1

A.1 Literature Review

A.1.1 Load Balancing Problem

In this section, we briefly review classical load balancing algorithm structures [37] (except for First-come-first-serve (FCFS) [38–40], which serves as the benchmark in

the paper and is discussed in Section 3) and elucidate their fundamental inefficiency or incompatibility in the LLM inference problem:

- *Join Shortest Queue (JSQ)*. JSQ [41–43] routes each arriving request to the worker with the smallest queue length (ties arbitrary). In practice, LLM serving systems in widely used (e.g., vLLM [44], SGLang [45]) implement a JSQ-style policy, so we take JSQ as the primary baseline. The core difficulty is that, in decode-time DP with sticky assignments, “queue length” is a poor proxy for per-step work: true workloads are unknown at assignment time and evolve as KV caches grow, so production systems typically measure the number of requests rather than their total workload. This makes JSQ brittle. Consider G workers and an adversarial arrival sequence with “heavy” requests of unknown long length L and “short” requests of length $s \ll L$. Because a heavy counts as one request, JSQ will place a heavy on the worker that currently has the fewest requests; subsequent bursts of many short requests inflate the counts on other workers while leaving the heavy worker’s count small, so the next heavy again goes to the same worker. After k such events, that worker holds k heavies while others hold many shorts. Since per-step time under the barrier model is

$$T_{\text{step}}(t) = \max_g T_{\text{local}}^{(g)},$$

we have $T_{\text{step}}^{\text{JSQ}}(t) \geq kc(L)$, where $c(L)$ is the per-step local cost of a single heavy (proportional to its resident KV). A balanced assignment would yield $T_{\text{step}}^*(t) \leq \lceil k/G \rceil c(L)$, so the ratio is $\Omega(G)$. The problem persists because assignments are non-preemptive: as heavies generate more tokens, their per-step cost grows, yet JSQ cannot correct earlier placements. Hence JSQ targets the wrong surrogate and can be highly inefficient in the decode-stage, barrier-synchronized setting.

- *Round-Robin (RR)*. RR [46–48] dispatch assigns the i -th arriving (post-prefill) request to worker $((i-1) \bmod G) + 1$, cycling through the G workers irrespective of job size, resident KV, or drift. Under sticky, non-preemptive assignments, this determinism is exploitable. Consider an online sequence in which requests with indices $i \in 1, 1+G, 1+2G, \dots$ have long decode length L (heavy), and all others have short length $s \ll L$. RR places **all** heavy jobs on worker 1 and none on workers $2, \dots, G$. Let H be the number of heavy jobs that arrive before any heavy completes (this is typical when L is large). Then, for each decode step in that interval, the per-step makespan under RR satisfies

$$T_{\text{step}}^{\text{RR}}(t) \geq H \cdot c(L),$$

where $c(L)$ is the per-step local cost contributed by one heavy (proportional to its resident KV), because the max local time occurs on worker 1 carrying H heavies. By contrast, an assignment that evenly spreads heavies yields

$$T_{\text{step}}^*(t) \leq \left\lceil \frac{H}{G} \right\rceil \cdot c(L),$$

so the ratio $T_{\text{step}}^{\text{RR}}/T_{\text{step}}^* \geq \frac{H}{\lceil H/G \rceil} \geq G$. This gap persists across many steps because jobs are sticky and heavy requests evolve slowly, so RR is not competitive for our LLM inference load balancing problem under adversarial arrivals.

- *Power-of-d.* At each arrival, Power-of-d [49–51] samples $d \ll G$ workers uniformly at random and routes the request to the one with the smallest queue length among the d sampled. This reduces coordination overhead from $O(G)$ to $O(d)$ per arrival and, in classical migratable/size-known settings, retains JSQ-like balance with strong tail guarantees. However, in decode-time DP with sticky assignments and barrier synchronization, power-of-d inherits the core JSQ shortcomings: queue length is a poor surrogate for workload when job sizes are unknown and evolve with KV growth; placements are non-preemptive, so early mistakes persist; and minimizing counts does not control the per-step maximum local time that gates progress.
- *Min-min.* The Min–Min scheduler [52–54] builds an “earliest completion time” (ECT) matrix and repeatedly assigns the task that can finish soonest on some worker. Concretely, for each unscheduled task i and worker g , compute $\text{ECT}_{ig} = r_g + p_{ig}$, where r_g is the worker’s ready time and p_{ig} is the estimated processing time of task i on g . Choose $i^* = \arg \min_i \min_g \text{ECT}_{ig}$, assign it to $g^* = \arg \min_g \text{ECT}_{i^*g}$, update r_{g^*} , and repeat. This strategy presumes reasonably accurate, worker-specific p_{ig} and is effective for static batches on heterogeneous clusters. However, it is incompatible in our decode-time setting it is ill-suited: (i) processing times are unknown and evolve token-by-token with KV growth, so p_{ig} is neither observable nor stationary; (ii) assignments are sticky (KV migration is impractical), so Min–Min’s advantage of revising choices before start or splitting jobs is unavailable; (iii) computing and maintaining a full ECT matrix is computationally prohibitive. Consequently, Min–Min cannot address the constraints of decode-stage load balancing in LLM serving.
- *Opportunistic Load Balancing and Load Balancing Min–Min (OLB+LBMM).* This hybrid couples opportunistic load balancing with a load-balancing Min–Min refinement [55–57]. OLB greedily dispatches arrivals to the first idle or least-busy worker (size-agnostic) to keep resources utilized; periodically, LBMM builds an earliest-completion-time table over the waiting pool (often after chunking tasks) and reassigns pending or not-yet-started chunks to heterogeneous workers that minimize predicted completion time. This can reduce transient idleness relative to pure Min–Min. However, it still relies on (i) accurate per-chunk processing-time estimates, (ii) the ability to split work before start, and (iii) periodic ECT recomputation overhead. Crucially, in our decode-time regime requests are indivisible: token generation is sequential and bound to a single KV cache, so pre-chunking across workers is not possible. Therefore, the OLB+LBMM architecture remains incompatible with the constraints in LLM serving.
- *Max–Min.* Max–Min [58–60] is the dual of Min–Min: for each unscheduled task i and worker g , compute the earliest–completion time $\text{ECT}_{ig} = r_g + p_{ig}$. For each task, take its best machine $g(i) = \arg \min_g \text{ECT}_{ig}$ with best time $m_i = \min_g \text{ECT}_{ig}$. Max–Min then selects $i^* = \arg \max_i m_i$ (the task whose best predicted finish time is largest), assigns it to $g(i^*)$, updates $r_{g(i^*)}$, and repeats. This choice favors long

tasks early to mitigate starvation on heterogeneous clusters. In decode-time LLM serving, the same incompatibilities as Min-Min apply: p_{ig} is unknown and evolves token by token (KV growth), assignments are sticky and requests are indivisible (no pre-chunking or migration), and maintaining ECT tables within millisecond is impractical. Consequently, Max-Min is not suitable for the decode-stage, barrier-synchronized LLM serving setting.

- *Ant Colony Optimization (ACO).* ACO [61–63] is a constructive metaheuristic that repeatedly builds task-worker assignments by sampling edges with probability $P_{ig} \propto \tau_{ig}^\alpha \eta_{ig}^\beta$, where τ_{ig} (pheromone) summarizes past good solutions and η_{ig} is a heuristic desirability. After evaluating an assignment, pheromones evaporate and are reinforced, and the process iterates over many ants/iterations. In our decode-time setting ACO is incompatible for two core reasons. *Information:* ACO needs informative processing-time estimates p_{ig} , but decode workloads are unknown at assignment and drift token by token with KV growth, so the signals required to guide sampling are unreliable. *Computation:* Even if perfect predictions existed, ACO requires multiple ants and iterations and is typically batch oriented; with online, non-stationary arrivals and a millisecond decision budget, recomputing pheromones and re-sampling assignments per arrival is computationally infeasible. Consequently, ACO and its variants are ill-suited to decode-stage load balancing.
- *Honey Bee Foraging Algorithm (HBFA).* HBFA-style schedulers [64, 65] emulate bee foraging: “employed” workers advertise their current load and the number of pending priority tasks (a waggle-dance-like signal), while “onlooker” tasks probabilistically select a destination with high advertised fitness (e.g., few priority tasks, low queue length, sufficient CPU/memory). This algorithm aims to raise utilization and cut mean response time on heterogeneous clusters. In decode-time LLM serving, HBFA is incompatible for the same structural reasons as ACO: (i) it relies on queue-length/priority signals, but per-request workloads are unknown at assignment and evolve token by token; (ii) its population-style selection/updates are infeasible to a millisecond scheduling budget under online, non-stationary arrivals. Consequently, HBFA does not satisfy the information, control, and timing constraints in decode-stage load balancing.
- *Throttled Load Balancing (TLB).* TLB [66, 67] maintains a catalog of workers with capability vectors and enforces a per-worker concurrency threshold Θ ; an arriving request is routed to the first worker that is under its threshold and appears “suitable” given current residual capacity. While this capacity-aware gating can outperform RR, it is misaligned with decode-time DP. First, TLB presumes a known, stable requirement vector $d(r)$ per request, but in decode the effective demand is unknown at admission and drifts token by token as the KV cache grows, so eligibility tests based on initial size or queue length are unreliable. Second, assignments are sticky: early misplacements cannot be corrected as $d(r)$ inflates. Third, throttling caps concurrency rather than minimizing the per-step maximum local work; depending on Θ , it can even increase idle time by admitting fewer short requests to otherwise underloaded workers while a heavy request gates progress. So, TLB is ineffective for decode-stage load balancing under unknown, evolving workloads and synchronous barriers.

- *Carton.* Carton [68–70] combines load balancing with distributed rate limiting: a controller spreads incoming work across workers, while each worker enforces a local rate cap so that measured performance levels are equalized with minimal coordination. This can work well when workloads and rate signals are stable. In decode-time DP, however, Carton is structurally incompatible for two reasons. First, the signals it relies on—per-worker rates, queue lengths, or smoothed performance counters—are poor surrogates for decode-time work: per-request workloads are unknown at admission and drift token by token as KV caches grow, so rate-based estimates become stale on the step-by-step timescale. Second, assignments are sticky: once a request is placed on a decode worker, its KV cache is not migrated, so DRL cannot reallocate in-flight work to correct early imbalances. Heavy requests then continue to dominate a worker’s local time while others idle at barriers, leaving Carton’s LB+DRL control loop without the information or actuation needed to repair decode-stage imbalance.

A.1.2 LLM Serving and Energy Consumption

Recent work on the energy footprint of LLM serving falls into two complementary directions: (i) characterization and accounting of energy, and (ii) control/optimization of GPU power under service-level objectives (SLOs). On characterization, [71] profile serving across batching and parallelism knobs and show stage-specific energy-latency trade-offs; [72] frame sustainability as a system-level challenge, highlighting that serving can rival or exceed training in operational energy; [73] quantify both operational and embodied emissions, showing that hardware generation and batching interact non-trivially with energy efficiency; and [21] model the fundamental power-utilization relationship, establishing that GPU power scales sublinearly with utilization—idle states draw substantial power without contributing throughput. On control, [74] build workload-based energy/runtime models to derive offline energy-optimal serving policies on heterogeneous systems, while iteration-level dynamic voltage frequency scaling (DVFS) emerges as a runtime lever: [75] propose SLO-aware GPU frequency control tailored to autoregressive decoding, and [76] separate prefill and decode into distinct control loops to reduce energy under trace replays without throughput loss. Together, these studies establish that serving’s energy footprint is large, that idle power is non-negligible, that prefill versus decode differ in performance–energy behavior, and that SLO-aware frequency control and hardware/batching choices are potent—but workload- and system-specific—tools

The studies above optimize per-device power or fleet-level energy/carbon via frequency control, hardware selection, or offline scheduling models. None addresses the decode-stage barrier objective where per-step time is governed by the maximum local workload across data-parallel workers—precisely the imbalance our paper targets. Our universal load-balancing principle is orthogonal and complementary: by provably shrinking the per-step maximum (thus reducing systematic idle at barriers), it converts wasted idle power into useful computation, lowering energy per token regardless of which DVFS or hardware policy is deployed. Moreover, it applies under unknown, drifting decode lengths where prediction-based controllers degrade. In short, prior work characterizes and tunes how fast and how green a given worker runs; we address

how evenly the decode-time work is distributed across workers—an upstream lever that tightens the energy/latency envelope that DVFS and carbon-aware schedulers can then exploit.

A.1.3 LLM Serving Optimization

Recent systems work has rearchitected the serving stack to expose structural levers that raise throughput and reduce latency/queuing contention. Engine designs such as vLLM introduce PagedAttention to virtualize and compact the KV cache, eliminating fragmentation and enabling large, flexible batches with near-zero KV waste [44]. SGLang provides a program/runtime interface for multi-call LLM applications (tools, control flow, structured I/O), co-designing execution with batching and caching to keep the accelerator pipeline busy [45]. At the cluster level, prefill–decode (PD) disaggregation separates prompt encoding from autoregressive decoding across GPUs to remove cross-phase interference and to co-optimize latency targets for TTFT (prefill) and TPOT (decode) [77, 78]. These structural choices interact with parallelism: decode commonly uses data parallelism (DP) over requests, while model parallelism mixes tensor and pipeline partitioning for large models and expert parallelism (MoE) for sparse activation [79–82]. Together, this body of work establishes the modern serving substrate—memory-efficient KV management, program-aware engines, PD disaggregation, and composable DP/TP/PP/EP—as the structural foundation on which scheduling and load-balancing policies operate.

Besides optimization in architecture of LLM serving, many recent works design scheduling algorithms to make LLM serving more efficient. Production LLM engines adopt iteration-level scheduling with continuous batching as the default control primitive: Orca introduced iteration-level scheduling and selective batching to keep accelerators busy despite heterogeneous request lengths [83], and vLLM co-designs Paged-Attention with preemptive request scheduling to admit and retire sequences at iteration granularity [44]. Building on these primitives, recent systems explore complementary schedulers: Sarathi-Serve proposes stall-free scheduling via chunked prefill to relieve the prefill–decode interference and improve the throughput–latency frontier [84, 85]; Fast-Serve adds token-granular preemption with a skip-join multi-level feed back queue (MLFQ) to reduce job completion time under bursty arrivals [86]. A parallel line uses learned or proxy signals to approximate shortest-first: proxy-model-based predictors to rank jobs and avoid head-of-line blocking [23], learned-to-rank policies that plug into vLLM [24], and embedding-based estimators with preemptive schedulers [26]. Fairness-aware policies integrate service fairness into continuous batching without preemption [87]. Beyond single-instance engines, decentralized or cross-replica schedulers have been proposed for heterogeneous or edge settings [88].

A growing subset of works tackles *load balancing* explicitly. ShuffleInfer disaggregates prefill and decode instances and introduces a two-level scheduler to spread mixed workloads across instances, reporting latency gains but relying on instance-level migration [89]. For MoE inference, HarMoEny balances expert load via dynamic token redistribution and asynchronous expert prefetching across GPUs [90], while DuoServe-MoE separates expert scheduling for prefill versus decode to match distinct activation

patterns [91]. At the router layer, performance-aware load balancers combine response-length prediction with mixing strategies to steer flows across replicas [92]. Systems surveys and empirical analyses further catalog scheduling variants and highlight the gap between academic schedulers and deployable, low-overhead policies [93]. Many of these works target expert-parallel (EP) balancing rather than data-parallel (DP) balancing of per-request decode work; the latter is more challenging because job sizes are unknown and evolving, assignments are sticky (KV non-migratable), and step progress is gated by synchronous barriers. Among approaches that could be adapted to DP, most are engine- or trace-specific heuristics without theoretical guarantees; their effectiveness varies across datasets and configurations and thus does not constitute a universal load-balancing principle.

Moreover, a recent theory stream formalizes LLM serving as online scheduling with KV-cache constraints and provides provable policies at the single-worker level. [94] develop a benchmark via a hindsight-optimal integer program, prove impossibility in the fully online adversarial setting (no constant competitive ratio for any algorithm), and design algorithms that are near-optimal in a semi-online model. Following this model, [95, 96] relax several assumptions in the model. They study heterogeneous prefill and unknown decode lengths with only interval prediction information. In parallel, [97] introduce a fluid-guided framework with memory constraints, deriving Nested-WAIT policies that are near-optimal against a fluid benchmark in heavy traffic. These works provide principled scheduling for batching and scheduling under a single worker and do not address problems under multiple workers.

A.1.4 Assignment and Scheduling Problem

Our decode worker selection problem is an instance of the *online assignment* paradigm: jobs (requests) arrive sequentially, some side information may be observed, and the decision maker must irrevocably assign each job to a resource so as to optimize a system objective. Foundationally, online assignment connects to online bipartite matching and budgeted allocation (AdWords): the classical RANKING algorithm achieves the optimal $(1 - 1/e)$ competitive ratio in adversarial arrival models for bipartite matching, while primal-dual methods underlie many extensions [98–101]. Subsequent work generalizes from linear objectives to concave returns and to learning or estimation within the primal-dual framework, as well as fairness-aware variants [102–106]. Beyond the classic “offline resources fixed, online jobs arrive” setting, fully online models allow both sides to arrive and sharpen competitive limits [107]. Parallel lines model task heterogeneity and worker qualities in crowdsourcing markets, formalizing how partial information at arrival influences assignment quality [108]. Taken together, these literatures provide baseline guarantees for irrevocable decisions under uncertainty, typically in profit/throughput objectives and without per-step synchronization.

A newer strand studies *reusable resource allocation*, where an assigned resource is occupied for some duration and then returns to the pool; this captures ridesharing, healthcare beds, and inventory with returns [109]. Recent results establish near-optimal guarantees in adversarial or stochastic arrivals by exploiting fluid or learning approximations and carefully designed dual controls [110–113]. These models are

closer to our setting (decode workers are reusable) but still differ in two crucial ways: (i) they optimize cumulative reward (linear) while our objective is the load balancing (non-linear); and (ii) they typically assume either known or stationary service-time models, whereas decode workloads are unknown at admission and evolve token-by-token. Thus, classical online assignment and reusable-resource frameworks inform admission/routing under uncertainty, but they do not directly address data-parallel decode with sticky assignments and synchronous barriers that gate progress each step.

The classical *online scheduling* literature studies how a decision maker allocates processing time to jobs that arrive sequentially, aiming to optimize latency/throughput objectives under limited lookahead [114–121]. Two strands are especially relevant to LLM inference on a *single* engine. First, *batch scheduling* groups jobs to amortize setup or memory costs and to raise effective utilization; models and algorithms range from static batch formation to fully online batching with competitive guarantees [122–126]. Second, *precedence-constrained* scheduling captures intra-job dependencies; here each task must respect a partial order, and objectives include makespan and total weighted completion time [127–130]. LLM decoding on a single worker fits this mold: tokens within a request obey a strict chain precedence (each token depends on its prefix), batching trades latency for throughput, and memory (KV-cache) constraints couple sequencing and admission. Results from these lines provide principled policies for admission, batching, and service order when processing times are known or learnable, but they operate at the level of one engine and do not account for cross-worker synchronization.

Multi-processor scheduling generalizes to identical/related/unrelated machines and mixes preemptive and non-preemptive models [115–117, 119]. Canonical approaches (e.g., list scheduling, longest-processing-time rules, or migration-based balancing) assume either known processing times or allow job preemption/migration to correct early placements; performance is typically analyzed for makespan or flow-time objectives. These models illuminate when per-machine queues equalize and when migration is essential, yet they remain misaligned with LLM decode in two ways: (i) unknown and evolving processing times undermine size-aware or learned dispatching; (ii) sticky assignments remove the main lever used to fix early mistakes. Classic multi-worker scheduling therefore informs local ordering and (where allowed) migration, but it does not address the barrier-synchronized, unknown-size, non-preemptive regime that governs data-parallel decoding; this gap motivates our universal load-balancing principle.

A.1.5 Online Algorithms under Adversarial Arrivals

An *online algorithm* chooses actions sequentially as inputs arrive, without seeing the future; an *adversarial arrival model* allows the input sequence to be chosen by an adversary, often either *oblivious* (fixes the entire sequence before seeing the algorithm’s random bits) or *adaptive* (may react to the algorithm’s past random choices). Performance is assessed by competitive analysis: finding out the largest gap between the performance of the online algorithm and the hindsight optimal algorithm (which has full access to all arrivals in advance).

Beyond our online assignment domain, a broad literature studies online algorithms under adversarial arrivals. In online resource allocation, booking-limit and protection-level policies [131, 132], together with primal–dual methods [133–136], yield constant or logarithmic competitive ratios for covering/packing and related network-allocation problems [137]. In online caching and paging, classic results show *least-recently-used* (LRU) is k -competitive, and randomized marking schemes achieve $O(\log k)$ competitiveness against an oblivious adversary [138–140]. The k -server problem and metrical task systems capture stateful movement on metric spaces; the work-function algorithm attains $(2k-1)$ -competitiveness for k -server on general metrics [141, 142]. In online convex optimization, regret-minimizing methods (e.g., online gradient and mirror descent) guarantee $O(\sqrt{T})$ adversarial regret [143]. In online facility location, Meyerson’s randomized algorithm is $O(\log n)$ -competitive in random-order models, whereas under oblivious adversaries the tight rate is $\Theta(\log n / \log \log n)$ [144, 145]. Our analysis likewise adopts an adversarial-arrival viewpoint—inputs (arrivals and lengths) are determined by an oblivious adversary—and establishes competitive optimality for decode-stage load balancing under synchronous barriers.

Appendix B Baseline Policy: First-Come-First-Serve (FCFS)

In this subsection, we formalize the baseline policy used throughout the paper: *First-Come-First-Serve* (FCFS). FCFS is widely deployed in real LLM serving systems’ scheduler [44, 45].

At each step k , the scheduler maintains a waiting queue $R_{\text{wait}}(k)$ that stores all requests that have arrived by time k but have not yet been assigned to any worker. Under FCFS, the scheduler scans workers in increasing index $g = 1, 2, \dots, G$ and fills any available slots on each worker up to the batch capacity B . Requests are always taken from $R_{\text{wait}}(k)$ in strict arrival order (the head of the queue), and no request that arrived later may be scheduled before an earlier one. The capacity constraint $|\mathcal{A}_g(k)| \leq B$ is always respected, and the loop terminates as soon as either all workers are full (no remaining capacity) or the waiting queue is empty.

This policy is extremely fast and deterministic (for a fixed arrival sequence), and it does not rely on any information about the workload profile W_i of individual requests. Precisely because it ignores workload heterogeneity, FCFS can easily accumulate many heavy requests on a single worker while others receive only light ones, leading to large per-step imbalance and, consequently, substantial idle time at the barrier. The pseudocode used in our analysis and implementation is given in Algorithm 2.

Appendix C Supplementary Materials for Section 5

C.1 Proof of Theorem 1

Proof of Theorem 1: We first reduce the statement to a single admission round, and then analyze BF-IO and FCFS separately.

Reduction to a single admission round. In the homogeneous-output setting $o_i = o$ for all i , the evolution naturally decomposes into *rounds*. At the beginning of a round, the cluster is

Algorithm 2: FCFS Baseline

Input: Waiting queue $R_{\text{wait}}(k)$ (arrival order), worker concurrency B , active sets $\{\mathcal{A}_g(k)\}_{g \in [G]}$

Output: Assignments at step k

Compute remaining slots on each worker: $\text{cap}[g] \leftarrow B - |\mathcal{A}_g(k)|$ for all $g \in [G]$;

if $\sum_{g \in [G]} \text{cap}[g] = 0$ **or** $R_{\text{wait}}(k) = \emptyset$ **then**
| **return**

while $R_{\text{wait}}(k)$ is not *None* **do**

Pop the oldest request i from $R_{\text{wait}}(k)$;
| Select $g^* \in \arg \max_g \text{cap}[g]$ with maximal free slots;
| Assign i to worker g^* : $\mathcal{A}_{g^*}(k) \leftarrow \mathcal{A}_{g^*}(k) \cup \{i\}$;
| $\text{cap}[g^*] \leftarrow \text{cap}[g^*] - 1$;

empty; GB jobs are admitted (up to capacity), with B jobs sent to each worker. All admitted jobs have the same decode length o , so they generate tokens in lockstep and terminate simultaneously after o steps. No further jobs are admitted until all GB jobs complete, at which point the next round begins.

Within a round, the instantaneous imbalance is the same at each of the o steps, because all workers advance in parallel, and the per-step workloads merely translate in time. Thus, the time-average imbalance over a long horizon is proportional to the average imbalance *per admission round*. Formally, let $\text{Imb}^{(r)}(\pi)$ be the (step-wise) imbalance in round r under a policy π immediately after the GB jobs of that round have been admitted. As argued above, this quantity also captures the imbalance at each step within the round, up to the fixed multiplicative factor o .

Under the prefill-length model in Section 5, and given any arrival instance I that satisfies the overloaded condition at every step, the multiset of prefill lengths entering each round consists of GB i.i.d. draws from the distribution of s ; different rounds use disjoint sets of jobs, and so the collections of GB prompts across rounds are independent. In particular, the random variables $\{\text{Imb}^{(r)}(\pi)\}_{r \geq 1}$ are i.i.d. for each fixed policy π , and their law does not depend on the specific overloaded arrival instance I .

Let $\text{AvgImbalance}(\pi; I)$ denote the time-average imbalance under policy π for arrival instance I as in Section 3. Over a long horizon, the law of large numbers implies that, for any π and any $I \in \mathcal{I}$,

$$\lim_{K \rightarrow \infty} \mathbb{E}[\text{AvgImbalance}(\pi; I)] = \mathbb{E}[\text{Imb}^{(1)}(\pi)],$$

because each round contributes o identical steps, and the rounds form an i.i.d. sequence. Consequently, the imbalance improvement ratio **IIR** simplifies to the ratio of one-round expectations:

$$\mathbf{IIR} = \inf_{I \in \mathcal{I}} \frac{\lim_{K \rightarrow \infty} \mathbb{E}[\text{AvgImbalance}(\text{FCFS}; I)]}{\lim_{K \rightarrow \infty} \mathbb{E}[\text{AvgImbalance}(\text{BF-IO}; I)]} = \frac{\mathbb{E}[\text{Imb}^{(1)}(\text{FCFS})]}{\mathbb{E}[\text{Imb}^{(1)}(\text{BF-IO})]}.$$

Thus, it suffices to lower bound the ratio

$$\frac{\mathbb{E}[\text{Imb}(\text{FCFS})]}{\mathbb{E}[\text{Imb}(\text{BF-IO})]}$$

in a *single* admission round, where we write $\text{Imb}(\pi)$ for $\text{Imb}^{(1)}(\pi)$ for brevity.

Step A: BF-IO is s_{\max} -balanced. Fix a realization of the GB prefill lengths in the current round. Since prefill lengths are independent across jobs and arrival times do not carry additional information about their values, we may regard these as an unordered multiset of GB numbers in $[0, s_{\max}]$. Any assignment that fills all devices in the round corresponds to a partition of this multiset into G disjoint groups S_1, \dots, S_G , each of cardinality $|S_g| = B$. Define the per-device loads

$$L_g := \sum_{s \in S_g} s, \quad M := \max_{1 \leq g \leq G} L_g, \quad m := \min_{1 \leq g \leq G} L_g.$$

Because all jobs have identical decode length o , the per-step imbalance within the round is constant and proportional to the deviation of the L_g from M . In particular, minimizing the sum of future imbalances over the round is equivalent to minimizing the maximum load M across devices in that round. Let $\{S_g^*\}_{g=1}^G$ be any assignment that minimizes M .

Lemma 1. *For any optimal assignment $\{S_g^*\}$ minimizing M , we have*

$$M - m \leq s_{\max}.$$

Proof of Lemma 1 Suppose for contradiction that $M - m > s_{\max}$. Let $p \in \arg \max_g L_g$ and $q \in \arg \min_g L_g$, so $L_p = M$ and $L_q = m$. Because $L_p - L_q > M - m > s_{\max}$ and every element of $S_p^* \cup S_q^*$ lies in $[0, s_{\max}]$, there must exist $x \in S_p^*$ and $y \in S_q^*$ with $x > y$; otherwise we would have $\max S_p^* \leq \min S_q^*$, which together with $|S_p^*| = |S_q^*| = B$ would imply

$$L_p \leq B \max_{s \in S_p^*} s \leq B \min_{s \in S_q^*} s \leq L_q,$$

contradicting $L_p > L_q$.

Construct a new assignment by swapping x and y between devices p and q :

$$S'_p := (S_p^* \setminus \{x\}) \cup \{y\}, \quad S'_q := (S_q^* \setminus \{y\}) \cup \{x\},$$

and $S'_r := S_r^*$ for all $r \notin \{p, q\}$. The new loads are

$$L'_p = L_p - (x - y) < L_p, \quad L'_q = L_q + (x - y) \leq L_q + s_{\max} < L_p,$$

and $L'_r = L_r$ for $r \notin \{p, q\}$. Thus every new load L'_r is strictly less than the old maximum $L_p = M$ except possibly those devices $r \neq p$ that already had $L_r = M$ before the swap. In particular, if p was the unique maximizer, then

$$\max_g L'_g < \max_g L_g = M,$$

which contradicts the optimality of $\{S_g^*\}$ as a minimizer of M .

If instead there were multiple devices achieving the maximum M before the swap, then after the swap, device p falls below M , while all other devices $r \neq p$ maintain their previous loads $L'_r \leq M$. Hence

$$\max_g L'_g = M,$$

but the number of devices attaining this maximum strictly decreases. Consequently, starting from any optimal assignment that is also *lexicographically minimal* in the pair

$$\left(\max_g L_g, \#\{g : L_g = M\} \right),$$

we cannot have $M - m > s_{\max}$, since the above swap produces another assignment with either a smaller maximum load or the same maximum load but fewer maximizers. This contradicts lexicographic minimality. Therefore $M - m \leq s_{\max}$ must hold for every optimal assignment. \square

For any assignment, the round-level imbalance is

$$\text{Imb} = \sum_{g=1}^G (M - L_g).$$

For the optimal assignment $\{S_g^*\}$, choose $p \in \arg \max_g L_g$ and note that $L_p = M$. Then

$$\text{Imb} = \sum_{g \neq p} (M - L_g) \leq \sum_{g \neq p} (M - m) = (G - 1)(M - m) \leq (G - 1)s_{\max}$$

by Lemma 1. Since this bound holds for every realization of the GB prompt lengths in the round, taking expectations yields

$$\mathbb{E}[\text{Imb}(\text{BF-IO})] \leq (G - 1)s_{\max}. \quad (\text{C1})$$

Step B: FCFS lower bound. We now derive a lower bound on the expected imbalance under FCFS in one round. Because of the overloaded assumption and size-agnostic FCFS admission, the GB jobs admitted in a round can be viewed as an unordered multiset of i.i.d. prefill lengths with law s , after which FCFS fills the G devices in arrival order. Conditioned on this multiset, the distribution of the B prompts assigned to each device is that of B samples drawn uniformly without replacement from the multiset. Since the underlying pool itself comprises GB i.i.d. draws from s , a standard exchangeability argument implies that the prompts $(s_{g,j})_{j=1}^B$ on each device g can be represented as B i.i.d. draws from s , and that the collections $\{(s_{g,j})_{j=1}^B : g \in [G]\}$ are independent across g .

Let

$$S_g := \sum_{j=1}^B s_{g,j}, \quad \mu := \mathbb{E}[s], \quad \sigma_s^2 := \text{Var}(s) > 0.$$

Then S_1, \dots, S_G are i.i.d. with

$$\mathbb{E}[S_g] = \mu B, \quad \text{Var}(S_g) = \sigma_s^2 B.$$

Define the standardized sums

$$Z_g := \frac{S_g - \mu B}{\sigma_s \sqrt{B}}, \quad g = 1, \dots, G.$$

Because $s \in [0, s_{\max}]$, the random variable s has a bounded third absolute moment, and the Berry–Esseen theorem (for sums of i.i.d. real variables) yields the existence of a universal constant C_{BE} such that

$$\sup_{x \in \mathbb{R}} \left| \Pr(Z_g \leq x) - \Phi(x) \right| \leq \frac{C_{\text{BE}}}{\sqrt{B}}, \quad (\text{C2})$$

where Φ is the standard normal distribution function.

Set $z_G := \sqrt{\frac{\log G}{2}}$ and consider the threshold z_G . For a standard normal $Z \sim N(0, 1)$ and large G , the Gaussian tail bound implies

$$\Pr(Z \geq z_G) \geq \frac{1}{\sqrt{2\pi}} \left(\frac{1}{z_G} - \frac{1}{z_G^3} \right) \exp\left(-\frac{z_G^2}{2}\right) \geq \frac{1}{2\sqrt{2\pi} z_G} G^{-1/4}.$$

Combining this with (C2), we obtain

$$\Pr(Z_g \geq z_G) \geq \frac{1}{2\sqrt{2\pi} z_G} G^{-1/4} - \frac{C_{\text{BE}}}{\sqrt{B}}.$$

Since $\sqrt{G} \log G = o(B)$, there exists $B_0(G)$ such that for all $B \geq B_0(G)$,

$$\frac{C_{\text{BE}}}{\sqrt{B}} \leq \frac{1}{2} \cdot \frac{1}{2\sqrt{2\pi} z_G} G^{-1/4},$$

and hence

$$\Pr(Z_g \geq z_G) \geq \frac{1}{4\sqrt{2\pi} z_G} G^{-1/4} =: p_G. \quad (\text{C3})$$

By independence across g , we have

$$\Pr\left(\max_{1 \leq g \leq G} Z_g \geq z_G\right) \geq 1 - (1 - p_G)^G.$$

Using the inequality $1 - x \leq e^{-x}$ for $x \geq 0$, we find

$$1 - (1 - p_G)^G \geq 1 - \exp(-Gp_G).$$

From (C3), $Gp_G \geq \frac{1}{4\sqrt{2\pi} z_G} G^{3/4}$, which is bounded away from zero for every fixed $G \geq 2$.

Thus, there exists a universal constant $c_1 \in (0, 1)$ (for instance $c_1 := 1 - e^{-1/(4\sqrt{2\pi})}$) such that

$$\Pr\left(\max_{1 \leq g \leq G} Z_g \geq z_G\right) \geq c_1 \quad \text{for all } \log G \geq 4 \text{ and all } B \geq B_0(G). \quad (\text{C4})$$

We now translate this into a lower bound on $\mathbb{E}[\max_g S_g]$. For any $t > 0$, an elementary inequality yields

$$\mathbb{E}\left[\max_{1 \leq g \leq G} S_g\right] = \mu B + \mathbb{E}\left[\max_{1 \leq g \leq G} (S_g - \mu B)\right] \geq \mu B + t \Pr\left(\max_g (S_g - \mu B) \geq t\right).$$

Choose $t := \sigma_s \sqrt{B} z_G$, so that the event $\{\max_g (S_g - \mu B) \geq t\}$ coincides with $\{\max_g Z_g \geq z_G\}$. Combining with (C4), we obtain

$$\mathbb{E}\left[\max_g S_g\right] \geq \mu B + \sigma_s \sqrt{B} z_G c_1 = \mu B + \frac{c_1}{\sqrt{2}} \sigma_s \sqrt{B \log G}.$$

Since $\mathbb{E}[\sum_{g=1}^G S_g] = G\mu B$, it follows that the expected imbalance in the round under FCFS satisfies

$$\mathbb{E}[\text{Imb}(\text{FCFS})] = G \mathbb{E}\left[\max_g S_g\right] - \mathbb{E}\left[\sum_{g=1}^G S_g\right] \geq c_2 G \sigma_s \sqrt{B \log G}, \quad (\text{C5})$$

for all $B \geq B_0(G)$, where $c_2 := c_1/\sqrt{2} > 0$ is a universal constant.

Conclusion. Combining the upper bound (C1) for BF-IO with the lower bound (C5) for FCFS, we find that for all $B \geq B_0(G)$,

$$\frac{\mathbb{E}[\text{Imb}(\text{FCFS})]}{\mathbb{E}[\text{Imb}(\text{BF-IO})]} \geq \frac{c_2 G \sigma_s \sqrt{B \log G}}{(G-1) s_{\max}} = \left(c_2 \frac{\sigma_s}{s_{\max}}\right) \sqrt{B \log G} \cdot \frac{G}{G-1}.$$

By the non-degeneracy assumption in Section 5, the ratio σ_s/s_{\max} is bounded below by $\kappa_0 > 0$. Setting $c := c_2$ and recalling that IIR equals the ratio of one-round expectations, we conclude that

$$\text{IIR} \geq c \kappa_0 \sqrt{B \log G} \cdot \frac{G}{G-1},$$

which is the claimed lower bound (3). This completes the proof. \square

C.2 Proof of Theorem 2

Proof of Theorem 2: We work on a probability space $(\Omega, \mathcal{F}, \mathbb{P})$ that supports the arrival instance \mathcal{I} , the prefill lengths $\mathcal{D}_{\text{prefill}}$, the geometric decode lengths $\mathcal{D}_{\text{decode}} = \text{Geo}(p)$, and the completion indicators. For each step $k \in [K]$, we define the *natural filtration*

$$\mathcal{F}_k := \sigma\left(\text{all arrivals, prefill, decode lengths, completions, and BF-IO assignments up to step } k\right),$$

and write $\mathbb{E}[\cdot \mid \mathcal{F}_k]$ for conditional expectations.

At the end of step $k-1$ (after BF-IO admission at that step), each device $g \in \{1, \dots, G\}$ holds exactly B active requests, indexed by $i = 1, \dots, B$, with sizes $a_{g,i}(k-1) \in \mathbb{N}$ (including prompt tokens and already generated output tokens). Let

$$L_g(k-1) := \sum_{i=1}^B a_{g,i}(k-1), \quad D(k-1) := \max_g L_g(k-1) - \min_g L_g(k-1),$$

and

$$\Lambda(k) := \max_{g,i} a_{g,i}(k-1),$$

be, respectively, the device loads, the inter-device gap, and the one-step envelope at the end of step $k-1$. These quantities are \mathcal{F}_{k-1} -measurable.

At the beginning of step k , every active request grows by exactly one token, then completes independently with probability p at the end of the step. Let $\xi_{g,i}(k) \sim \text{Bernoulli}(p)$ be the completion indicator of slot (g, i) in step k , independent of \mathcal{F}_{k-1} and across (g, i) . The number of completions (free slots) on device g in step k is

$$c_g(k) := \sum_{i=1}^B \xi_{g,i}(k) \sim \text{Binomial}(B, p),$$

independent across g and of \mathcal{F}_{k-1} , and we write $C_k := \sum_{g=1}^G c_g(k)$ for the total number of completions.

Before admitting new requests at step k , the total *pre-admission* load on device g is

$$a_g^{\text{pre}}(k) := L_g(k-1) + B - R_g(k), \quad R_g(k) := \sum_{i=1}^B \xi_{g,i}(k)(a_{g,i}(k-1) + 1),$$

where $R_g(k)$ is the load removed by completions (each surviving job contributes +1 token). The corresponding pre-admission spread is

$$A^{\text{pre}}(k) := \max_g a_g^{\text{pre}}(k) - \min_g a_g^{\text{pre}}(k).$$

After BF-IO admission at step k , we write $L_g(k)$ for the post-admission loads and

$$D(k) := \max_g L_g(k) - \min_g L_g(k)$$

for the post-admission gap. Finally, we set

$$\Lambda(k+1) := \max_{g,i} a_{g,i}(k),$$

the one-step envelope at the end of step k . By construction, $L_g(k)$, $D(k)$, and $\Lambda(k+1)$ are \mathcal{F}_k -measurable.

Part 1 (Upper Bound of Imbalance of BF-IO)

Step 1.A: Separation and one-step drift

The first lemma is a geometric statement about the BF-IO assignment at step k .

Lemma 2 (Separation and gap reduction). *Fix $\delta \in (0, (2s_{\max} - 1)^{-1})$ and set*

$$\gamma := 1 - \delta(2s_{\max} - 1) \in (0, 1).$$

Then, for every $k \geq 1$,

$$\mathbb{P}\left(D(k) \leq \max\{s_{\max}, A^{\text{pre}}(k) - \gamma Bp\} \mid \mathcal{F}_{k-1}\right) \geq 1 - 2G \exp\left(-\frac{\delta^2}{3} Bp\right). \quad (\text{C6})$$

Proof of Lemma 2: Fix a step k and condition on \mathcal{F}_{k-1} . Given \mathcal{F}_{k-1} , the collection of sizes $\{a_{g,i}(k-1)\}$ and loads $\{L_g(k-1)\}$ is deterministic, and the randomness at step k comes only from the completion indicators $\{\xi_{g,i}(k)\}$ and the prompt lengths of newly admitted requests. Let

$$E_{\text{cnt}}(k) := \{|c_g(k) - Bp| \leq \delta Bp \text{ for all } g \in \{1, \dots, G\}\}.$$

The event $E_{\text{cnt}}(k)$ depends only on $\{\xi_{g,i}(k)\}$, and thus is independent of \mathcal{F}_{k-1} . By the Chernoff bound for binomial variables,

$$\mathbb{P}(E_{\text{cnt}}(k)^c \mid \mathcal{F}_{k-1}) = \mathbb{P}(E_{\text{cnt}}(k)^c) \leq 2G \exp\left(-\frac{\delta^2}{3} Bp\right).$$

On the event $E_{\text{cnt}}(k)$, we have

$$c_{\min}(k) := \min_g c_g(k) \geq (1 - \delta)Bp, \quad c_{\max}(k) := \max_g c_g(k) \leq (1 + \delta)Bp.$$

Fix an outcome $\omega \in E_{\text{cnt}}(k)$ and consider deterministically the BF-IO assignment at step k on that outcome. Let $S_g(k)$ denote the multiset of prompt sizes of the new requests admitted to device g at step k ; by construction $|S_g(k)| = c_g(k)$, and

$$L_g(k) = a_g^{\text{pre}}(k) + \sum_{s \in S_g(k)} s.$$

We first establish a separation property for the minimizer of $D(k)$. For each feasible family of multisets $\{S_g(k)\}_{g=1}^G$ with $|S_g(k)| = c_g(k)$ and using only jobs from the waiting pool, define

$$L_g(k) := a_g^{\text{pre}}(k) + \sum_{s \in S_g(k)} s, \quad D(k) := \max_g L_g(k) - \min_g L_g(k).$$

Among all such assignments, BF-IO chooses one that minimizes $D(k)$. Let $\{S_g^*(k)\}$ be such a minimizer, and let

$$L_g^*(k) := a_g^{\text{pre}}(k) + \sum_{s \in S_g^*(k)} s, \quad D^*(k) := \max_g L_g^*(k) - \min_g L_g^*(k),$$

denote the corresponding loads and gap. If $D^*(k) \leq s_{\max}$, then $D(k) = D^*(k) \leq s_{\max}$ and the claimed inequality (C6) trivially holds on this outcome. Hence it suffices to analyze the case $D^*(k) > s_{\max}$.

Let $p \in \arg \max_g L_g^*(k)$ and $q \in \arg \min_g L_g^*(k)$, so that

$$L_p^*(k) - L_q^*(k) = D^*(k) > s_{\max}.$$

We first show that, under this strict gap and the optimality of $\{S_g^*(k)\}$, the assignment must be “separated” between any such heavy–light pair (p, q) . That is, for the sets $S_p^*(k)$ and $S_q^*(k)$ there exists an integer $\theta \in \{0, \dots, s_{\max} - 1\}$ such that

$$s \leq \theta \text{ for all } s \in S_p^*(k), \quad s \geq \theta + 1 \text{ for all } s \in S_q^*(k).$$

We prove by contradiction. Suppose not, then there exist $x \in S_p^*(k)$ and $y \in S_q^*(k)$ with $x > y$. Consider the assignment $\{\tilde{S}_g(k)\}$ obtained by swapping x and y between devices p and q ,

$$\tilde{S}_p(k) := (S_p^*(k) \setminus \{x\}) \cup \{y\}, \quad \tilde{S}_q(k) := (S_q^*(k) \setminus \{y\}) \cup \{x\},$$

and $\tilde{S}_r(k) := S_r^*(k)$ for all $r \notin \{p, q\}$. This swap preserves $|S_g(k)| = c_g(k)$ for every g and uses only jobs from the waiting pool (by the overloaded definition 1, the pool contains sufficiently many jobs of each size to support such exchanges). The new loads are

$$\tilde{L}_p(k) = a_p^{\text{pre}}(k) + \sum_{s \in \tilde{S}_p(k)} s = L_p^*(k) - (x - y) < L_p^*(k),$$

and

$$\tilde{L}_q(k) = a_q^{\text{pre}}(k) + \sum_{s \in \tilde{S}_q(k)} s = L_q^*(k) + (x - y) \leq L_q^*(k) + s_{\max} < L_p^*(k),$$

using $x - y \leq s_{\max}$ and $L_p^*(k) - L_q^*(k) > s_{\max}$. All other loads $\tilde{L}_r(k)$ equal $L_r^*(k) \leq L_p^*(k)$. If p is the unique maximizer of $\{L_g^*(k)\}$, then

$$\max_g \tilde{L}_g(k) < \max_g L_g^*(k),$$

contradicting the minimality of $D^*(k)$. If there are multiple maximizers, then the swap strictly reduces the number of devices attaining the maximum load while keeping the maximum value at most $L_p^*(k)$. Repeating this argument finitely many times, we either strictly reduce the maximum load or obtain a contradiction to the choice of $\{S_g^*(k)\}$ as a minimizer with minimal number of maximizers. Hence no such pair (x, y) can exist, and the desired threshold θ exists.

Condition on $E_{\text{cnt}}(k)$ and fix an outcome with $D^*(k) > s_{\max}$. Using the separation property, for device p every $s \in S_p^*(k)$ satisfies $s \leq \theta$, while for q every $s \in S_q^*(k)$ satisfies $s \geq \theta + 1$. Therefore,

$$\sum_{s \in S_p^*(k)} s \leq \theta c_p(k), \quad \sum_{s \in S_q^*(k)} s \geq (\theta + 1) c_q(k),$$

and hence

$$\begin{aligned} D^*(k) &= L_p^*(k) - L_q^*(k) \\ &= \left(a_p^{\text{pre}}(k) + \sum_{s \in S_p^*(k)} s \right) - \left(a_q^{\text{pre}}(k) + \sum_{s \in S_q^*(k)} s \right) \\ &\leq a_p^{\text{pre}}(k) - a_q^{\text{pre}}(k) + \theta c_p(k) - (\theta + 1) c_q(k). \end{aligned}$$

Using $c_p(k) \leq c_{\max}(k)$ and $c_q(k) \geq c_{\min}(k)$, we obtain

$$\begin{aligned} \theta c_p(k) - (\theta + 1) c_q(k) &\leq \theta c_{\max}(k) - (\theta + 1) c_{\min}(k) \leq \theta(1 + \delta) Bp - (\theta + 1)(1 - \delta) Bp \\ &= Bp(\theta(1 + \delta) - (\theta + 1)(1 - \delta)) = Bp(-1 + \delta(2\theta + 1)) \\ &\leq Bp(-1 + \delta(2s_{\max} - 1)) = -\gamma Bp, \end{aligned}$$

where we used $\theta \leq s_{\max} - 1$ and the definition of γ . Consequently,

$$D^*(k) \leq a_p^{\text{pre}}(k) - a_q^{\text{pre}}(k) - \gamma Bp \leq A^{\text{pre}}(k) - \gamma Bp.$$

Combining this with the trivial bound $D^*(k) \leq s_{\max}$ in the case $D^*(k) \leq s_{\max}$, and recalling that $D(k) = D^*(k)$ under **BF-IO**, we obtain, for every outcome in $E_{\text{cnt}}(k)$,

$$D(k) \leq \max \{s_{\max}, A^{\text{pre}}(k) - \gamma Bp\}.$$

Since $E_{\text{cnt}}(k)$ is independent of \mathcal{F}_{k-1} , taking conditional probability given \mathcal{F}_{k-1} yields $\mathbb{P}(D(k) \leq \max \{s_{\max}, A^{\text{pre}}(k) - \gamma Bp\} \mid \mathcal{F}_{k-1}) \geq \mathbb{P}(E_{\text{cnt}}(k) \mid \mathcal{F}_{k-1}) \geq 1 - 2G \exp\left(-\frac{\delta^2}{3} Bp\right)$, as claimed. \square

Step 1.B: Concentration of pre-admission spread

We now control $A^{\text{pre}}(k)$ around its conditional baseline $(1 - p)D(k - 1)$.

Define the range functional $r(x) := \max_g x_g - \min_g x_g$ for $x \in \mathbb{R}^G$. For step k , recall that

$$R_g(k) = \sum_{i=1}^B \xi_{g,i}(k)(a_{g,i}(k-1) + 1), \quad \mu_g(k) := \mathbb{E}[R_g(k) \mid \mathcal{F}_{k-1}] = p \sum_{i=1}^B (a_{g,i}(k-1) + 1),$$

and set

$$Z_g(k) := R_g(k) - \mu_g(k), \quad Z(k) := (Z_g(k))_{g=1}^G.$$

The one-step envelope

$$\Lambda(k) := \max_{g,i} a_{g,i}(k-1)$$

is \mathcal{F}_{k-1} -measurable and bounds every summand in $R_g(k)$.

Lemma 3 (One-step concentration of $A^{\text{pre}}(k)$). *For each step $k \geq 1$ and every \mathcal{F}_{k-1} -measurable $\Lambda(k)$, define*

$$\alpha_B := 3 \log(GB), \quad u_A(k) := 8 \Lambda(k) \max \left\{ \sqrt{p(1-p)B\alpha_B}, \alpha_B \right\}.$$

Then, for all $k \geq 1$,

$$\mathbb{P}\left(A^{\text{pre}}(k) - (1-p)D(k-1) > u_A(k) \mid \mathcal{F}_{k-1}\right) \leq 2G e^{-\alpha_B} \leq 2G^{-2}B^{-3}. \quad (\text{C7})$$

Proof of Lemma 3: Given \mathcal{F}_{k-1} , the vector of loads $L(k-1) = (L_g(k-1))_{g=1}^G$ is deterministic, and

$$a_g^{\text{pre}}(k) = L_g(k-1) + B - R_g(k) = (1-p)(L_g(k-1) + B) - Z_g(k).$$

Let $X_g := (1-p)(L_g(k-1) + B)$ and $X := (X_g)_{g=1}^G$. Then

$$A^{\text{pre}}(k) = r(a^{\text{pre}}(k)) = r(X - Z(k)).$$

For any vectors $x, z \in \mathbb{R}^G$, comparing coordinates achieving the maximum and minimum of $x - z$ gives the elementary inequality

$$r(x - z) \leq r(x) + 2\|z\|_\infty,$$

where $\|z\|_\infty := \max_g |z_g|$. Applying this with $x = X$ and $z = Z(k)$, and using $r(X) = (1-p)D(k-1)$, we obtain

$$A^{\text{pre}}(k) - (1-p)D(k-1) = r(X - Z(k)) - r(X) \leq 2\|Z(k)\|_\infty = 2 \max_g |Z_g(k)|.$$

Thus, for any $u > 0$,

$$\mathbb{P}\left(A^{\text{pre}}(k) - (1-p)D(k-1) > u \mid \mathcal{F}_{k-1}\right) \leq \sum_{g=1}^G \mathbb{P}\left(|Z_g(k)| > u/2 \mid \mathcal{F}_{k-1}\right).$$

It remains to control each tail $\mathbb{P}(|Z_g(k)| > u/2 \mid \mathcal{F}_{k-1})$. Conditional on \mathcal{F}_{k-1} , the variables $\{(\xi_{g,i}(k) - p)(a_{g,i}(k-1) + 1)\}_{i=1}^B$ are independent, mean-zero, and bounded in absolute value by $\Lambda(k) + 1 \leq 2\Lambda(k)$. Their conditional variance satisfies

$$\text{Var}\left(\sum_{i=1}^B (\xi_{g,i}(k) - p)(a_{g,i}(k-1) + 1) \mid \mathcal{F}_{k-1}\right) = \sum_{i=1}^B p(1-p) (a_{g,i}(k-1) + 1)^2 \leq p(1-p) B 4\Lambda(k)^2.$$

By Bernstein's inequality for bounded summands, for every g and $u > 0$,

$$\mathbb{P}\left(|Z_g(k)| > u/2 \mid \mathcal{F}_{k-1}\right) \leq 2 \exp\left(-\min\left\{\frac{(u/2)^2}{16p(1-p)B\Lambda(k)^2}, \frac{3(u/2)}{8\Lambda(k)}\right\}\right).$$

Summing over $g = 1, \dots, G$ and recalling the earlier inequality, we obtain

$$\mathbb{P}\left(A^{\text{pre}}(k) - (1-p)D(k-1) > u \mid \mathcal{F}_{k-1}\right) \leq 2G \exp\left(-\min\left\{\frac{(u/2)^2}{16p(1-p)B\Lambda(k)^2}, \frac{3(u/2)}{8\Lambda(k)}\right\}\right).$$

Choosing

$$u = u_A(k) = 8 \Lambda(k) \max \left\{ \sqrt{p(1-p) B \alpha_B}, \alpha_B \right\},$$

forces

$$\frac{(u/2)^2}{16 p(1-p) B \Lambda(k)^2} \geq \alpha_B, \quad \frac{3(u/2)}{8 \Lambda(k)} \geq \alpha_B,$$

so that the minimum in the exponent is at least $2\alpha_B$. This yields

$$\mathbb{P} \left(A^{\text{pre}}(k) - (1-p)D(k-1) > u_A(k) \mid \mathcal{F}_{k-1} \right) \leq 2G e^{-\alpha_B}.$$

With $\alpha_B = 3 \log(GB)$ we have $2G e^{-\alpha_B} \leq 2G^{-2} B^{-3}$, completing the proof. \square

Step 1.C: Average gap bound for BF-IO

We now combine Lemmas 2 and 3 to obtain a uniform bound on the long-run average of $D(k)$. Recall that at each step, the instantaneous imbalance under any policy satisfies

$$\text{Imbalance}(k; \text{BF-IO}) = \sum_{g=1}^G (\max_h L_h(k) - L_g(k)) \leq (G-1) \left(\max_h L_h(k) - \min_h L_h(k) \right) = (G-1) D(k).$$

Lemma 4 (Average gap under geometric outputs for BF-IO). *Let $\delta := 1/(4s_{\max})$, set $\gamma := 1 - \delta(2s_{\max} - 1) \in (0, 1)$, and let $\alpha_B := 3 \log(GB)$. Define*

$$x_{\star}(B, G) := \left\lceil \frac{3}{p} \log(GB) \right\rceil, \quad U_B := 8(s_{\max} + x_{\star}(B, G)) \max \left\{ \sqrt{p(1-p) B \alpha_B}, \alpha_B \right\},$$

and

$$\varepsilon_B := 2G e^{-(\delta^2/3)Bp} + 2G^{-2} B^{-3}.$$

Take B is large enough (depending on (p, s_{\max}, G)) so that

$$\gamma Bp \geq 2U_B. \quad (\text{C8})$$

Then, under the overloaded-arrival regime, the BF-IO policy with $H = 0$ satisfies

$$\limsup_{K \rightarrow \infty} \frac{1}{K} \sum_{k=0}^{K-1} \mathbb{E}[D(k)] \leq \frac{s_{\max}}{p} + o_{B,G}(1), \quad (\text{C9})$$

where $o_{B,G}(1) \geq 0$ depends only on (B, G, p, s_{\max}) and $o_{B,G}(1) \rightarrow 0$ whenever $B, G \rightarrow \infty$ with $\sqrt{G} = o(B)$.

Proof of Lemma 4: Fix B, G , and simplify the notation $x_{\star} := x_{\star}(B, G)$. For each step k define the events

$$E_{\text{cnt}}(k) := \{|c_g(k) - Bp| \leq \delta Bp \ \forall g\}, \quad E_{\text{snap}}(k) := \{\Lambda(k) \leq s_{\max} + x_{\star}\},$$

and

$$E_{\text{dev}}(k) := \{A^{\text{pre}}(k) - (1-p)D(k-1) \leq U_B\}.$$

By Lemma 2,

$$\mathbb{P}(E_{\text{cnt}}(k)^c \mid \mathcal{F}_{k-1}) \leq 2G \exp \left(-\frac{\delta^2}{3} Bp \right),$$

and by Lemma 3 (applied with x_{\star} and using $\Lambda(k) \leq s_{\max} + x_{\star}$ on $E_{\text{snap}}(k)$),

$$\mathbb{P}(E_{\text{dev}}(k)^c \cap E_{\text{snap}}(k) \mid \mathcal{F}_{k-1}) \leq 2G^{-2} B^{-3}.$$

Abbreviate

$$\varepsilon_B := 2G \exp \left(-\frac{\delta^2}{3} Bp \right) + 2G^{-2} B^{-3}.$$

On the “good” event

$$E_{\text{good}}(k) := E_{\text{cnt}}(k) \cap E_{\text{snap}}(k) \cap E_{\text{dev}}(k),$$

we combine Lemma 2 and the bound on $A^{\text{pre}}(k)$ to obtain

$$D(k) \leq \max \left\{ s_{\max}, (1-p)D(k-1) + U_B - \gamma B p \right\}.$$

As $\gamma B p \geq 2U_B$, we have

$$(1-p)D(k-1) + U_B - \gamma B p \leq (1-p)D(k-1) - U_B \leq (1-p)D(k-1),$$

and hence

$$D(k) \leq s_{\max} + (1-p)D(k-1) \quad \text{on } E_{\text{good}}(k). \quad (\text{C10})$$

On the complement $E_{\text{good}}(k)^c$, we use a uniform bound. At the beginning of step k , before completions, every alive request grows by one token and new arrivals have size at most s_{\max} , so

$$\Lambda(k+1) \leq \max\{\Lambda(k) + 1, s_{\max}\} \leq s_{\max} + (\Lambda(k) + 1 - s_{\max})_+.$$

Therefore,

$$B\Lambda(k+1) \leq B(s_{\max} + x_*) + B(\Lambda(k) + 1 - s_{\max} - x_*)_+,$$

and since each device holds B requests after admission, we have

$$D(k) \leq B\Lambda(k+1) \quad \text{on } E_{\text{good}}(k)^c.$$

Combining the two cases and using the union bound $\mathbf{1}_{E_{\text{good}}(k)^c} \leq \mathbf{1}_{E_{\text{cnt}}(k)^c} + \mathbf{1}_{E_{\text{snap}}(k)^c} + \mathbf{1}_{E_{\text{dev}}(k)^c \cap E_{\text{snap}}(k)}$, we obtain the pathwise decomposition

$$\begin{aligned} D(k) &\leq (s_{\max} + (1-p)D(k-1)) \mathbf{1}_{E_{\text{good}}(k)} \\ &\quad + B(s_{\max} + x_*)(\mathbf{1}_{E_{\text{cnt}}(k)^c} + \mathbf{1}_{E_{\text{dev}}(k)^c \cap E_{\text{snap}}(k)} + \mathbf{1}_{E_{\text{snap}}(k)^c}) + B(\Lambda(k) + 1 - s_{\max} - x_*)_+. \end{aligned}$$

Taking conditional expectations given \mathcal{F}_{k-1} and using the bounds on event probabilities, we have

$$\begin{aligned} \mathbb{E}[D(k) | \mathcal{F}_{k-1}] &\leq (s_{\max} + (1-p)D(k-1)) \\ &\quad + \varepsilon_B B(s_{\max} + x_*) + B(s_{\max} + x_*) \mathbb{P}(E_{\text{snap}}(k)^c | \mathcal{F}_{k-1}) \\ &\quad + B \mathbb{E}[(\Lambda(k) + 1 - s_{\max} - x_*)_+ | \mathcal{F}_{k-1}]. \end{aligned} \quad (\text{C11})$$

We use the simple bound, $\mathbf{1}_{\{\Lambda(k) > s_{\max} + x_*\}} \leq (\Lambda(k) + 1 - s_{\max} - x_*)_+$, and hence

$$\mathbb{P}(E_{\text{snap}}(k)^c | \mathcal{F}_{k-1}) \leq \mathbb{E}[(\Lambda(k) + 1 - s_{\max} - x_*)_+ | \mathcal{F}_{k-1}].$$

Substituting into (C11) and taking unconditional expectations yields the one-step inequality

$$\begin{aligned} \mathbb{E}[D(k)] &\leq (s_{\max} + (1-p)\mathbb{E}[D(k-1)]) + \varepsilon_B B(s_{\max} + x_*) \\ &\quad + B(s_{\max} + x_* + 1) \mathbb{E}[(\Lambda(k) + 1 - s_{\max} - x_*)_+]. \end{aligned} \quad (\text{C12})$$

To complete the proof, we bound the horizon average of the envelope term. In any step k , the size of an alive request equals the sum of its prompt length (at most s_{\max}) and the number of tokens it has generated up to step k (its age). Thus $\Lambda(k) - s_{\max}$ is bounded by the maximal age among alive requests at step k . Summing over the horizon and exchanging the order of summation (first over requests, then over the steps they are alive), we obtain

$$\sum_{k=0}^{K-1} (\Lambda(k) + 1 - s_{\max} - x_*)_+ \leq \sum_j \sum_{r=0}^{o_j-1} (r + 1 - x_*)_+,$$

where the outer sum is over all requests j whose lifetime intersects $[0:K-1]$, and o_j is the (geometric) output length of request j . For a single geometric random variable $o_j \sim \text{Geo}(p)$,

$$\mathbb{E}\left[\sum_{r=0}^{o_j-1} (r+1-x_\star)_+\right] = \sum_{r=x_\star+1}^{\infty} (r-x_\star) \mathbb{P}(o_j \geq r) = \sum_{r=x_\star+1}^{\infty} (r-x_\star)(1-p)^{r-1} = \frac{(1-p)^{x_\star}}{p^2}.$$

Let N_K be the number of distinct requests whose lifetime intersects the horizon $[0:K-1]$. At each step there are exactly GB alive items, and each item counted in N_K is alive for at least one step, so deterministically $N_K \leq GBK$ and hence $N_K/K \leq GB$. By linearity of expectation,

$$\frac{1}{K} \sum_{k=0}^{K-1} \mathbb{E}[(\Lambda(k) + 1 - s_{\max} - x_\star)_+] \leq \frac{\mathbb{E}[N_K]}{K} \cdot \frac{(1-p)^{x_\star}}{p^2} \leq GB \frac{(1-p)^{x_\star}}{p^2}.$$

Averaging (C12) over $k = 0, \dots, K-1$ and rearranging, we obtain

$$\begin{aligned} \frac{1}{K} \sum_{k=0}^{K-1} \mathbb{E}[D(k)] &\leq \left(s_{\max} + (1-p) \frac{1}{K} \sum_{k=0}^{K-1} \mathbb{E}[D(k-1)] \right) \\ &\quad + \varepsilon_B B (s_{\max} + x_\star) + \frac{GB^2}{p^2} (s_{\max} + x_\star + 1) (1-p)^{x_\star}. \end{aligned} \quad (\text{C13})$$

The sequence $\{\mathbb{E}[D(k)]\}_{k \geq 0}$ is nonnegative, so its Cesàro average is bounded, and the right-hand side of (C13) is an affine contraction in the horizon average. Letting $K \rightarrow \infty$ and using $(1-p) < 1$, we obtain

$$\limsup_{K \rightarrow \infty} \frac{1}{K} \sum_{k=0}^{K-1} \mathbb{E}[D(k)] \leq \frac{s_{\max} + \varepsilon_B B (s_{\max} + x_\star) + \frac{GB^2}{p^2} (s_{\max} + x_\star + 1) (1-p)^{x_\star}}{p}.$$

Finally, for $x_\star(B, G) = \lceil 3 \log(GB)/p \rceil$, the term $(1-p)^{x_\star}$ decays fast in GB ; more precisely,

$$(1-p)^{x_\star} \leq \exp(-px_\star) \leq (GB)^{-3},$$

so

$$\frac{GB^2}{p^2} (s_{\max} + x_\star + 1) (1-p)^{x_\star} = o_{B,G}(1)$$

whenever $B, G \rightarrow \infty$. Similarly, by definition of ε_B and the assumption $\log G = o(B)$,

$$\varepsilon_B B (s_{\max} + x_\star) = o_{B,G}(1).$$

Absorbing these vanishing terms into $o_{B,G}(1)$, we obtain (C9). This completes the proof of Part 1. \square

Part 2 (Lower Bound of Imbalance of FCFS)

We now analyze the lower bound of average imbalance of the FCFS baseline. Under the overloaded arrival definition, FCFS is size-agnostic: whenever a completion occurs in any slot, the slot is immediately refilled by the earliest pending request, whose prompt length is i.i.d. distributed by the distribution $S = \mathcal{D}_{\text{prefill}}$ with $\mathbb{E}[S] = \mu_s$ and $\text{Var}(S) = \sigma_s^2 > 0$.

Step 2.A: Slot-level recursion and Markov structure.

Index slots by (g, b) with $g \in \{1, \dots, G\}$ and $b \in \{1, \dots, B\}$. Let $Y_{g,b}(k)$ denote the *post-admission* size in slot (g, b) at the end of step k . Under **FCFS**, we have the slot-level recursion

$$Y_{g,b}(k) = (1 - \xi_{g,b}(k))(Y_{g,b}(k-1) + 1) + \xi_{g,b}(k)S_{g,b}(k), \quad k \geq 1, \quad (\text{C14})$$

where, for each (g, b, k) ,

$$\xi_{g,b}(k) \sim \text{Bernoulli}(p), \quad S_{g,b}(k) \stackrel{\text{i.i.d.}}{\sim} S = \mathcal{D}_{\text{prefill}},$$

and all these random variables are mutually independent across (g, b, k) and independent of the initial configuration $\{Y_{g,b}(0)\}$. Thus, for each fixed slot (g, b) , the process $(Y_{g,b}(k))_{k \geq 0}$ is a time-homogeneous Markov chain on \mathbb{N} , and the chains corresponding to different slots evolve independently.

For each device g , the post-admission load at step k is

$$S_g(k) := \sum_{b=1}^B Y_{g,b}(k),$$

and the instantaneous **FCFS** imbalance at step k is

$$\text{Imbalance}(k; \text{FCFS}) := G \cdot \max_{1 \leq g \leq G} S_g(k) - \sum_{g=1}^G S_g(k).$$

By symmetry across devices, for any k and any initial configuration,

$$\mathbb{E}[\text{Imbalance}(k; \text{FCFS})] = G \left(\mathbb{E} \left[\max_g S_g(k) \right] - \mathbb{E}[S_1(k)] \right).$$

Step 2.B: Single-slot stationary law.

Fix a slot (g, b) and suppress the indices. The chain $(Y_k)_{k \geq 0}$ defined by (C14) satisfies, for every measurable $A \subseteq \mathbb{N}$ and $y \in \mathbb{N}$,

$$\mathbb{P}(Y_1 \in A \mid Y_0 = y) = \mathbb{P}((1 - \xi_1)(y + 1) + \xi_1 S_1 \in A) \geq \mathbb{P}(\xi_1 = 1, S_1 \in A) = p \mathbb{P}(S \in A).$$

Thus the transition kernel admits a Doeblin minorization with parameter $p > 0$. In particular, $(Y_k)_{k \geq 0}$ is uniformly ergodic and admits a unique stationary distribution, which we denote by U . To identify U explicitly, it is convenient to track the *age* process:

$$A_k := \text{number of steps elapsed since the current job in the slot started}, \quad k \geq 0.$$

Each time a completion occurs ($\xi_k = 1$), a fresh job with prompt $S_k \sim S$ starts in that slot and the age resets to zero; otherwise, the job survives and the age increases by one. The age process alone evolves via

$$A_{k+1} = \begin{cases} 0, & \text{with probability } p, \\ A_k + 1, & \text{with probability } 1 - p. \end{cases}$$

This is a Markov chain on \mathbb{N} with transition kernel

$$\mathbb{P}(A_{k+1} = 0 \mid A_k = a) = p, \quad \mathbb{P}(A_{k+1} = a + 1 \mid A_k = a) = 1 - p.$$

A direct calculation shows that the geometric distribution

$$A \sim \text{Geo}(p) - 1, \quad \mathbb{P}(A = a) = p(1 - p)^a, \quad a = 0, 1, \dots,$$

is invariant for the age chain:

$$\mathbb{P}(A_{k+1} = a) = p \mathbb{P}(A_k \geq a) = p \sum_{j=a}^{\infty} p(1 - p)^j = p(1 - p)^a = \mathbb{P}(A = a).$$

Since the prompts $\{S_k\}$ are i.i.d. and independent of the completions $\{\xi_k\}$, in stationarity the prompt of the current job S_{cur} and the age A are independent, with $S_{\text{cur}} \stackrel{d}{=} S$ and $A \sim \text{Geo}(p) - 1$. At a stationary snapshot, the slot size U has the representation

$$U \stackrel{d}{=} S_{\text{cur}} + A, \quad S_{\text{cur}} \stackrel{d}{=} S, \quad A \sim \text{Geo}(p) - 1, \quad S_{\text{cur}} \perp\!\!\!\perp A.$$

Consequently,

$$\mu_U := \mathbb{E}[U] = \mu_s + \frac{1-p}{p}, \quad \sigma_{\text{snap}}^2 := \text{Var}(U) = \sigma_s^2 + \frac{1-p}{p^2}. \quad (\text{C15})$$

Because S is bounded and A has geometric tails, U has finite moments of all orders, in particular $\mathbb{E}[|U|^3] < \infty$.

Step 2.C: Device-level loads at stationarity.

Since the slot chains are independent and identically distributed, and their transition kernels do not couple different slots, the stationary distribution of the entire collection $\{Y_{g,b}(k)\}_{g,b}$ is the product measure under which all $Y_{g,b}$ are i.i.d. with law U . Let $(U_{g,b})_{g,b}$ be i.i.d. copies of U and define the stationary per-device loads

$$S_g^{\text{st}} := \sum_{b=1}^B U_{g,b}, \quad g = 1, \dots, G.$$

Then $\{S_g^{\text{st}}\}_{g=1}^G$ are i.i.d. with

$$\mathbb{E}[S_g^{\text{st}}] = \mu_U B, \quad \text{Var}(S_g^{\text{st}}) = \sigma_{\text{snap}}^2 B.$$

We now invoke the same Berry–Esseen and extreme-value argument as in the homogeneous-output case, but with U replacing s . Define the standardized sums

$$W_g := \frac{S_g^{\text{st}} - \mu_U B}{\sigma_{\text{snap}} \sqrt{B}}, \quad g = 1, \dots, G.$$

Because U has finite third absolute moment, the Berry–Esseen theorem (for sums of i.i.d. real variables) guarantees the existence of a universal constant C_{BE} such that

$$\sup_{x \in \mathbb{R}} \left| \mathbb{P}(W_g \leq x) - \Phi(x) \right| \leq \frac{C_{\text{BE}}}{\sqrt{B}},$$

for each g , where Φ is the standard normal distribution function.

Set $z_G := \sqrt{\frac{\log G}{2}}$ and consider the threshold z_G . For a standard normal $Z \sim N(0, 1)$ and all sufficiently large G (say $\log G \geq 4$), the Gaussian tail bound implies

$$\mathbb{P}(Z \geq z_G) \geq \frac{1}{\sqrt{2\pi}} \left(\frac{1}{z_G} - \frac{1}{z_G^3} \right) \exp\left(-\frac{z_G^2}{2}\right) \geq \frac{1}{2\sqrt{2\pi} z_G} G^{-1/4}.$$

Combining this with Berry–Esseen, we obtain

$$\mathbb{P}(W_g \geq z_G) \geq \frac{1}{2\sqrt{2\pi} z_G} G^{-1/4} - \frac{C_{\text{BE}}}{\sqrt{B}}.$$

Since $\sqrt{G} = \tilde{o}(B)$, there exists $B_0(G)$ such that, for all $B \geq B_0(G)$,

$$\frac{C_{\text{BE}}}{\sqrt{B}} \leq \frac{1}{2} \cdot \frac{1}{2\sqrt{2\pi} z_G} G^{-1/4},$$

and hence

$$\mathbb{P}(W_g \geq z_G) \geq \frac{1}{4\sqrt{2\pi} z_G} G^{-1/4} =: p_G. \quad (\text{C16})$$

By independence across g , we have

$$\mathbb{P}\left(\max_{1 \leq g \leq G} W_g \geq z_G\right) \geq 1 - (1 - p_G)^G.$$

Using the inequality $1 - x \leq e^{-x}$ for $x \geq 0$, we find

$$1 - (1 - p_G)^G \geq 1 - \exp(-Gp_G).$$

From (C16), $Gp_G \geq \frac{1}{4\sqrt{2\pi}z_G}G^{3/4}$, which is bounded away from zero for every fixed $G \geq 2$.

Thus, there exists a universal constant $c_1 \in (0, 1)$ (for instance $c_1 := 1 - e^{-1/(4\sqrt{2\pi})}$) such that

$$\mathbb{P}\left(\max_{1 \leq g \leq G} W_g \geq z_G\right) \geq c_1 \quad \text{for all } \log G \geq 4 \text{ and all } B \geq B_0(G).$$

Finally, for any $t > 0$,

$$\mathbb{E}\left[\max_{1 \leq g \leq G} S_g^{\text{st}}\right] = \mu_U B + \mathbb{E}\left[\max_{1 \leq g \leq G} (S_g^{\text{st}} - \mu_U B)\right] \geq \mu_U B + t \mathbb{P}\left(\max_g (S_g^{\text{st}} - \mu_U B) \geq t\right).$$

Choosing $t := \sigma_{\text{snap}}\sqrt{B}z_G$, so that the event $\{\max_g (S_g^{\text{st}} - \mu_U B) \geq t\}$ coincides with $\{\max_g W_g \geq z_G\}$, we obtain

$$\mathbb{E}\left[\max_{1 \leq g \leq G} S_g^{\text{st}}\right] \geq \mu_U B + \sigma_{\text{snap}}\sqrt{B}z_G c_1 = \mu_U B + c' \sigma_{\text{snap}} \sqrt{B \log G},$$

for some absolute constant $c' > 0$. Since $\mathbb{E}[\sum_{g=1}^G S_g^{\text{st}}] = G\mu_U B$, the stationary expected imbalance under FCFS satisfies

$$\mathbb{E}[\text{Imbalance}^{\text{st}}] := \mathbb{E}\left[G \max_g S_g^{\text{st}} - \sum_{g=1}^G S_g^{\text{st}}\right] \geq c' G \sigma_{\text{snap}} \sqrt{B \log G}, \quad (\text{C17})$$

for all $G \geq 2$ and all $B \geq B_0(G)$, where $B_0(G)$ is as above.

Step 2.D: Time-average imbalance under FCFS.

The global collection of slot loads

$$Y(k) := (Y_{g,b}(k))_{g \in [G], b \in [B]}$$

is a Markov chain on \mathbb{N}^{GB} with transition kernel induced by (C14). By the Doeblin minorization on each coordinate, the product chain is uniformly ergodic and admits the unique stationary distribution Π , which is precisely the product law of i.i.d. copies of U . Moreover, by uniform ergodicity, for any initial configuration $Y(0)$ and any integrable function f ,

$$\lim_{k \rightarrow \infty} \mathbb{E}[f(Y(k))] = \mathbb{E}_{\Pi}[f(Y)].$$

Applying this to $f(Y) = \text{Imbalance}(k; \text{FCFS})$, which has finite second moment under Π in view of (C15), we deduce that

$$\lim_{k \rightarrow \infty} \mathbb{E}[\text{Imbalance}(k; \text{FCFS})] = \mathbb{E}[\text{Imbalance}^{\text{st}}].$$

By Cesàro averaging, it follows that the long-run expected time-average imbalance under FCFS,

$$\text{AvgImbalance}(\text{FCFS}; \mathcal{I}) := \lim_{K \rightarrow \infty} \frac{1}{K} \sum_{k=0}^{K-1} \mathbb{E}[\text{Imbalance}(k; \text{FCFS})],$$

exists and equals the stationary expectation $\mathbb{E}[\text{Imbalance}^{\text{st}}]$, independently of the arrival instance \mathcal{I} and the initial configuration. Combining with (C17), we obtain

$$\text{AvgImbalance}(\text{FCFS}; \mathcal{I}) \geq c' G \sigma_{\text{snap}} \sqrt{B \log G}, \quad \sigma_{\text{snap}}^2 = \sigma_s^2 + \frac{1-p}{p^2}, \quad (\text{C18})$$

for all $G \geq 2$ and all B sufficiently large, uniformly over all overloaded arrival instances \mathcal{I} .

Part 3: BF-IO vs. FCFS

We now combine the BF-IO average-gap bound from Lemma 4 with the FCFS lower bound (C18) to obtain the imbalance-reduction rate in the geometric-output setting. By Lemma 4, for any overloaded arrival instance \mathcal{I} we have

$$\limsup_{K \rightarrow \infty} \frac{1}{K} \sum_{k=0}^{K-1} \mathbb{E}[D(k)] \leq \frac{s_{\max}}{p} + o_{B,G}(1), \quad \text{with } o_{B,G}(1) \rightarrow 0 \text{ as } B, G \rightarrow \infty.$$

Since, for every step k and any policy,

$$\text{Imbalance}(k; \text{BF-IO}) = \sum_{g=1}^G \left(\max_h L_h(k) - L_g(k) \right) \leq (G-1) D(k),$$

it follows that

$$\text{AvgImbalance}(\text{BF-IO}; \mathcal{I}) = \limsup_{K \rightarrow \infty} \frac{1}{K} \sum_{k=0}^{K-1} \mathbb{E}[\text{Imbalance}(k; \text{BF-IO})] \leq (G-1) \frac{s_{\max}}{p} + o_{B,G}(1),$$

with the same $o_{B,G}(1)$.

On the other hand, by (C18), for every overloaded arrival instance \mathcal{I} ,

$$\text{AvgImbalance}(\text{FCFS}; \mathcal{I}) \geq c' G \sigma_{\text{snap}} \sqrt{B \log G}, \quad \sigma_{\text{snap}}^2 = \sigma_s^2 + \frac{1-p}{p^2},$$

for some universal constant $c' > 0$ and all B sufficiently large. Therefore, for every such \mathcal{I} ,

$$\frac{\text{AvgImbalance}(\text{FCFS}; \mathcal{I})}{\text{AvgImbalance}(\text{BF-IO}; \mathcal{I})} \gtrsim \frac{G \sigma_{\text{snap}} \sqrt{B \log G}}{(G-1) s_{\max} / p} = c \frac{p \sigma_{\text{snap}}}{s_{\max}} \cdot \frac{G}{G-1} \sqrt{B \log G},$$

for a possibly smaller universal constant $c > 0$, where we absorb the $o_{B,G}(1)$ term into c for B large enough. Since $\sigma_{\text{snap}} \geq \sqrt{1-p}/p$, the prefactor $\frac{p \sigma_{\text{snap}}}{s_{\max}}$ is strictly positive (up to the fixed scale s_{\max}), and the scaling $\sqrt{B \log G}$ is inherited from the FCFS lower bound. Taking the infimum over all overloaded arrival instances \mathcal{I} completes the proof. \square

C.3 Proof of Theorem 3

Proof of Theorem 3 We work on a probability space $(\Omega, \mathcal{F}, \mathbb{P})$ that supports the arrival instance \mathcal{I} , the prefill lengths $\mathcal{D}_{\text{prefill}}$, the geometric decode lengths $\mathcal{D}_{\text{decode}} = \text{Geo}(p)$, and the completion indicators. For each step $k \in \mathbb{N}$ we define the *natural filtration*

$$\mathcal{F}_k := \sigma(\text{all arrivals, prefill, decode lengths, completions, and BF-IO assignments up to step } k),$$

and write $\mathbb{E}[\cdot | \mathcal{F}_k]$ for conditional expectations.

At the end of step $k-1$ (after BF-IO admission at that step), each device $g \in \{1, \dots, G\}$ holds exactly B active requests, indexed by $i = 1, \dots, B$, with sizes $a_{g,i}(k-1) \in \mathbb{N}$ (including prompt tokens and already generated output tokens). Let

$$L_g(k-1) := \sum_{i=1}^B a_{g,i}(k-1), \quad D(k-1) := \max_g L_g(k-1) - \min_g L_g(k-1),$$

and

$$\Lambda(k) := \max_{g,i} a_{g,i}(k-1),$$

be, respectively, the device loads, the inter-device gap, and the one-step envelope at the end of step $k-1$. These quantities are \mathcal{F}_{k-1} -measurable.

At the beginning of step k , every active request grows by exactly δ_k units of workload and then completes independently with probability p at the end of the step. Let $\xi_{g,i}(k) \sim \text{Bernoulli}(p)$ be the completion indicator of slot (g, i) in step k , independent of \mathcal{F}_{k-1} and across (g, i) . The number of completions (free slots) on device g in step k is

$$c_g(k) := \sum_{i=1}^B \xi_{g,i}(k) \sim \text{Binomial}(B, p),$$

independent across g and of \mathcal{F}_{k-1} , and we write $C_k := \sum_{g=1}^G c_g(k)$ for the total number of completions.

Before admitting new requests at step k , the total *pre-admission* load on device g is

$$a_g^{\text{pre}}(k) := L_g(k-1) + B\delta_k - R_g(k), \quad R_g(k) := \sum_{i=1}^B \xi_{g,i}(k)(a_{g,i}(k-1) + \delta_k),$$

where $R_g(k)$ is the load removed by completions in step k . The corresponding pre-admission spread is

$$A^{\text{pre}}(k) := \max_g a_g^{\text{pre}}(k) - \min_g a_g^{\text{pre}}(k).$$

After BF-IO admission at step k , we write $L_g(k)$ for the post-admission loads and

$$D(k) := \max_g L_g(k) - \min_g L_g(k)$$

for the post-admission gap. Finally, we set

$$\Lambda(k+1) := \max_{g,i} a_{g,i}(k),$$

the one-step envelope at the end of step k . By construction, $L_g(k)$, $D(k)$, and $\Lambda(k+1)$ are \mathcal{F}_k -measurable.

Part 1 (Upper Bound of Imbalance of BF-IO)

Step 1.A: Separation and one-step drift

The first lemma is a geometric statement about the BF-IO assignment at step k . Note that its proof does not depend on the specific value of δ_k , only on prompt sizes and completion counts.

Lemma 5 (Separation and gap reduction). *Fix $\delta \in (0, (2s_{\max} - 1)^{-1})$ and set*

$$\gamma := 1 - \delta(2s_{\max} - 1) \in (0, 1).$$

Then, for every $k \geq 1$,

$$\mathbb{P}\left(D(k) \leq \max\{s_{\max}, A^{\text{pre}}(k) - \gamma Bp\} \mid \mathcal{F}_{k-1}\right) \geq 1 - 2G \exp\left(-\frac{\delta^2}{3} Bp\right). \quad (\text{C19})$$

Proof of Lemma 5 Fix a step k and condition on \mathcal{F}_{k-1} . Given \mathcal{F}_{k-1} , the collection of sizes $\{a_{g,i}(k-1)\}$ and loads $\{L_g(k-1)\}$ is deterministic, and the randomness at step k comes only from the completion indicators $\{\xi_{g,i}(k)\}$ and the prompt lengths of newly admitted requests. Define

$$E_{\text{cnt}}(k) := \{|c_g(k) - Bp| \leq \delta Bp \text{ for all } g \in \{1, \dots, G\}\}.$$

The event $E_{\text{cnt}}(k)$ depends only on $\{\xi_{g,i}(k)\}$ and thus is independent of \mathcal{F}_{k-1} . By a standard Chernoff bound for binomial variables,

$$\mathbb{P}(E_{\text{cnt}}(k)^c \mid \mathcal{F}_{k-1}) = \mathbb{P}(E_{\text{cnt}}(k)^c) \leq 2G \exp\left(-\frac{\delta^2}{3} Bp\right).$$

On the event $E_{\text{cnt}}(k)$, we have

$$c_{\min}(k) := \min_g c_g(k) \geq (1 - \delta)Bp, \quad c_{\max}(k) := \max_g c_g(k) \leq (1 + \delta)Bp.$$

Fix an outcome $\omega \in E_{\text{cnt}}(k)$ and consider deterministically the BF-IO assignment at step k on that outcome. Let $S_g(k)$ denote the multiset of prompt sizes of the new requests admitted to device g at step k ; by construction $|S_g(k)| = c_g(k)$, and

$$L_g(k) = a_g^{\text{pre}}(k) + \sum_{s \in S_g(k)} s.$$

For each feasible family of multisets $\{S_g(k)\}_{g=1}^G$ with $|S_g(k)| = c_g(k)$, define

$$L_g(k) := a_g^{\text{pre}}(k) + \sum_{s \in S_g(k)} s, \quad D(k) := \max_g L_g(k) - \min_g L_g(k).$$

Among all such assignments, BF-IO chooses one that minimizes $D(k)$. Let $\{S_g^*(k)\}$ be such a minimizer, and let

$$L_g^*(k) := a_g^{\text{pre}}(k) + \sum_{s \in S_g^*(k)} s, \quad D^*(k) := \max_g L_g^*(k) - \min_g L_g^*(k),$$

denote the corresponding loads and gap. If $D^*(k) \leq s_{\max}$, then $D(k) = D^*(k) \leq s_{\max}$ and the claimed inequality (C19) holds trivially on this outcome. Hence it suffices to analyze the case $D^*(k) > s_{\max}$.

Let $p \in \arg \max_g L_g^*(k)$ and $q \in \arg \min_g L_g^*(k)$, so that

$$L_p^*(k) - L_q^*(k) = D^*(k) > s_{\max}.$$

We first show that, under this strict gap and the optimality of $\{S_g^*(k)\}$, the assignment must be “separated” between any such heavy–light pair (p, q) : there exists an integer $\theta \in \{0, \dots, s_{\max} - 1\}$ such that

$$s \leq \theta \quad \text{for all } s \in S_p^*(k), \quad s \geq \theta + 1 \quad \text{for all } s \in S_q^*(k).$$

Suppose not. Then there exist $x \in S_p^*(k)$ and $y \in S_q^*(k)$ with $x > y$. Consider the assignment $\{\tilde{S}_g(k)\}$ obtained by swapping x and y between devices p and q ,

$$\tilde{S}_p(k) := (S_p^*(k) \setminus \{x\}) \cup \{y\}, \quad \tilde{S}_q(k) := (S_q^*(k) \setminus \{y\}) \cup \{x\},$$

and $\tilde{S}_r(k) := S_r^*(k)$ for all $r \notin \{p, q\}$. This swap preserves $|S_g(k)| = c_g(k)$ for every g and uses only jobs from the waiting pool (by the overloaded definition of \mathcal{I} , the pool contains sufficiently many jobs of each size to support such exchanges). The new loads are

$$\tilde{L}_p(k) = a_p^{\text{pre}}(k) + \sum_{s \in \tilde{S}_p(k)} s = L_p^*(k) - (x - y) < L_p^*(k),$$

and

$$\tilde{L}_q(k) = a_q^{\text{pre}}(k) + \sum_{s \in \tilde{S}_q(k)} s = L_q^*(k) + (x - y) \leq L_q^*(k) + s_{\max} < L_p^*(k),$$

using $x - y \leq s_{\max}$ and $L_p^*(k) - L_q^*(k) > s_{\max}$. All other loads $\tilde{L}_r(k)$ equal $L_r^*(k) \leq L_p^*(k)$.

If p is the unique maximizer of $\{L_g^*(k)\}$, then

$$\max_g \tilde{L}_g(k) < \max_g L_g^*(k),$$

contradicting the minimality of $D^*(k)$. If there are multiple maximizers, then the swap strictly reduces the number of devices attaining the maximum load while keeping the maximum value

at most $L_p^*(k)$. Repeating this argument finitely many times, we either strictly reduce the maximum load or obtain a contradiction to the choice of $\{S_g^*(k)\}$ as a minimizer with minimal number of maximizers. Hence no such pair (x, y) can exist, and the desired threshold θ exists.

Condition on $E_{\text{cnt}}(k)$ and fix an outcome with $D^*(k) > s_{\max}$. Using the separation property, for device p every $s \in S_p^*(k)$ satisfies $s \leq \theta$, while for q every $s \in S_q^*(k)$ satisfies $s \geq \theta + 1$. Therefore,

$$\sum_{s \in S_p^*(k)} s \leq \theta c_p(k), \quad \sum_{s \in S_q^*(k)} s \geq (\theta + 1) c_q(k),$$

and hence

$$\begin{aligned} D^*(k) &= L_p^*(k) - L_q^*(k) \\ &= \left(a_p^{\text{pre}}(k) + \sum_{s \in S_p^*(k)} s \right) - \left(a_q^{\text{pre}}(k) + \sum_{s \in S_q^*(k)} s \right) \\ &\leq a_p^{\text{pre}}(k) - a_q^{\text{pre}}(k) + \theta c_p(k) - (\theta + 1) c_q(k). \end{aligned}$$

Using $c_p(k) \leq c_{\max}(k)$ and $c_q(k) \geq c_{\min}(k)$, we obtain

$$\begin{aligned} \theta c_p(k) - (\theta + 1) c_q(k) &\leq \theta c_{\max}(k) - (\theta + 1) c_{\min}(k) \leq \theta(1 + \delta) Bp - (\theta + 1)(1 - \delta) Bp \\ &= Bp(\theta(1 + \delta) - (\theta + 1)(1 - \delta)) = Bp(-1 + \delta(2\theta + 1)) \\ &\leq Bp(-1 + \delta(2s_{\max} - 1)) = -\gamma Bp, \end{aligned}$$

where we used $\theta \leq s_{\max} - 1$ and the definition of γ . Consequently,

$$D^*(k) \leq a_p^{\text{pre}}(k) - a_q^{\text{pre}}(k) - \gamma Bp \leq A^{\text{pre}}(k) - \gamma Bp.$$

Combining this with the trivial bound $D^*(k) \leq s_{\max}$ in the case $D^*(k) \leq s_{\max}$, and recalling that $D(k) = D^*(k)$ under **BF-IO**, we obtain, for every outcome in $E_{\text{cnt}}(k)$,

$$D(k) \leq \max \{s_{\max}, A^{\text{pre}}(k) - \gamma Bp\}.$$

Since $E_{\text{cnt}}(k)$ is independent of \mathcal{F}_{k-1} , taking conditional probability given \mathcal{F}_{k-1} yields

$$\mathbb{P}(D(k) \leq \max \{s_{\max}, A^{\text{pre}}(k) - \gamma Bp\} \mid \mathcal{F}_{k-1}) \geq \mathbb{P}(E_{\text{cnt}}(k) \mid \mathcal{F}_{k-1}) \geq 1 - 2G \exp\left(-\frac{\delta^2}{3} Bp\right),$$

which is (C19). \square

Step 1.B: Concentration of pre-admission spread

We now control $A^{\text{pre}}(k)$ around its conditional baseline $(1 - p)D(k - 1)$, taking into account the general per-step increments $\{\delta_k\}$.

Define the range functional $r(x) := \max_g x_g - \min_g x_g$ for $x \in \mathbb{R}^G$. For step k , recall that

$$R_g(k) = \sum_{i=1}^B \xi_{g,i}(k)(a_{g,i}(k-1) + \delta_k), \quad \mu_g(k) := \mathbb{E}[R_g(k) \mid \mathcal{F}_{k-1}] = p \sum_{i=1}^B (a_{g,i}(k-1) + \delta_k),$$

and set

$$Z_g(k) := R_g(k) - \mu_g(k), \quad Z(k) := (Z_g(k))_{g=1}^G.$$

The one-step envelope

$$\Lambda(k) := \max_{g,i} a_{g,i}(k-1)$$

is \mathcal{F}_{k-1} -measurable. As $0 \leq \delta_k \leq \delta_{\max}$, each summand $(\xi_{g,i}(k) - p)(a_{g,i}(k-1) + \delta_k)$ is bounded in absolute value by $\Lambda(k) + \delta_{\max}$.

Lemma 6 (One-step concentration of $A^{\text{pre}}(k)$ under general increments). *For each step $k \geq 1$ and every \mathcal{F}_{k-1} -measurable $\Lambda(k)$, define*

$$\alpha_B := 3 \log(GB), \quad \tilde{\Lambda}(k) := \Lambda(k) + \delta_{\max}, \quad u_A(k) := C_0 \tilde{\Lambda}(k) \max \left\{ \sqrt{p(1-p)B\alpha_B}, \alpha_B \right\},$$

where $C_0 > 0$ is a universal numerical constant. Then, for all $k \geq 1$,

$$\mathbb{P} \left(A^{\text{pre}}(k) - (1-p)D(k-1) > u_A(k) \mid \mathcal{F}_{k-1} \right) \leq 2G e^{-\alpha_B} \leq 2G^{-2} B^{-3}. \quad (\text{C20})$$

Proof of Lemma 6 Given \mathcal{F}_{k-1} , the vector of loads $L(k-1) = (L_g(k-1))_{g=1}^G$ is deterministic, and

$$a_g^{\text{pre}}(k) = L_g(k-1) + B\delta_k - R_g(k) = (1-p)(L_g(k-1) + B\delta_k) - Z_g(k).$$

Let $X_g := (1-p)(L_g(k-1) + B\delta_k)$ and $X := (X_g)_{g=1}^G$. Then

$$A^{\text{pre}}(k) = r(a^{\text{pre}}(k)) = r(X - Z(k)).$$

For any vectors $x, z \in \mathbb{R}^G$, comparing coordinates achieving the maximum and minimum of $x - z$ gives the elementary inequality

$$r(x - z) \leq r(x) + 2\|z\|_\infty,$$

where $\|z\|_\infty := \max_g |z_g|$. Applying this with $x = X$ and $z = Z(k)$, and noting that $r(X) = (1-p)D(k-1)$ (since adding the common offset $(1-p)B\delta_k$ to all coordinates does not change the range), we obtain

$$A^{\text{pre}}(k) - (1-p)D(k-1) = r(X - Z(k)) - r(X) \leq 2\|Z(k)\|_\infty = 2 \max_g |Z_g(k)|.$$

Thus, for any $u > 0$,

$$\mathbb{P} \left(A^{\text{pre}}(k) - (1-p)D(k-1) > u \mid \mathcal{F}_{k-1} \right) \leq \sum_{g=1}^G \mathbb{P} \left(|Z_g(k)| > u/2 \mid \mathcal{F}_{k-1} \right).$$

It remains to control each tail $\mathbb{P}(|Z_g(k)| > u/2 \mid \mathcal{F}_{k-1})$. Conditional on \mathcal{F}_{k-1} , the variables

$$X_{g,i}(k) := (\xi_{g,i}(k) - p)(a_{g,i}(k-1) + \delta_k), \quad i = 1, \dots, B,$$

are independent, mean-zero, and bounded in absolute value by $\tilde{\Lambda}(k) = \Lambda(k) + \delta_{\max}$. Their conditional variance satisfies

$$\text{Var} \left(\sum_{i=1}^B X_{g,i}(k) \mid \mathcal{F}_{k-1} \right) = \sum_{i=1}^B p(1-p)(a_{g,i}(k-1) + \delta_k)^2 \leq p(1-p)B\tilde{\Lambda}(k)^2.$$

By Bernstein's inequality for bounded summands, there exists a universal constant $C_1 > 0$ such that, for every g and $u > 0$,

$$\mathbb{P} \left(|Z_g(k)| > u/2 \mid \mathcal{F}_{k-1} \right) \leq 2 \exp \left(-C_1 \min \left\{ \frac{(u/2)^2}{p(1-p)B\tilde{\Lambda}(k)^2}, \frac{u/2}{\tilde{\Lambda}(k)} \right\} \right).$$

Summing over $g = 1, \dots, G$ and recalling the earlier inequality, we obtain

$$\mathbb{P} \left(A^{\text{pre}}(k) - (1-p)D(k-1) > u \mid \mathcal{F}_{k-1} \right) \leq 2G \exp \left(-C_1 \min \left\{ \frac{(u/2)^2}{p(1-p)B\tilde{\Lambda}(k)^2}, \frac{u/2}{\tilde{\Lambda}(k)} \right\} \right).$$

Choosing

$$u = u_A(k) = C_0 \tilde{\Lambda}(k) \max \left\{ \sqrt{p(1-p)B\alpha_B}, \alpha_B \right\},$$

with C_0 sufficiently large (depending only on C_1), forces

$$\frac{(u/2)^2}{p(1-p)B\tilde{\Lambda}(k)^2} \geq 2\alpha_B, \quad \frac{u}{2\tilde{\Lambda}(k)} \geq 2\alpha_B,$$

so that the minimum in the exponent is at least $2\alpha_B$. This yields

$$\mathbb{P}\left(A^{\text{pre}}(k) - (1-p)D(k-1) > u_A(k) \mid \mathcal{F}_{k-1}\right) \leq 2Ge^{-\alpha_B}.$$

With $\alpha_B = 3\log(GB)$ we have $2Ge^{-\alpha_B} \leq 2G^{-2}B^{-3}$, completing the proof. \square

Step 1.C: Average gap bound for BF-IO under general per-step growth

We now combine Lemmas 5 and 6 to obtain a uniform bound on the long-run average of $D(k)$ when per-step growth is governed by (δ_k) so that $0 \leq \delta_k \leq \delta_{\max}$. As before, at each step the instantaneous imbalance under any policy satisfies

$$\text{Imbalance}(k; \text{BF-IO}) = \sum_{g=1}^G \left(\max_h L_h(k) - L_g(k) \right) \leq (G-1) \left(\max_h L_h(k) - \min_h L_h(k) \right) = (G-1) D(k).$$

Lemma 7 (Average gap under geometric outputs with general increments). *Let $\delta := 1/(4s_{\max})$, set $\gamma := 1 - \delta(2s_{\max} - 1) \in (0, 1)$, and let $\alpha_B := 3\log(GB)$. Define*

$$x_{\star}(B, G) := \left\lceil \frac{3}{p} \log(GB) \right\rceil, \quad U_B := C_2 (s_{\max} + x_{\star}(B, G) + \delta_{\max}) \max \left\{ \sqrt{p(1-p)B\alpha_B}, \alpha_B \right\},$$

and

$$\varepsilon_B := 2G e^{-(\delta^2/3)Bp} + 2G^{-2}B^{-3},$$

for a universal constant $C_2 > 0$. Assume B is large enough (depending on $(p, s_{\max}, \delta_{\max}, G)$) so that

$$\gamma Bp \geq 2U_B. \quad (\text{C21})$$

Then, the BF-IO policy with $H = 0$ satisfies

$$\limsup_{K \rightarrow \infty} \frac{1}{K} \sum_{k=0}^{K-1} \mathbb{E}[D(k)] \leq \frac{s_{\max}}{p} + o_{B,G}(1), \quad (\text{C22})$$

where $o_{B,G}(1) \geq 0$ depends only on $(B, G, p, s_{\max}, \delta_{\max})$ and $o_{B,G}(1) \rightarrow 0$ whenever $B, G \rightarrow \infty$ with $\sqrt{G} \log G = o(B)$.

Proof Fix B, G , and write $x_{\star} := x_{\star}(B, G)$. For each step k define the events

$$E_{\text{cnt}}(k) := \{ |c_g(k) - Bp| \leq \delta Bp \ \forall g\}, \quad E_{\text{snap}}(k) := \{ \Lambda(k) \leq s_{\max} + x_{\star} \},$$

and

$$E_{\text{dev}}(k) := \{ A^{\text{pre}}(k) - (1-p)D(k-1) \leq U_B \}.$$

By Lemma 5,

$$\mathbb{P}(E_{\text{cnt}}(k)^c \mid \mathcal{F}_{k-1}) \leq 2G \exp\left(-\frac{\delta^2}{3}Bp\right),$$

and by Lemma 6 (applied with $\tilde{\Lambda}(k) = \Lambda(k) + \delta_{\max}$ and using $\Lambda(k) \leq s_{\max} + x_{\star}$ on $E_{\text{snap}}(k)$),

$$\mathbb{P}(E_{\text{dev}}(k)^c \cap E_{\text{snap}}(k) \mid \mathcal{F}_{k-1}) \leq 2G^{-2}B^{-3},$$

provided C_2 is chosen large enough so that U_B dominates the bound $u_A(k)$ from Lemma 6 on $E_{\text{snap}}(k)$. Abbreviate

$$\varepsilon_B := 2G \exp\left(-\frac{\delta^2}{3}Bp\right) + 2G^{-2}B^{-3}.$$

On the “good” event

$$E_{\text{good}}(k) := E_{\text{cnt}}(k) \cap E_{\text{snap}}(k) \cap E_{\text{dev}}(k),$$

we combine Lemma 5 and the bound on $A^{\text{pre}}(k)$ to obtain

$$D(k) \leq \max \left\{ s_{\max}, (1-p)D(k-1) + U_B - \gamma B p \right\}.$$

Under (C21), $\gamma B p \geq 2U_B$, so

$$(1-p)D(k-1) + U_B - \gamma B p \leq (1-p)D(k-1) - U_B \leq (1-p)D(k-1),$$

and hence

$$D(k) \leq s_{\max} + (1-p)D(k-1) \quad \text{on } E_{\text{good}}(k). \quad (\text{C23})$$

On the complement $E_{\text{good}}(k)^c$, we use a uniform bound. At the beginning of step k , before completions, every alive request grows by $\delta_k \leq \delta_{\max}$ and new arrivals have size at most s_{\max} , so

$$\Lambda(k+1) \leq \max\{\Lambda(k) + \delta_k, s_{\max}\} \leq s_{\max} + (\Lambda(k) + \delta_{\max} - s_{\max})_+.$$

Therefore,

$$B \Lambda(k+1) \leq B(s_{\max} + x_{\star} + \delta_{\max}) + B(\Lambda(k) + \delta_{\max} - s_{\max} - x_{\star})_+,$$

and since each device holds B requests after admission, we have

$$D(k) \leq B \Lambda(k+1) \quad \text{on } E_{\text{good}}(k)^c.$$

Combining the two cases and using the union bound $\mathbf{1}_{E_{\text{good}}(k)^c} \leq \mathbf{1}_{E_{\text{cnt}}(k)^c} + \mathbf{1}_{E_{\text{snap}}(k)^c} + \mathbf{1}_{E_{\text{dev}}(k)^c \cap E_{\text{snap}}(k)}$, we obtain the pathwise decomposition

$$\begin{aligned} D(k) &\leq (s_{\max} + (1-p)D(k-1)) \mathbf{1}_{E_{\text{good}}(k)} \\ &\quad + B(s_{\max} + x_{\star} + \delta_{\max})(\mathbf{1}_{E_{\text{cnt}}(k)^c} + \mathbf{1}_{E_{\text{dev}}(k)^c \cap E_{\text{snap}}(k)} + \mathbf{1}_{E_{\text{snap}}(k)^c}) \\ &\quad + B(\Lambda(k) + \delta_{\max} - s_{\max} - x_{\star})_+. \end{aligned}$$

Taking conditional expectations given \mathcal{F}_{k-1} and using the bounds on event probabilities, we have

$$\begin{aligned} \mathbb{E}[D(k) | \mathcal{F}_{k-1}] &\leq (s_{\max} + (1-p)D(k-1)) \\ &\quad + \varepsilon_B B(s_{\max} + x_{\star} + \delta_{\max}) + B(s_{\max} + x_{\star} + \delta_{\max}) \mathbb{P}(E_{\text{snap}}(k)^c | \mathcal{F}_{k-1}) \\ &\quad + B \mathbb{E}[(\Lambda(k) + \delta_{\max} - s_{\max} - x_{\star})_+ | \mathcal{F}_{k-1}]. \end{aligned} \quad (\text{C24})$$

We use the simple bound $\mathbf{1}_{\{\Lambda(k) > s_{\max} + x_{\star}\}} \leq (\Lambda(k) + \delta_{\max} - s_{\max} - x_{\star})_+$, and hence

$$\mathbb{P}(E_{\text{snap}}(k)^c | \mathcal{F}_{k-1}) \leq \mathbb{E}[(\Lambda(k) + \delta_{\max} - s_{\max} - x_{\star})_+ | \mathcal{F}_{k-1}].$$

Substituting into (C24) and taking unconditional expectations yields the one-step inequality

$$\begin{aligned} \mathbb{E}[D(k)] &\leq s_{\max} + (1-p)\mathbb{E}[D(k-1)] + \varepsilon_B B(s_{\max} + x_{\star} + \delta_{\max}) \\ &\quad + B(s_{\max} + x_{\star} + \delta_{\max}) \mathbb{E}[(\Lambda(k) + \delta_{\max} - s_{\max} - x_{\star})_+]. \end{aligned} \quad (\text{C25})$$

To bound the horizon average of the envelope term, observe that in any step k , the size of an alive request equals the sum of its prompt length (at most s_{\max}) and the cumulative increments $\sum_{r=1}^{\text{age}} \delta_r$ over its age. Since $0 \leq \delta_k \leq \delta_{\max}$, we have

$$\text{size}(k) \leq s_{\max} + \delta_{\max} \cdot \text{age}(k),$$

so $\Lambda(k) - s_{\max}$ is bounded by δ_{\max} times the maximal age among alive requests at step k . Summing over the horizon and exchanging the order of summation (first over requests, then over the steps they are alive), we obtain

$$\sum_{k=0}^{K-1} (\Lambda(k) + \delta_{\max} - s_{\max} - x_{\star})_+ \leq \delta_{\max} \sum_j \sum_{r=0}^{o_j-1} (r+1 - y_{\star})_+,$$

where the outer sum is over all requests j whose lifetime intersects $[0:K-1]$, $o_j \sim \text{Geo}(p)$ is the decode length of request j , and $y_\star := \lfloor x_\star / \delta_{\max} \rfloor$ is an integer threshold on age. For a single geometric random variable $o_j \sim \text{Geo}(p)$,

$$\mathbb{E} \left[\sum_{r=0}^{o_j-1} (r+1-y_\star)_+ \right] = \sum_{r=y_\star+1}^{\infty} (r-y_\star) \mathbb{P}(o_j \geq r) = \sum_{r=y_\star+1}^{\infty} (r-y_\star)(1-p)^{r-1} = \frac{(1-p)^{y_\star}}{p^2}.$$

Let N_K be the number of distinct requests whose lifetime intersects the horizon $[0:K-1]$. At each step there are exactly GB alive items, and each item counted in N_K is alive for at least one step, so deterministically $N_K \leq GBK$ and hence $N_K/K \leq GB$. By linearity of expectation,

$$\frac{1}{K} \sum_{k=0}^{K-1} \mathbb{E}[(\Lambda(k) + \delta_{\max} - s_{\max} - x_\star)_+] \leq \frac{\delta_{\max} \mathbb{E}[N_K]}{K} \cdot \frac{(1-p)^{y_\star}}{p^2} \leq GB \delta_{\max} \frac{(1-p)^{y_\star}}{p^2}.$$

Averaging (C25) over $k = 0, \dots, K-1$ and rearranging, we obtain

$$\begin{aligned} \frac{1}{K} \sum_{k=0}^{K-1} \mathbb{E}[D(k)] &\leq s_{\max} + (1-p) \frac{1}{K} \sum_{k=0}^{K-1} \mathbb{E}[D(k-1)] \\ &\quad + \varepsilon_B B (s_{\max} + x_\star + \delta_{\max}) + \frac{GB^2}{p^2} \delta_{\max} (s_{\max} + x_\star + \delta_{\max}) (1-p)^{y_\star}. \end{aligned} \tag{C26}$$

The sequence $\{\mathbb{E}[D(k)]\}_{k \geq 0}$ is nonnegative, so its Cesàro average is bounded, and the right-hand side of (C26) is an affine contraction in the horizon average. Letting $K \rightarrow \infty$ and using $(1-p) < 1$, we obtain

$$\limsup_{K \rightarrow \infty} \frac{1}{K} \sum_{k=0}^{K-1} \mathbb{E}[D(k)] \leq \frac{s_{\max} + \varepsilon_B B (s_{\max} + x_\star + \delta_{\max}) + \frac{GB^2}{p^2} \delta_{\max} (s_{\max} + x_\star + \delta_{\max}) (1-p)^{y_\star}}{p}.$$

Finally, for $x_\star(B, G) = \lceil 3 \log(GB)/p \rceil$, we have $y_\star \geq \frac{3}{p \delta_{\max}} \log(GB)$, so

$$(1-p)^{y_\star} \leq \exp(-p y_\star) \leq (GB)^{-3},$$

and thus

$$\frac{GB^2}{p^2} \delta_{\max} (s_{\max} + x_\star + \delta_{\max}) (1-p)^{y_\star} = o_{B,G}(1)$$

whenever $B, G \rightarrow \infty$ with $\sqrt{G} \log G = o(B)$. Similarly, by the definition of ε_B and the same growth condition,

$$\varepsilon_B B (s_{\max} + x_\star + \delta_{\max}) = o_{B,G}(1).$$

Absorbing these vanishing terms into $o_{B,G}(1)$ and dividing by p yields (C22). This completes the proof. \square

Part 2 (Lower bound of Imbalance of FCFS)

We now extend the FCFS lower-bound analysis to the setting with general per-step drift: at each step k , every alive request gains a common increment $\delta_k \geq 0$, with δ_k independent of (B, G) and of the stochastic primitives. As before, each active request has an output length $o \sim \text{Geo}(p)$, independent across requests and of prompt lengths $S \sim \mathcal{D}_{\text{prefill}}$ supported on $\{0, 1, \dots, s_{\max}\}$, with

$$\mathbb{E}[S] = \mu_s, \quad \text{Var}(S) = \sigma_s^2 > 0.$$

Step 2.A: Slot-level dynamics under FCFS.

Index slots by (g, b) with $g \in \{1, \dots, G\}$ and $b \in \{1, \dots, B\}$. Let $Y_{g,b}(k)$ denote the *post-admission* size in slot (g, b) at the end of step k . Under FCFS, when the pool is overloaded and size-agnostic, each completion in any slot is immediately refilled by the earliest pending request whose prompt length is an i.i.d. draw from S . Thus, for each (g, b, k) , we have the recursion

$$Y_{g,b}(k) = (1 - \xi_{g,b}(k))(Y_{g,b}(k-1) + \delta_k) + \xi_{g,b}(k) S_{g,b}(k), \quad k \geq 1, \quad (\text{C27})$$

where

$$\xi_{g,b}(k) \sim \text{Bernoulli}(p), \quad S_{g,b}(k) \stackrel{\text{i.i.d.}}{\sim} S,$$

and all $\{\xi_{g,b}(k), S_{g,b}(k)\}_{g,b,k}$ are mutually independent and independent of the initial configuration $\{Y_{g,b}(0)\}$. The completion probability p and the drift δ_k do not depend on the current size $Y_{g,b}(k-1)$.

For device g , define the post-admission load and the instantaneous FCFS imbalance at step k by

$$S_g(k) := \sum_{b=1}^B Y_{g,b}(k), \quad \text{Imbalance}(k; \text{FCFS}) := G \cdot \max_{1 \leq g \leq G} S_g(k) - \sum_{g=1}^G S_g(k).$$

By symmetry of the FCFS rule across devices, for any arrival instance \mathcal{I} and any k ,

$$\mathbb{E}[\text{Imbalance}(k; \text{FCFS})] = G \left(\mathbb{E} \left[\max_g S_g(k) \right] - \frac{1}{G} \mathbb{E} \left[\sum_g S_g(k) \right] \right).$$

We now show that, for every step k , the G device loads have fluctuations of order \sqrt{B} with variance uniformly bounded away from zero, and that the maximum across devices therefore exhibits an excess of order $\sqrt{B \log G}$.

Step 2.B: Per-slot decomposition and moment bounds.

Fix a slot (g, b) and suppress its indices. For each step k , let $A(k)$ denote the *age* of the current job in this slot at the end of step k : the number of steps elapsed since the last completion in this slot (and since time 0 if no completion has occurred). The completion indicators $\{\xi(k)\}_{k \geq 1}$ form an i.i.d. Bernoulli(p) sequence. Therefore:

- At the end of step k , the event $\{A(k) \geq n\}$ implies that no completion occurred in the last n steps, hence

$$\mathbb{P}(A(k) \geq n) \leq (1-p)^n, \quad n \geq 0, k \geq 1. \quad (\text{C28})$$

- Every time a completion occurs in this slot, the new job's prompt length is drawn as $S_j \sim S$, independently of the completion history and the past prompts. Consequently, at any fixed time k , the prompt length $S_{\text{cur}}(k)$ of the job currently in this slot is independent of the completion history up to time k , and in particular independent of $A(k)$, with

$$S_{\text{cur}}(k) \stackrel{d}{=} S, \quad S_{\text{cur}}(k) \perp\!\!\!\perp A(k).$$

Given the age $A(k)$ and the sequence (δ_t) , the total increment accumulated since the last completion is deterministic:

$$H_k(A(k)) := \sum_{r=0}^{A(k)-1} \delta_{k-r},$$

with the convention that an empty sum is zero when $A(k) = 0$. Thus, at the end of step k ,

$$Y(k) = S_{\text{cur}}(k) + H_k(A(k)),$$

and $S_{\text{cur}}(k)$ and $H_k(A(k))$ are independent.

From this representation we can immediately extract uniform moment bounds.

Lemma 8 (Per-slot variance and third moment). *For any slot and any step $k \geq 1$,*

$$\text{Var}(Y(k)) \geq \sigma_s^2, \quad (\text{C29})$$

and there exists a constant $C_3 < \infty$ depending only on $(p, \sigma_s^2, \delta_{\max}, s_{\max})$ such that

$$\mathbb{E}[|Y(k) - \mathbb{E}[Y(k)]|^3] \leq C_3 \quad \text{for all } k \geq 1. \quad (\text{C30})$$

Proof of Lemma 8 Because $S_{\text{cur}}(k)$ and $H_k(A(k))$ are independent,

$$\text{Var}(Y(k)) = \text{Var}(S_{\text{cur}}(k)) + \text{Var}(H_k(A(k))) \geq \text{Var}(S) = \sigma_s^2,$$

establishing (C29).

For the third moment, we use that S is bounded and that $H_k(A(k))$ has uniformly bounded moments. From (C28),

$$\mathbb{P}(A(k) \geq n) \leq (1-p)^n, \quad n \geq 0.$$

Hence, by the tail-sum formula,

$$\mathbb{E}[A(k)^3] \leq 3 \sum_{n=0}^{\infty} n^2 \mathbb{P}(A(k) \geq n) \leq 3 \sum_{n=0}^{\infty} n^2 (1-p)^n < \infty,$$

and this bound is uniform in k . As $0 \leq \delta_k \leq \delta_{\max}$, we have $|H_k(A(k))| \leq \delta_{\max} A(k)$ and therefore

$$\mathbb{E}[|H_k(A(k))|^3] \leq \delta_{\max}^3 \mathbb{E}[A(k)^3] \leq C'_H,$$

for some C'_H depending only on (p, δ_{\max}) . Since $S_{\text{cur}}(k)$ is supported in $\{0, \dots, s_{\max}\}$, its centered third absolute moment is bounded by a constant C'_S depending only on s_{\max} . Writing

$$Y(k) - \mathbb{E}[Y(k)] = (S_{\text{cur}}(k) - \mu_s) + (H_k(A(k)) - \mathbb{E}[H_k(A(k))]) + (\mu_s - \mathbb{E}[Y(k)]),$$

and using the triangle inequality and the elementary bound $(x+y+z)^3 \leq 27(x^3+y^3+z^3)$ for $x, y, z \geq 0$, we obtain

$$\mathbb{E}[|Y(k) - \mathbb{E}[Y(k)]|^3] \leq C'' \left(\mathbb{E}[|S_{\text{cur}}(k) - \mu_s|^3] + \mathbb{E}[|H_k(A(k))|^3] + 1 \right) \leq C_3,$$

for some finite constant C_3 depending only on $(p, \sigma_s^2, \delta_{\max}, s_{\max})$. This proves (C30). \square

Step 2.C: Berry–Esseen for device-level loads.

Fix a device g and a step k . The B slot sizes $\{Y_{g,b}(k)\}_{b=1}^B$ are independent (across b) by construction: completions $\{\xi_{g,b}(k')\}$ and prompts $\{S_{g,b}(k')\}$ are independent across slots, and the FCFS assignment is size-agnostic under the overloaded regime. Their marginal distributions may not be identical, but Lemma 8 provides uniform variance and third-moment bounds.

Let

$$\mu_{g,b}(k) := \mathbb{E}[Y_{g,b}(k)], \quad X_{g,b}(k) := Y_{g,b}(k) - \mu_{g,b}(k),$$

and

$$V_g(k) := \text{Var}(S_g(k)) = \text{Var}\left(\sum_{b=1}^B Y_{g,b}(k)\right) = \sum_{b=1}^B \text{Var}(Y_{g,b}(k)).$$

By (C29),

$$V_g(k) \geq B \sigma_s^2 \quad \text{for all } g, k. \quad (\text{C31})$$

Moreover,

$$\sum_{b=1}^B \mathbb{E}[|X_{g,b}(k)|^3] \leq BC_3.$$

Define the normalized sum

$$W_g(k) := \frac{S_g(k) - \mathbb{E}[S_g(k)]}{\sqrt{V_g(k)}}.$$

By the Berry–Esseen theorem for sums of independent, non-identically distributed random variables, there exists an absolute constant $C_{\text{BE}} \in (0, \infty)$ such that, for each g, k ,

$$\sup_{x \in \mathbb{R}} \left| \mathbb{P}(W_g(k) \leq x) - \Phi(x) \right| \leq \frac{C_{\text{BE}} \sum_{b=1}^B \mathbb{E}[|X_{g,b}(k)|^3]}{V_g(k)^{3/2}} \leq \frac{C_{\text{BE}} C_3}{\sigma_s^3} \frac{1}{\sqrt{B}} =: \frac{C_*}{\sqrt{B}}, \quad (\text{C32})$$

where Φ denotes the standard normal distribution function and $C_* := C_{\text{BE}} C_3 / \sigma_s^3$ depends only on $(p, \sigma_s^2, \delta_{\max}, s_{\max})$.

We now derive a uniform lower bound on the right-tail probabilities of $W_g(k)$. Let

$$z_G := \sqrt{\frac{\log G}{2}},$$

and assume $\log G \geq 4$ (the case of smaller G can be absorbed into constants). For $Z \sim N(0, 1)$, the Gaussian tail bound gives

$$\mathbb{P}(Z \geq z_G) \geq \frac{1}{\sqrt{2\pi}} \left(\frac{1}{z_G} - \frac{1}{z_G^3} \right) \exp\left(-\frac{z_G^2}{2}\right) \geq \frac{1}{2\sqrt{2\pi} z_G} G^{-1/4} \quad (\text{C33})$$

for all $\log G \geq 4$. Combining (C32) and (C33) yields

$$\mathbb{P}(W_g(k) \geq z_G) \geq \frac{1}{2\sqrt{2\pi} z_G} G^{-1/4} - \frac{C_*}{\sqrt{B}}. \quad (\text{C34})$$

Since we assume $\sqrt{G} = \tilde{o}(B)$, there exists $B_0 < \infty$ and $G_0 \geq 2$ such that, for all $G \geq G_0$ and all $B \geq B_0$ satisfying this growth condition,

$$\frac{C_*}{\sqrt{B}} \leq \frac{1}{4\sqrt{2\pi} z_G} G^{-1/4}.$$

Hence, for all such (B, G) and for all devices g and steps k ,

$$\mathbb{P}(W_g(k) \geq z_G) \geq \frac{1}{4\sqrt{2\pi} z_G} G^{-1/4} =: p_G. \quad (\text{C35})$$

Step 2.D: Extreme-value lower bound across devices.

For a fixed step k , the collections $\{Y_{g,b}(k)\}_{b=1}^B$ are independent across g , because the slot primitives $(\xi_{g,b}(k), S_{g,b}(k))$ are independent across both g and b and FCFS acts independently on each device under the overloaded regime. Therefore, the device loads $\{S_g(k)\}_{g=1}^G$ are independent (though not necessarily identically distributed). By (C35), for each g ,

$$\mathbb{P}(W_g(k) \geq z_G) \geq p_G,$$

so by independence across g ,

$$\mathbb{P}\left(\max_{1 \leq g \leq G} W_g(k) \geq z_G\right) = 1 - \prod_{g=1}^G \mathbb{P}(W_g(k) < z_G) \geq 1 - (1 - p_G)^G \geq 1 - \exp(-Gp_G), \quad (\text{C36})$$

where we used $1 - x \leq e^{-x}$ for $x \geq 0$. From (C35),

$$Gp_G \geq \frac{1}{4\sqrt{2\pi} z_G} G^{3/4},$$

which is bounded away from zero for every fixed $G \geq 2$. Thus there exists an absolute $c_1 \in (0, 1)$ such that, for all $G \geq 2$ and all $B \geq B_0$,

$$\mathbb{P}\left(\max_{1 \leq g \leq G} W_g(k) \geq z_G\right) \geq c_1, \quad \forall k \geq 1. \quad (\text{C37})$$

Next, define

$$t_{B,G} := \sigma_s \sqrt{B} z_G.$$

By (C31), for every g, k ,

$$\sqrt{V_g(k)} \geq \sigma_s \sqrt{B},$$

so on the event $\{W_g(k) \geq z_G\}$ we have

$$S_g(k) - \mathbb{E}[S_g(k)] = W_g(k) \sqrt{V_g(k)} \geq z_G \sqrt{V_g(k)} \geq t_{B,G}.$$

Therefore,

$$\left\{ \max_{1 \leq g \leq G} W_g(k) \geq z_G \right\} \subseteq \left\{ \max_{1 \leq g \leq G} (S_g(k) - \mathbb{E}[S_g(k)]) \geq t_{B,G} \right\}.$$

Using the standard inequality $\mathbb{E}[\max_i X_i] \geq \max_i a_i + t \mathbb{P}(\max_i (X_i - a_i) \geq t)$ for any family $\{X_i\}$ and any $t > 0$, with $X_i = S_i(k)$ and $a_i = \mathbb{E}[S_i(k)]$, we obtain

$$\begin{aligned} \mathbb{E}\left[\max_{1 \leq g \leq G} S_g(k)\right] &\geq \max_{1 \leq g \leq G} \mathbb{E}[S_g(k)] + t_{B,G} \mathbb{P}\left(\max_{1 \leq g \leq G} (S_g(k) - \mathbb{E}[S_g(k)]) \geq t_{B,G}\right) \\ &\geq \max_{1 \leq g \leq G} \mathbb{E}[S_g(k)] + t_{B,G} \mathbb{P}\left(\max_{1 \leq g \leq G} W_g(k) \geq z_G\right). \end{aligned} \quad (\text{C38})$$

Combining (C38) with (C37), we obtain

$$\mathbb{E}\left[\max_{1 \leq g \leq G} S_g(k)\right] \geq \max_{1 \leq g \leq G} \mathbb{E}[S_g(k)] + c_1 t_{B,G} = \max_{1 \leq g \leq G} \mathbb{E}[S_g(k)] + c_1 \sigma_s \sqrt{B} z_G. \quad (\text{C39})$$

Step 2.E: Lower bound on FCFS imbalance and its time average.

For any step k , the expected imbalance under FCFS is

$$\mathbb{E}[\text{Imbalance}(k; \text{FCFS})] = G \mathbb{E}\left[\max_{1 \leq g \leq G} S_g(k)\right] - \sum_{g=1}^G \mathbb{E}[S_g(k)].$$

Writing

$$M_k := \max_{1 \leq g \leq G} \mathbb{E}[S_g(k)], \quad \bar{m}_k := \frac{1}{G} \sum_{g=1}^G \mathbb{E}[S_g(k)],$$

we may rewrite

$$\mathbb{E}[\text{Imbalance}(k; \text{FCFS})] = G \left(\mathbb{E}\left[\max_g S_g(k)\right] - \bar{m}_k \right).$$

Using (C39) and $M_k \geq \bar{m}_k$, we obtain

$$\begin{aligned}\mathbb{E}[\text{Imbalance}(k; \text{FCFS})] &\geq G \left(M_k + c_1 \sigma_s \sqrt{B} z_G - \bar{m}_k \right) \\ &= G(M_k - \bar{m}_k) + c_1 G \sigma_s \sqrt{B} z_G \\ &\geq c_1 G \sigma_s \sqrt{B} z_G.\end{aligned}\tag{C40}$$

Recalling $z_G = \sqrt{(\log G)/2}$, we conclude that there exists a constant $c > 0$, depending only on $(p, \sigma_s^2, \delta_{\max}, s_{\max})$, such that, for all $G \geq 2$ and all B sufficiently large with $\sqrt{G} = \tilde{o}(B)$,

$$\mathbb{E}[\text{Imbalance}(k; \text{FCFS})] \geq c G \sigma_s \sqrt{B \log G}, \quad \forall k \geq 1. \tag{C41}$$

Define the long-run expected time-average imbalance under **FCFS** and arrival instance \mathcal{I} by

$$\text{AvgImbalance}(\text{FCFS}; \mathcal{I}) := \liminf_{K \rightarrow \infty} \frac{1}{K} \sum_{k=0}^{K-1} \mathbb{E}[\text{Imbalance}(k; \text{FCFS})].$$

Since the lower bound (C41) holds uniformly for all $k \geq 1$, we have

$$\text{AvgImbalance}(\text{FCFS}; \mathcal{I}) \geq c G \sigma_s \sqrt{B \log G},$$

uniformly over all overloaded arrival instances \mathcal{I} .

In particular, as in the homogeneous-drift case, **FCFS** incurs imbalance of order $G\sqrt{B \log G}$, with the constant depending only on the prompt-length dispersion σ_s^2 , the geometric parameter p , and the drift bound δ_{\max} , but not on (B, G) .

Part 3: **BF-IO** vs. **FCFS**

We now combine the **BF-IO** average-gap bound from Lemma 7 with the **FCFS** lower bound from Part 2 to obtain the imbalance-reduction rate under geometric outputs with general per-step growth.

Recall the definition of the long-run expected average imbalance for a policy $\pi \in \{\text{BF-IO}, \text{FCFS}\}$ and an arrival instance \mathcal{I} :

$$\text{AvgImbalance}(\pi; \mathcal{I}) := \limsup_{K \rightarrow \infty} \frac{1}{K} \sum_{k=0}^{K-1} \mathbb{E}[\text{Imbalance}(k; \pi)].$$

As in the homogeneous-output case, we define the imbalance-reduction ratio of **BF-IO** against **FCFS** by

$$\text{IIR} := \inf_{\mathcal{I}} \frac{\text{AvgImbalance}(\text{FCFS}; \mathcal{I})}{\text{AvgImbalance}(\text{BF-IO}; \mathcal{I})},$$

where the infimum ranges over all overloaded arrival instances \mathcal{I} .

From Lemma 7, under our growth assumption $\sqrt{G} = \tilde{o}(B)$ we have, for any overloaded arrival instance \mathcal{I} ,

$$\limsup_{K \rightarrow \infty} \frac{1}{K} \sum_{k=0}^{K-1} \mathbb{E}[D(k)] \leq \frac{s_{\max}}{p} + o_{B,G}(1),$$

where $o_{B,G}(1) \rightarrow 0$ as $B, G \rightarrow \infty$ with $\sqrt{G} = \tilde{o}(B)$. Since for every step k ,

$$\text{Imbalance}(k; \text{BF-IO}) = \sum_{g=1}^G \left(\max_h L_h(k) - L_g(k) \right) \leq (G-1) D(k),$$

we obtain

$$\text{AvgImbalance}(\text{BF-IO}; \mathcal{I}) = \limsup_{K \rightarrow \infty} \frac{1}{K} \sum_{k=0}^{K-1} \mathbb{E}[\text{Imbalance}(k; \text{BF-IO})] \leq (G-1) \frac{s_{\max}}{p} + (G-1) o_{B,G}(1). \quad (\text{C42})$$

On the other hand, from the **FCFS** analysis in Part 2 we showed that, for all $G \geq 2$ and all B sufficiently large satisfying $\sqrt{G} \log G = o(B)$, there exists a constant $c_F > 0$ (depending only on $\sigma_s^2, p, \delta_{\max}, s_{\max}$) such that, uniformly over all overloaded arrival instances \mathcal{I} ,

$$\text{AvgImbalance}(\text{FCFS}; \mathcal{I}) \geq c_F G \sigma_s \sqrt{B \log G}. \quad (\text{C43})$$

Combining (C42) and (C43), we obtain, for every such \mathcal{I} ,

$$\begin{aligned} \frac{\text{AvgImbalance}(\text{FCFS}; \mathcal{I})}{\text{AvgImbalance}(\text{BF-IO}; \mathcal{I})} &\geq \frac{c_F G \sigma_s \sqrt{B \log G}}{(G-1) \frac{s_{\max}}{p} + (G-1) o_{B,G}(1)} \\ &= \left(\frac{c_F p \sigma_s}{s_{\max}} \frac{G}{G-1} \right) \frac{\sqrt{B \log G}}{1 + \frac{p}{s_{\max}} o_{B,G}(1)}. \end{aligned}$$

Since $o_{B,G}(1) \rightarrow 0$, we can choose B large enough (as a function of G) so that $\frac{p}{s_{\max}} o_{B,G}(1) \leq \frac{1}{2}$. For all such (B, G) ,

$$\frac{1}{1 + \frac{p}{s_{\max}} o_{B,G}(1)} \geq \frac{2}{3},$$

and we obtain the uniform lower bound

$$\frac{\text{AvgImbalance}(\text{FCFS}; \mathcal{I})}{\text{AvgImbalance}(\text{BF-IO}; \mathcal{I})} \geq c \frac{p \sigma_s}{s_{\max}} \frac{G}{G-1} \sqrt{B \log G},$$

for some universal constant $c > 0$ depending only on $(\sigma_s^2, p, \delta_{\max}, s_{\max})$. Taking the infimum over all overloaded arrival instances \mathcal{I} yields

$$\text{IIR} = \inf_{\mathcal{I}} \frac{\text{AvgImbalance}(\text{FCFS}; \mathcal{I})}{\text{AvgImbalance}(\text{BF-IO}; \mathcal{I})} \geq c \frac{p \sigma_s}{s_{\max}} \frac{G}{G-1} \sqrt{B \log G} = \Omega(\sqrt{B \log G}),$$

which shows that **BF-IO** achieves the same $\sqrt{B \log G}$ -order improvement over **FCFS** in the general per-step drift setting as in the homogeneous +1 model. \square

Appendix D Supplementary Materials for Section 6

D.1 Energy and MFU Computation

This appendix provides details on the energy consumption metric used in our experiments.

Model FLOPs Utilization (MFU).

MFU measures how efficiently the GPU's computational capacity is utilized, defined as the ratio of actual floating-point operations performed to the theoretical peak:

$$\text{mfu} = \frac{\text{Observed FLOPs/second}}{\text{Peak FLOPs/second}} \quad (\text{D44})$$

For LLM inference, the FLOPs required to generate one token is approximately $6 \times N_{\text{params}}$, arising from the matrix multiplications in the forward pass (approximately $2 \times N_{\text{params}}$ multiply-accumulate operations, each counting as 2 FLOPs, with an additional factor from attention computation). Thus, for a throughput of \mathcal{T} tokens per second on a model with N_{params} parameters:

$$\text{mfu} \approx \frac{\mathcal{T} \times 6 \times N_{\text{params}}}{\text{FLOPs}_{\text{peak}}} \quad (\text{D45})$$

where $\text{FLOPs}_{\text{peak}}$ is the GPU's theoretical peak throughput (e.g., 312 TFLOPs for NVIDIA A100 at FP16/BF16 precision).

Power Model and Parameters.

We adopt the power-utilization model from [21]:

$$P(\text{mfu}) = P_{\text{idle}} + (P_{\text{max}} - P_{\text{idle}}) \cdot \left(\frac{\text{mfu}}{\text{mfu}_{\text{sat}}} \right)^{\gamma} \quad (\text{D46})$$

The parameters are set as follows:

- $P_{\text{idle}} = 100\text{W}$: baseline power draw when the GPU is powered but not computing, reflecting memory refresh, control logic, and leakage current.
- $P_{\text{max}} = 400\text{W}$: peak power draw at full utilization, consistent with NVIDIA A100/H100 thermal design power specifications.
- $\text{mfu}_{\text{sat}} = 0.45$: the utilization level at which power consumption saturates. In practice, inference workloads rarely exceed this threshold due to memory bandwidth limitations.
- $\gamma = 0.7$: the sublinear scaling exponent, empirically calibrated in [21] for inference workloads. The value $\gamma < 1$ implies diminishing power increase per unit utilization gain, but also substantial power draw (P_{idle}) even at zero useful throughput.

Implications for Load Balancing.

The sublinear power model has a direct implication for barrier-synchronized systems. At each decode step, the wall-clock duration is $\Delta t = C + t_{\ell} \cdot \max_g L_g$. Workers with load $L_g < \max_{g'} L_{g'}$ complete their local computation early and idle until the barrier clears. During this idle period, these workers draw power near P_{idle} while generating zero tokens. Therefore, the total energy consumed is the discrete approximation of the integral (Equation (10)) :

$$E = \sum_{k=1}^K \sum_{g=1}^G \left[P(\text{mfu}_g^{(k)}) \cdot \Delta t^{(k)} \right] \quad (\text{D47})$$

where $\text{mfu}_g^{(k)}$ reflects worker g 's effective utilization at step k . Workers idling at barriers have $\text{mfu}_g^{(k)} \approx 0$ for a fraction of the step, drawing P_{idle} without contributing to

throughput. By reducing load imbalance, **BF-IO** ensures that all workers remain productively utilized throughout each step, converting idle power into useful computation and thereby reducing total energy consumption.

References

- [1] Hess, B., Kutzner, C., Spoel, D., Lindahl, E.: Gromacs 4: Algorithms for highly efficient, load-balanced, and scalable molecular simulation. *Journal of Chemical Theory and Computation* **4**(3), 435–447 (2008) <https://doi.org/10.1021/ct700301q>
- [2] Deng, Y., Cai, W.: An adaptive load balancing method for parallel molecular dynamics simulations. *Journal of Computational Physics* **161**(1), 250–263 (2000) <https://doi.org/10.1006/jcph.2000.6501>
- [3] Foster, I.T., Toonen, B.R.: Load-balancing algorithms for climate models. In: *Proceedings of IEEE Scalable High Performance Computing Conference*, pp. 674–681 (1994). IEEE
- [4] Rodrigues, E.R., Navaux, P.O., Panetta, J., Fazenda, A., Mendes, C.L., Kale, L.V.: A comparative analysis of load balancing algorithms applied to a weather forecast model. In: *2010 22nd International Symposium on Computer Architecture and High Performance Computing*, pp. 71–78 (2010). IEEE
- [5] Mishra, S.K., Sahoo, B., Parida, P.P.: Load balancing in cloud computing: a big picture. *Journal of King Saud University-Computer and Information Sciences* **32**(2), 149–158 (2020)
- [6] Khiyaita, A., El Bakkali, H., Zbakh, M., El Kettani, D.: Load balancing cloud computing: state of art. *2012 National Days of Network Security and Systems*, 106–109 (2012)
- [7] Chen, C., Lee, C., McGillem, C.: Task assignment and load balancing of autonomous vehicles in a flexible manufacturing system. *IEEE Journal on Robotics and Automation* **3**(6), 659–671 (1987)
- [8] Li, D., Tang, H., Wang, S., Liu, C.: A big data enabled load-balancing control for smart manufacturing of industry 4.0. *Cluster Computing* **20**(2), 1855–1864 (2017)
- [9] Kolomvatsos, K., Panagidi, K., Hadjiefthymiades, S.: A load balancing module for post-emergency management. *Expert systems with applications* **42**(1), 657–667 (2015)
- [10] Friesen, M.R., McLeod, R., Strome, T., Mukhi, S.: Load balancing at emergency departments using ‘crowdinforming’. In: *2011 IEEE 13th International Conference on e-Health Networking, Applications and Services*, pp. 364–370 (2011).

- [11] Brown, T., Mann, B., Ryder, N., Subbiah, M., Kaplan, J.D., Dhariwal, P., Neelakantan, A., Shyam, P., Sastry, G., Askell, A., *et al.*: Language models are few-shot learners. *Advances in neural information processing systems* **33**, 1877–1901 (2020)
- [12] Chowdhery, A., Narang, S., Devlin, J., Bosma, M., Mishra, G., Roberts, A., Barham, P., Chung, H.W., Sutton, C., Gehrmann, S., *et al.*: Palm: Scaling language modeling with pathways. *Journal of Machine Learning Research* **24**(240), 1–113 (2023)
- [13] OpenAI: GPT-4 technical report. arxiv 2303.08774. View in Article **2**(5) (2023)
- [14] Kaplan, J., McCandlish, S., Henighan, T., Brown, T.B., Chess, B., Child, R., Gray, S., Radford, A., Wu, J., Amodei, D.: Scaling laws for neural language models. arXiv preprint arXiv:2001.08361 (2020)
- [15] Wei, J., Tay, Y., Bommasani, R., Raffel, C., Zoph, B., Borgeaud, S., Yogatama, D., Bosma, M., Zhou, D., Metzler, D., *et al.*: Emergent abilities of large language models. arXiv preprint arXiv:2206.07682 (2022)
- [16] Kim, J., Lee, J., Park, G., Kim, B., Kwon, S.J., Lee, D., Lee, Y.: An inquiry into datacenter tco for llm inference with fp8. arXiv preprint arXiv:2502.01070 (2025)
- [17] Milmo, D.: Ai could account for nearly half of datacentre power usage by end of year. <https://www.theguardian.com/environment/2025/may/22/ai-data-centre-power-consumption> (2025)
- [18] Roth, E.: Openai says chatgpt users send over 2.5 billion prompts every day. <https://www.theverge.com/news/710867/openai-chatgpt-daily-prompts-2-billionutmsource=chatgpt.com> (2025)
- [19] You, J.: How much energy does chatgpt use? <https://epoch.ai/gradient-updates/how-much-energy-does-chatgpt-use> (2025)
- [20] Blunt, K., Hiller, J.: Big tech’s latest obsession is finding enough energy. <https://www.wsj.com/business/energy-oil/big-techs-latest-obsession-is-finding-enough-energy-f00055b2>
- [21] Özcan, M., Wiesner, P., Weiß, P., Kao, O.: Quantifying the energy consumption and carbon emissions of llm inference via simulations. arXiv preprint arXiv:2507.11417 (2025)
- [22] Zheng, Z., Ren, X., Xue, F., Luo, Y., Jiang, X., You, Y.: Response length perception and sequence scheduling: An llm-empowered llm inference pipeline.

- [23] Qiu, H., Mao, W., Patke, A., Cui, S., Jha, S., Wang, C., Franke, H., Kalbarczyk, Z.T., Başar, T., Iyer, R.K.: Efficient interactive LLM serving with proxy model-based sequence length prediction. arXiv preprint arXiv:2404.08509 (2024)
- [24] Fu, Y., Zhu, S., Su, R., Qiao, A., Stoica, I., Zhang, H.: Efficient llm scheduling by learning to rank. arXiv preprint arXiv:2408.15792 (2024)
- [25] Chen, S., Jiang, R., Yu, D., Xu, J., Chao, M., Meng, F., Jiang, C., Xu, W., Liu, H.: Kvdirect: Distributed disaggregated llm inference. arXiv preprint arXiv:2501.14743 (2024)
- [26] Shahout, R., Malach, E., Liu, C., Jiang, W., Yu, M., Mitzenmacher, M.: Don't stop me now: Embedding based scheduling for llms. arXiv preprint arXiv:2410.01035 (2024)
- [27] Luenberger, D.G., Ye, Y., *et al.*: Linear and Nonlinear Programming vol. 2. Springer, New York (1984)
- [28] Dantzig, G.B.: Linear programming. Operations research **50**(1), 42–47 (2002)
- [29] Schrijver, A.: Theory of Linear and Integer Programming. John Wiley & Sons, New York (1998)
- [30] Wang, G., Cheng, S., Zhan, X., Li, X., Song, S., Liu, Y.: Openchat: Advancing open-source language models with mixed-quality data. arXiv preprint arXiv:2309.11235 (2023)
- [31] Wang, Y., Chen, Y., Li, Z., Kang, X., Tang, Z., He, X., Guo, R., Wang, X., Wang, Q., Zhou, A.C., *et al.*: Burstgpt: A real-world workload dataset to optimize llm serving systems. arXiv preprint arXiv:2401.17644 (2024)
- [32] Zheng, L., Chiang, W.-L., Sheng, Y., Li, T., Zhuang, S., Wu, Z., Zhuang, Y., Li, Z., Lin, Z., Xing, E., *et al.*: LMSYS-Chat-1M: A large-scale real-world LLM conversation dataset. arXiv preprint arXiv:2309.11998 (2023)
- [33] Zhao, W., Ren, X., Hessel, J., Cardie, C., Choi, Y., Deng, Y.: Wildchat: 1m chatgpt interaction logs in the wild. arXiv preprint arXiv:2405.01470 (2024)
- [34] Wang, Y., Chen, Y., Li, Z., Kang, X., Fang, Y., Zhou, Y., Zheng, Y., Tang, Z., He, X., Guo, R., *et al.*: Burstgpt: A real-world workload dataset to optimize llm serving systems. In: Proceedings of the 31st ACM SIGKDD Conference on Knowledge Discovery and Data Mining V. 2, pp. 5831–5841 (2025)
- [35] Berger, M.J., Oliger, J.: Adaptive mesh refinement for hyperbolic partial differential equations. Journal of computational Physics **53**(3), 484–512 (1984)

- [36] Berger, M.J., Colella, P.: Local adaptive mesh refinement for shock hydrodynamics. *Journal of computational Physics* **82**(1), 64–84 (1989)
- [37] Aslam, S., Shah, M.A.: Load balancing algorithms in cloud computing: A survey of modern techniques. In: 2015 National Software Engineering Conference (NSEC), pp. 30–35 (2015). IEEE
- [38] Saeed, F., Javaid, N., Zubair, M., Ismail, M., Zakria, M., Ashraf, M.H., Kamal, M.B.: Load balancing on cloud analyst using first come first serve scheduling algorithm. In: International Conference on Intelligent Networking and Collaborative Systems, pp. 463–472 (2018). Springer
- [39] Rathi, R., Narkhede, N., Hasamnis, M.: Design and implementation of first-in-first-out (fifo) buffer for distributed load balancing systems. In: International Conference on Smart Computing and Communication, pp. 11–21 (2024). Springer
- [40] Tarandeep, Bhushan, K.: Load balancing in cloud through task scheduling. In: Recent Trends in Communication and Intelligent Systems: Proceedings of ICRTCIS 2019, pp. 195–204. Springer, New York (2020)
- [41] Whitt, W.: Deciding which queue to join: Some counterexamples. *Operations research* **34**(1), 55–62 (1986)
- [42] Dai, J.G., Hasenbein, J.J., Kim, B.: Stability of join-the-shortest-queue networks. *Queueing Systems* **57**(4), 129–145 (2007)
- [43] Foley, R.D., McDonald, D.R.: Join the shortest queue: stability and exact asymptotics. *Annals of Applied Probability*, 569–607 (2001)
- [44] Kwon, W., Li, Z., Zhuang, S., Sheng, Y., Zheng, L., Yu, C.H., Gonzalez, J., Zhang, H., Stoica, I.: Efficient memory management for large language model serving with PagedAttention. In: Proceedings of the 29th Symposium on Operating Systems Principles, pp. 611–626 (2023)
- [45] Zheng, L., Yin, L., Xie, Z., Sun, C.L., Huang, J., Yu, C.H., Cao, S., Kozyrakis, C., Stoica, I., Gonzalez, J.E., *et al.*: Sglang: Efficient execution of structured language model programs. *Advances in neural information processing systems* **37**, 62557–62583 (2024)
- [46] Sran, N., Kaur, N.: Comparative analysis of existing load balancing techniques in cloud computing. *International Journal of Engineering Science Invention* **2**(1), 60–63 (2013)
- [47] Subashini, S., Kavitha, V.: A survey on security issues in service delivery models of cloud computing. *Journal of network and computer applications* **34**(1), 1–11 (2011)

[48] Swarnkar, N., Singh, A.K., Shankar, R.: A survey of load balancing techniques in cloud computing. *Int J Eng Res Technol (IJERT)* **2**(8), 800–804 (2013)

[49] Gardner, K., Harchol-Balter, M., Scheller-Wolf, A., Velednitsky, M., Zbarsky, S.: Redundancy-d: The power of d choices for redundancy. *Operations Research* **65**(4), 1078–1094 (2017)

[50] Hellemans, T., Van Houdt, B.: On the power-of-d-choices with least loaded server selection. *Proceedings of the ACM on Measurement and Analysis of Computing Systems* **2**(2), 1–22 (2018)

[51] Mukherjee, D., Borst, S.C., Van Leeuwaarden, J.S., Whiting, P.A.: Universality of power-of-d load balancing in many-server systems. *Stochastic Systems* **8**(4), 265–292 (2018)

[52] Patel, G., Mehta, R., Bhoi, U.: Enhanced load balanced min-min algorithm for static meta task scheduling in cloud computing. *Procedia Computer Science* **57**, 545–553 (2015)

[53] Chen, H., Wang, F., Helian, N., Akanmu, G.: User-priority guided min-min scheduling algorithm for load balancing in cloud computing. In: *2013 National Conference on Parallel Computing Technologies (PARCOMPTECH)*, pp. 1–8 (2013). IEEE

[54] Bhoi, U., Ramanuj, P.N., *et al.*: Enhanced max-min task scheduling algorithm in cloud computing. *International Journal of Application or Innovation in Engineering and Management (IJAIEM)* **2**(4), 259–264 (2013)

[55] Rewehel, E.M., Mostafa, M.-S.M., Ragaie, M.O.: New subtask load balancing algorithm based on olb and lbmm scheduling algorithms in cloud. In: *Proceedings of the 2014 International Conference on Computer Network and Information Science*, pp. 9–14 (2014)

[56] Kunwar, V., Agarwal, N., Rana, A., Pandey, J.: Load balancing in cloud—a systematic review. *Big Data Analytics: Proceedings of CSI 2015*, 583–593 (2017)

[57] Kansal, N.J., Chana, I.: Cloud load balancing techniques: A step towards green computing. *IJCSI International Journal of Computer Science Issues* **9**(1), 238–246 (2012)

[58] Nace, D., Pióro, M.: Max-min fairness and its applications to routing and load-balancing in communication networks: a tutorial. *IEEE Communications Surveys & Tutorials* **10**(4), 5–17 (2009)

[59] Mao, Y., Chen, X., Li, X.: Max–min task scheduling algorithm for load balance in cloud computing. In: *Proceedings of International Conference on Computer Science and Information Technology: CSAIT 2013*, September 21–23, 2013,

Kunming, China, pp. 457–465 (2014). Springer

- [60] Ghosh, T.K., Goswami, R., Bera, S., Barman, S.: Load balanced static grid scheduling using max-min heuristic. In: 2012 2nd IEEE International Conference on Parallel, Distributed and Grid Computing, pp. 419–423 (2012). IEEE
- [61] Sim, K.M., Sun, W.H.: Ant colony optimization for routing and load-balancing: survey and new directions. *IEEE transactions on systems, man, and cybernetics-Part A: systems and humans* **33**(5), 560–572 (2003)
- [62] Nishant, K., Sharma, P., Krishna, V., Gupta, C., Singh, K.P., Rastogi, R., *et al.*: Load balancing of nodes in cloud using ant colony optimization. In: 2012 UKSim 14th International Conference on Computer Modelling and Simulation, pp. 3–8 (2012). IEEE
- [63] Li, K., Xu, G., Zhao, G., Dong, Y., Wang, D.: Cloud task scheduling based on load balancing ant colony optimization. In: 2011 Sixth Annual ChinaGrid Conference, pp. 3–9 (2011). IEEE
- [64] LD, D.B., Krishna, P.V.: Honey bee behavior inspired load balancing of tasks in cloud computing environments. *Applied soft computing* **13**(5), 2292–2303 (2013)
- [65] Thapliyal, N., Dimri, P.: Load balancing in cloud computing based on honey bee foraging behavior and load balance min-min scheduling algorithm. *International Journal of Electrical and Electronics Research (IJEER)* **10**(1), 1–6 (2022)
- [66] Domanal, S.G., Reddy, G.R.M.: Load balancing in cloud computing using modified throttled algorithm. In: 2013 IEEE International Conference on Cloud Computing in Emerging Markets (CCEM), pp. 1–5 (2013). IEEE
- [67] Panigrahi, A., Sahu, B., Rout, S.K., Rath, A.K.: M-throttled: Dynamic load balancing algorithm for cloud computing. In: Intelligent and Cloud Computing: Proceedings of ICICC 2019, Volume 1, pp. 3–10. Springer, New York (2020)
- [68] Hu, J., Gu, J., Sun, G., Zhao, T.: A scheduling strategy on load balancing of virtual machine resources in cloud computing environment. In: 2010 3rd International Symposium on Parallel Architectures, Algorithms and Programming, pp. 89–96 (2010). IEEE
- [69] Singh, J., Blumer, T., Roy, S., Saha, K.: Carton clamp test methodologies and the effects on load containment and retention. *Packaging Technology and Science* **28**(1), 15–30 (2015)
- [70] Ramesh, D., Dey, S.: Sclba-cc: slot based carton load balancing approach for cloud environment. In: 2018 International Conference on Current Trends Towards Converging Technologies (ICCTCT), pp. 1–5 (2018). IEEE

[71] Stojkovic, J., Choukse, E., Zhang, C., Goiri, I., Torrellas, J.: Towards greener llms: Bringing energy-efficiency to the forefront of llm inference. arXiv preprint arXiv:2403.20306 (2024)

[72] Ding, Y., Shi, T.: Sustainable llm serving: Environmental implications, challenges, and opportunities. In: Proceedings of the 15th IEEE International Green and Sustainable Computing Conference (IGSC), pp. 37–38 (2024). <https://doi.org/10.1109/IGSC64514.2024.00016>

[73] Nguyen, S., Zhou, B., Ding, Y., Liu, S.: Towards sustainable large language model serving. In: Proceedings of the 3rd Workshop on Sustainable Computer Systems (HotCarbon '24) (2024). <https://hotcarbon.org/assets/2024/pdf/hotcarbon24-final3.pdf>

[74] Wilkins, G., Keshav, S., Mortier, R.: Offline energy-optimal llm serving: Workload-based energy models for llm inference on heterogeneous systems. arXiv preprint arXiv:2407.04014 (2024)

[75] Kakolyris, A.K., Masouros, D., Xydis, S., Soudris, D.: Slo-aware gpu dvfs for energy-efficient llm inference serving. IEEE Computer Architecture Letters **23**(2), 150–153 (2024) <https://doi.org/10.1109/LCA.2024.3406038>

[76] Liu, Q., Huang, D., Zapater, M., Atienza, D.: Greenllm: Slo-aware dynamic frequency scaling for energy-efficient llm serving. arXiv preprint arXiv:2508.16449 (2025)

[77] Zhong, Y., Liu, S., Chen, J., Hu, J., Zhu, Y., Liu, X., Jin, X., Zhang, H.: Dist-serve: Disaggregating prefill and decoding for goodput-optimized large language model serving. arXiv preprint arXiv:2401.09670 (2024)

[78] Patel, P., Choukse, E., Zhang, C., Shah, A., Goiri, I., Maleki, S., Bianchini, R.: Splitwise: Efficient generative LLM inference using phase splitting. Power **400**(700W), 1–75 (2023)

[79] Liu, A., Feng, B., Wang, B., Wang, B., Liu, B., Zhao, C., Dengr, C., Ruan, C., Dai, D., Guo, D., et al.: Deepseek-v2: A strong, economical, and efficient mixture-of-experts language model. arXiv preprint arXiv:2405.04434 (2024)

[80] Shoeybi, M., Patwary, M., Puri, R., LeGresley, P., Casper, J., Catanzaro, B.: Megatron-lm: Training multi-billion parameter language models using model parallelism. arXiv preprint arXiv:1909.08053 (2019)

[81] Narayanan, D., Shoeybi, M., Casper, J., LeGresley, P., Patwary, M., Korthikanti, V., Vainbrand, D., Kashinkunti, P., Bernauer, J., Catanzaro, B., et al.: Efficient large-scale language model training on gpu clusters using megatron-lm. In: Proceedings of the International Conference for High Performance Computing, Networking, Storage and Analysis, pp. 1–15 (2021)

[82] Fedus, W., Zoph, B., Shazeer, N.: Switch transformers: Scaling to trillion parameter models with simple and efficient sparsity. *Journal of Machine Learning Research* **23**(120), 1–39 (2022)

[83] Yu, G.-I., Jeong, J.S., Kim, G.-W., Kim, S., Chun, B.-G.: Orca: A distributed serving system for {Transformer-Based} generative models. In: 16th USENIX Symposium on Operating Systems Design and Implementation (OSDI 22), pp. 521–538 (2022)

[84] Agrawal, A., Panwar, A., Mohan, J., Kwatra, N., Gulavani, B.S., Ramjee, R.: Sarathi: Efficient LLM inference by piggybacking decodes with chunked prefills. arXiv preprint arXiv:2308.16369 (2023)

[85] Agrawal, A., Kedia, N., Panwar, A., Mohan, J., Kwatra, N., Gulavani, B.S., Tumanov, A., Ramjee, R.: Taming throughput-latency tradeoff in LLM inference with Sarathi-Serve. arXiv preprint arXiv:2403.02310 (2024)

[86] Wu, B., Zhong, Y., Zhang, Z., Liu, S., Liu, F., Sun, Y., Huang, G., Liu, X., Jin, X.: Fast distributed inference serving for large language models. arXiv preprint arXiv:2305.05920 (2023)

[87] Sheng, Y., Cao, S., Li, D., Zhu, B., Li, Z., Zhuo, D., Gonzalez, J.E., Stoica, I.: Fairness in serving large language models. In: 18th USENIX Symposium on Operating Systems Design and Implementation (OSDI 24), pp. 965–988 (2024)

[88] Srivatsa, V., He, Z., Abhyankar, R., Li, D., Zhang, Y.: Preble: Efficient distributed prompt scheduling for llm serving. arXiv preprint arXiv:2407.00023 (2024)

[89] Hu, C., Huang, H., Xu, L., Chen, X., Wang, C., Xu, J., Chen, S., Feng, H., Wang, S., Bao, Y., et al.: Shuffleinfer: Disaggregate llm inference for mixed downstream workloads. *ACM Transactions on Architecture and Code Optimization* (2025)

[90] Doucet, Z., Sharma, R., Vos, M., Pires, R., Kermarrec, A.-M., Balmau, O.: Harmoeny: Efficient multi-gpu inference of moe models. arXiv preprint arXiv:2506.12417 (2025)

[91] Zhang, Y., Pinkert, G., Yang, N., Li, Y., Yuan, D.: Duoserve-moe: Dual-phase expert prefetch and cache scheduling for efficient moe llm inference. arXiv preprint arXiv:2509.07379 (2025)

[92] Jain, K., Parayil, A., Mallick, A., Choukse, E., Qin, X., Zhang, J., Goiri, I., Wang, R., Bansal, C., Rühle, V., et al.: Performance aware llm load balancer for mixed workloads. In: Proceedings of the 5th Workshop on Machine Learning and Systems, pp. 19–30 (2025)

[93] Kim, K., Hong, K., Gulcehre, C., Ailamaki, A.: The effect of scheduling

and preemption on the efficiency of llm inference serving. arXiv preprint arXiv:2411.07447 (2024)

[94] Jaillet, P., Jiang, J., Mellou, K., Molinaro, M., Podimata, C., Zhou, Z.: Online scheduling for llm inference with kv cache constraints. arXiv preprint arXiv:2502.07115 (2025)

[95] Wang, M., Ye, Y., Zhou, Z.: Llm serving optimization with variable prefill and decode lengths. arXiv preprint arXiv:2508.06133 (2025)

[96] Chen, Z., Ye, Y., Zhou, Z.: Adaptively robust llm inference optimization under prediction uncertainty. arXiv preprint arXiv:2508.14544 (2025)

[97] Ao, R., Luo, G., Simchi-Levi, D., Wang, X.: Optimizing llm inference: Fluid-guided online scheduling with memory constraints. arXiv preprint arXiv:2504.11320 (2025)

[98] Karp, R.M., Vazirani, U.V., Vazirani, V.V.: An optimal algorithm for online bipartite matching. In: Proceedings of the Twenty-second Annual ACM Symposium on Theory of Computing, pp. 352–358 (1990)

[99] Mehta, A., Saberi, A., Vazirani, U., Vazirani, V.: Adwords and generalized online matching. *Journal of the ACM (JACM)* **54**(5), 22 (2007)

[100] Devanur, N.R., Hayes, T.P.: The adwords problem: online keyword matching with budgeted bidders under random permutations. In: Proceedings of the 10th ACM Conference on Electronic Commerce, pp. 71–78 (2009)

[101] Mehta, A., *et al.*: Online matching and ad allocation. *Foundations and Trends® in Theoretical Computer Science* **8**(4), 265–368 (2013)

[102] Jaillet, P., Lu, X.: Online stochastic matching: New algorithms with better bounds. *Mathematics of Operations Research* **39**(3), 624–646 (2014)

[103] Gallego, G., Li, A., Truong, V.-A., Wang, X.: Online resource allocation with customer choice. arXiv preprint arXiv:1511.01837 (2015)

[104] Ma, W., Simchi-Levi, D.: Online resource allocation under arbitrary arrivals: Optimal algorithms and tight competitive ratios. Available at SSRN **2989332** (2017)

[105] Wang, L., Jiao, L., Li, J., Mühlhäuser, M.: Online resource allocation for arbitrary user mobility in distributed edge clouds. In: 2017 IEEE 37th International Conference on Distributed Computing Systems (ICDCS), pp. 1281–1290 (2017). IEEE

[106] Ma, W., Xu, P., Xu, Y.: Fairness maximization among offline agents in online-matching markets. *ACM Transactions on Economics and Computation* **10**(4),

- [107] Huang, Z., Kang, N., Tang, Z.G., Wu, X., Zhang, Y., Zhu, X.: Fully online matching. *Journal of the ACM (JACM)* **67**(3), 1–25 (2020)
- [108] Ho, C.-J., Vaughan, J.: Online task assignment in crowdsourcing markets. In: *Proceedings of the AAAI Conference on Artificial Intelligence*, vol. 26, pp. 45–51 (2012)
- [109] Sumita, H., Ito, S., Takemura, K., Hatano, D., Fukunaga, T., Kakimura, N., Kawarabayashi, K.-i.: Online task assignment problems with reusable resources. In: *Proceedings of the AAAI Conference on Artificial Intelligence*, vol. 36, pp. 5199–5207 (2022)
- [110] Goyal, V., Iyengar, G., Udwani, R.: Online allocation of reusable resources via algorithms guided by fluid approximations. *arXiv preprint arXiv:2010.03983* (2020)
- [111] Zhang, X., Cheung, W.C.: Online resource allocation for reusable resources. *arXiv preprint arXiv:2212.02855* (2022)
- [112] Huo, T., Cheung, W.C.: Online reusable resource allocations with multi-class arrivals. Available at SSRN 4320423 (2022)
- [113] Ao, R., Fu, H., Simchi-Levi, D.: Two-stage online reusable resource allocation: Reservation, overbooking and confirmation call. *arXiv preprint arXiv:2410.15245* (2024)
- [114] Chen, B., Potts, C.N., Woeginger, G.J.: A review of machine scheduling: Complexity, algorithms and approximability. *Handbook of Combinatorial Optimization: Volume1–3*, 1493–1641 (1998)
- [115] Brucker, P., Drexl, A., Möhring, R., Neumann, K., Pesch, E.: Resource-constrained project scheduling: Notation, classification, models, and methods. *European journal of operational research* **112**(1), 3–41 (1999)
- [116] Xing, W., Zhang, J.: Parallel machine scheduling with splitting jobs. *Discrete Applied Mathematics* **103**(1-3), 259–269 (2000)
- [117] Leung, J.Y.- (ed.): *Handbook of Scheduling - Algorithms, Models, and Performance Analysis*. Chapman and Hall/CRC, Boca Raton, FL (2004). <http://www.crcnetbase.com/isbn/978-1-58488-397-5>
- [118] Allahverdi, A., Ng, C.T., Cheng, T.E., Kovalyov, M.Y.: A survey of scheduling problems with setup times or costs. *European journal of operational research* **187**(3), 985–1032 (2008)
- [119] Kong, Q., Lee, C.-Y., Teo, C.-P., Zheng, Z.: Scheduling arrivals to a stochastic

service delivery system using copositive cones. *Operations research* **61**(3), 711–726 (2013)

[120] Mak, H.-Y., Rong, Y., Zhang, J.: Appointment scheduling with limited distributional information. *Management Science* **61**(2), 316–334 (2015)

[121] Roughgarden, T. (ed.): *Beyond the Worst-Case Analysis of Algorithms*. Cambridge University Press, Cambridge (2020). <https://doi.org/10.1017/9781108637435> . <https://doi.org/10.1017/9781108637435>

[122] Brucker, P., Gladky, A., Hoogeveen, H., Kovalyov, M.Y., Potts, C.N., Tautenhahn, T., Van De Velde, S.L.: Scheduling a batching machine. *Journal of scheduling* **1**(1), 31–54 (1998)

[123] Chen, B., Lee, C.-Y.: Logistics scheduling with batching and transportation. *European journal of operational research* **189**(3), 871–876 (2008)

[124] Lucier, B., Menache, I., Naor, J., Yaniv, J.: Efficient online scheduling for deadline-sensitive jobs. In: *Proceedings of the Twenty-fifth Annual ACM Symposium on Parallelism in Algorithms and Architectures*, pp. 305–314 (2013)

[125] Im, S., Moseley, B.: Online batch scheduling for flow objectives. In: *Proceedings of the Twenty-fifth Annual ACM Symposium on Parallelism in Algorithms and Architectures*, pp. 102–104 (2013)

[126] Li, W., Wang, L., Chai, X., Yuan, H.: Online batch scheduling of simple linear deteriorating jobs with incompatible families. *Mathematics* **8**(2), 170 (2020)

[127] Azar, Y., Epstein, L.: On-line scheduling with precedence constraints. *Discrete Applied Mathematics* **119**(1), 169–180 (2002) [https://doi.org/10.1016/S0166-218X\(01\)00272-4](https://doi.org/10.1016/S0166-218X(01)00272-4) . Special Issue devoted to Foundation of Heuristics in Combinatorics 1 Optimization

[128] Robert, J., Schabanel, N.: Non-clairvoyant scheduling with precedence constraints. In: Teng, S. (ed.) *Proceedings of the Nineteenth Annual ACM-SIAM Symposium on Discrete Algorithms*, SODA 2008, San Francisco, California, USA, January 20-22, 2008, pp. 491–500. SIAM, San Francisco, CA (2008). <http://dl.acm.org/citation.cfm?id=1347082.1347136>

[129] Agrawal, K., Li, J., Lu, K., Moseley, B.: Scheduling parallel dag jobs online to minimize average flow time. In: *Proceedings of the Twenty-Seventh Annual ACM-SIAM Symposium on Discrete Algorithms*. SODA '16, pp. 176–189. Society for Industrial and Applied Mathematics, USA (2016)

[130] Garg, N., Gupta, A., Kumar, A., Singla, S.: Non-clairvoyant precedence constrained scheduling. In: Baier, C., Chatzigiannakis, I., Flocchini, P., Leonardi, S. (eds.) *46th International Colloquium on Automata, Languages,*

and Programming, ICALP 2019, July 9-12, 2019, Patras, Greece. LIPIcs, vol. 132, pp. 63–16314. Schloss Dagstuhl - Leibniz-Zentrum für Informatik, Patras, Greece (2019). <https://doi.org/10.4230/LIPIcs.ICALP.2019.63> . <https://doi.org/10.4230/LIPIcs.ICALP.2019.63>

- [131] Ball, M.O., Queyranne, M.: Toward robust revenue management: Competitive analysis of online booking. *Operations Research* **57**(4), 950–963 (2009)
- [132] Golrezaei, N., Jaillet, P., Zhou, Z.: Online resource allocation with convex-set machine-learned advice. *arXiv preprint arXiv:2306.12282* (2023)
- [133] Agrawal, S., Wang, Z., Ye, Y.: A dynamic near-optimal algorithm for online linear programming. *Operations Research* **62**(4), 876–890 (2014)
- [134] Li, X., Sun, C., Ye, Y.: Simple and fast algorithm for binary integer and online linear programming. *Advances in Neural Information Processing Systems* **33**, 9412–9421 (2020)
- [135] Li, X., Ye, Y.: Online linear programming: Dual convergence, new algorithms, and regret bounds. *Operations Research* **70**(5), 2948–2966 (2022)
- [136] Jiang, J., Li, X., Zhang, J.: Online stochastic optimization with wasserstein-based nonstationarity. *Management Science* (2025)
- [137] Buchbinder, N., Naor, J.: Online primal-dual algorithms for covering and packing. *Mathematics of Operations Research* **34**(2), 270–286 (2009)
- [138] Sleator, D.D., Tarjan, R.E.: Amortized efficiency of list update and paging rules. *Communications of the ACM* **28**(2), 202–208 (1985)
- [139] Fiat, A., Karp, R.M., Luby, M., McGeoch, L.A., Sleator, D.D., Young, N.E.: Competitive paging algorithms. *Journal of Algorithms* **12**(4), 685–699 (1991)
- [140] Lykouris, T., Vassilvitskii, S.: Competitive caching with machine learned advice. *Journal of the ACM (JACM)* **68**(4), 1–25 (2021)
- [141] Koutsoupias, E., Papadimitriou, C.H.: On the k-server conjecture. *Journal of the ACM (JACM)* **42**(5), 971–983 (1995)
- [142] Borodin, A., Linial, N., Saks, M.E.: An optimal on-line algorithm for metrical task system. *Journal of the ACM (JACM)* **39**(4), 745–763 (1992)
- [143] Zinkevich, M.: Online convex programming and generalized infinitesimal gradient ascent. In: *Proceedings of the 20th International Conference on Machine Learning (icml-03)*, pp. 928–936 (2003)
- [144] Meyerson, A.: Online facility location. In: *Proceedings 42nd IEEE Symposium on Foundations of Computer Science*, pp. 426–431 (2001). IEEE

[145] Fotakis, D.: On the competitive ratio for online facility location. *Algorithmica* **50**(1), 1–57 (2008)